Volume 4, Number 2 (Cumulative No.32) February 25, 2012 ISSN:1553-992X

Academia Arena

Marsland Press
PO Box 180432
Richmond Hill, New York 11418, USA

Websites:
http://www.sciencepub.net/academia
http://www.sciencepub.net

Emails:
aarena@gmail.com
editor@sciencepub.net

Phone: (347) 321-7172

Cover design: MA,Hongbao
Photograph: YOUNG, Mary

ISSN 1553-992X

Volume 4, Number 2 February 25, 2012 ISSN:1553-992X

Academia Arena

Academia Arena 2012;4 (2)

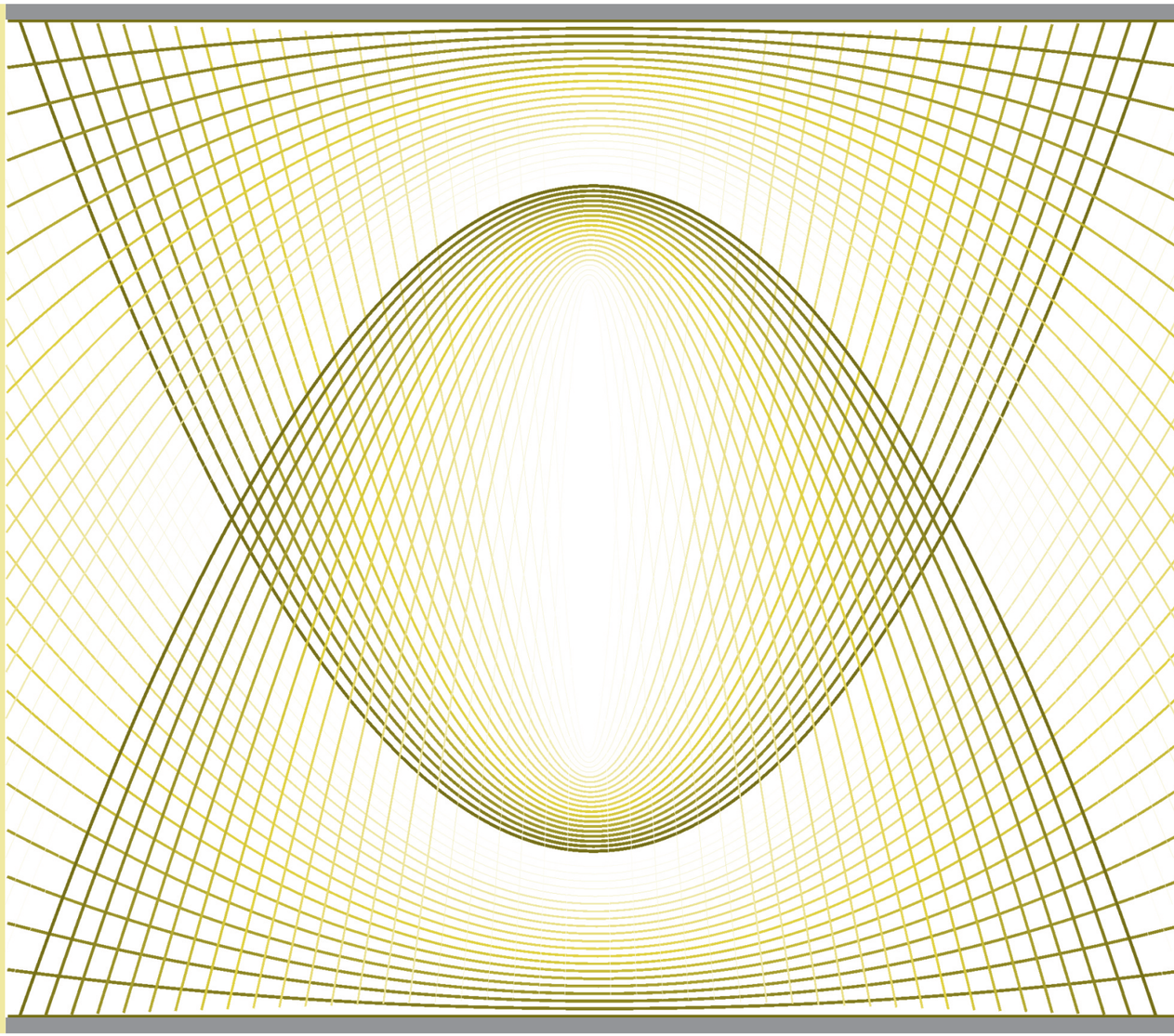

MARSLAND PRESS
Multidisciplinary Academic Journal Publisher

Websites:
http://www.sciencepub.net/academia
http://www.sciencepub.net

Emails:
aarena@gmail.com
editor@sciencepub.net

Volume 4, Number 2 February 25, 2012 ISSN:1553-992X

Academia Arena

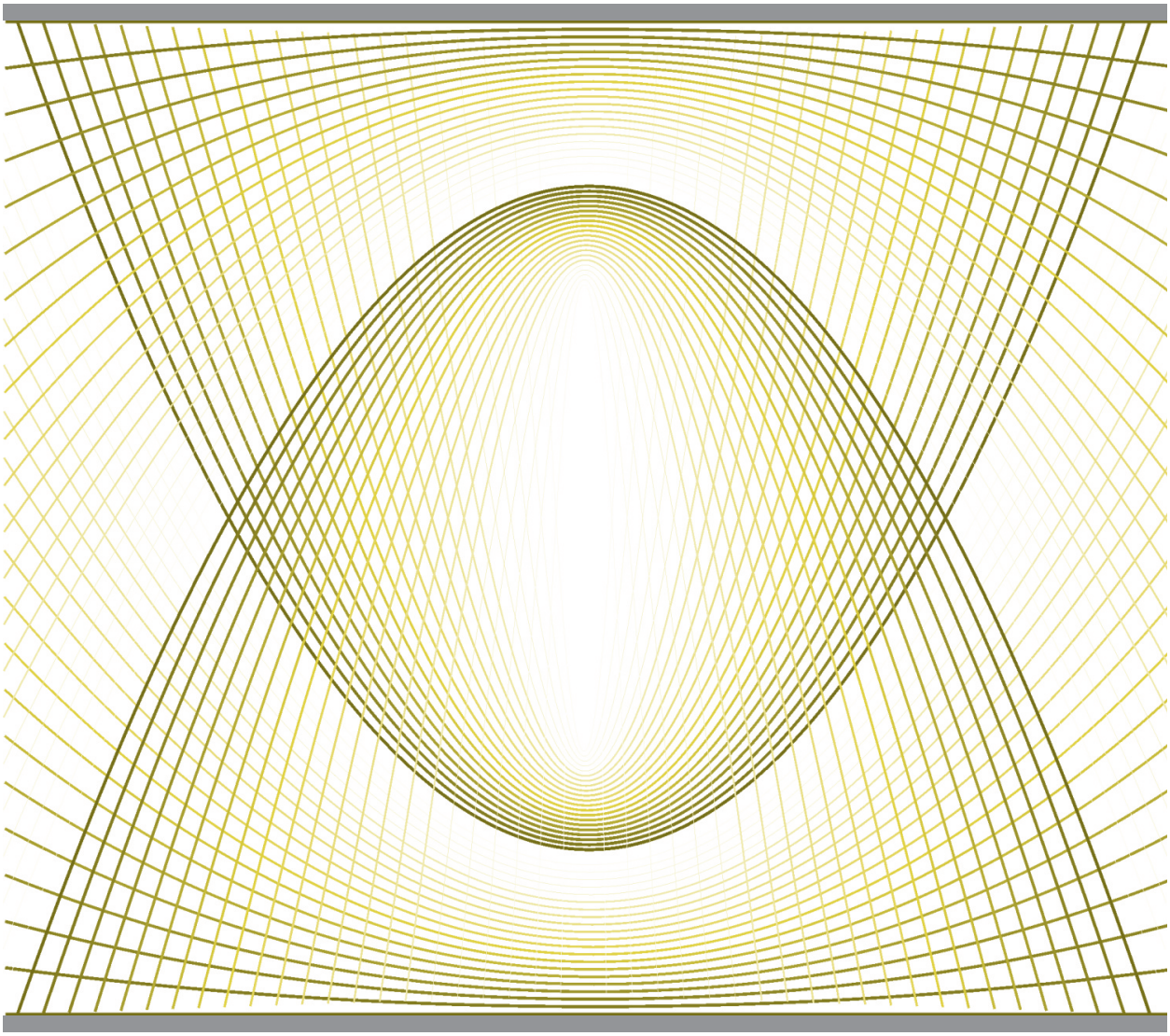

MARSLAND PRESS
Multidisciplinary Academic Journal Publisher

Websites:
http://www.sciencepub.net/academia
http://www.sciencepub.net

Emails:
aarena@gmail.com
editor@sciencepub.net

Academia Arena

(*Academ Arena*)
ISSN 1553-992X

学术争鸣

Academia Arena is published bi-linguistically with English and Chinese for the scientists and Engineers. The journal founded in January 1, 2009 aims to present an arena of science and engineering. The Editor-in-Chief, Associate Editors-in-Chief and Editors have backgrounds in Philosophy, Science, Technology, Cosmology, Mathematics, Physics, Chemistry, Biology, Medicine, Civil, Electrical, Mechanical Engineering, etc. Papers submitted could be reviews, objective descriptions, research reports, opinions/debates, news, letters, and other types of writings.
学术争鸣于2009年元月1日在美国纽约马斯兰德出版社发刊，主要目标为提供科学家与工程师及社会工作者学术辩论的发表园地，专业领域包含哲学、科学、技术、宇宙学、数学、物理、化学、生物学、医学、土木、电机、化工、机械工程，等，编辑群将以最专业客观的立场为所有投稿作者服务。

Information for Authors

1. Manuscripts Submission
(1) Submission Methods: Electronic submission through email would be accepted.
(2) Software: The Microsoft Word file is preferred.
(3) Font: Normal, Times New Roman, 10 pt, single space.
(4) Indent: Type 4 spaces in the beginning of each new paragraph.
(5) Manuscript: Don't use "Footnote" or "Header and Footer".
(6) Cover Page: Put detail information of authors and a short running title in the cover page.
(7) Title: Use Title Case in the title and subtitles, e.g. "**Debt and Agency Costs".**
(8) Figures and Tables: Use full word of figure and table, e.g. **"Figure 1.** Annul Income of Different Groups**", Table 1. List Data".**
(9) References: Cite references by "last name, year", e.g. "(Smith, 2003)". References should include all the authors' last names and initials, title, journal, year, volume, issue, and pages etc.

Reference Examples:

Journal Article: Hacker J, Hentschel U, Dobrindt U. Prokaryotic chromosomes and disease. Science 2003;301(34):790-3.

Book: Berkowitz BA, Katzung BG. Basic and clinical evaluation of new drugs. In: Katzung BG, ed. Basic and clinical pharmacology. Appleton & Lange Publisher. Norwalk, Connecticut, USA. 1995:60-9.

(10) Submission Address: Marsland Press
PO Box 180432, Richmond Hill, New York 11418, USA; Telephone: (347) 321-7172; Email: editor@sciencepub.net.
(11) Reviewers: Authors should suggest 2-8 competent reviewers with their name and email.

2. Manuscript Preparation

Each manuscript should be formatted to include the following components:

(1) Title: Complete article title;
(2) Author(s): Each author's full name; institution(s) with which each author is affiliated, with city, state/province, zip code, and country; and the name, complete mailing address, telephone number, facsimile number (if available), and e-mail address for all correspondence.
(3) Abstract: including Background, Materials and Methods, Results, and Discussions.
(4) Key Words.
(5) Introduction.
(6) Materials and Methods.
(7) Results.
(8) Discussions.
(9) Acknowledgments.
(10) References.
(11) Date submitted

3. Copyright and Responsibility of Authors to their Articles: When the manuscript(s) is submitted to the journal, the authors agree the following: All the authors have participated sufficiently in this work; The article is not published elsewhere; Authors are responsibility on the contents of the article; The journal and author(s) have same right for the copyright of the article and either of the journal or author(s) can use it by anyway without noting the other party.

Journal Address:
Marsland Press
PO Box 180432
Richmond Hill, New York 11418, USA
Telephone: (347) 321-7172
E-mail: sciencepub@gmail.com;
editor@sciencepub.net
Websites: http://www.sciencepub.net

CONTENTS

Extrinsic Factors Influencing Antibacterial Activities of *Tapinanthus bangwensis* Against Diarrhoeal Causing Organsims

B.T. Thomas[1], H. I. Effedua[2], G.C. Agu[5], O.S. Musa, P.A. Akinduti[3], O. Ejilude[4], A. Oluwadun[1]

1. Department of Medical Microbiology and Parasitology, Olabisi Onabanjo University, Ago-Iwoye, Ogun State, Nigeria.
2. Department of Medical Laboratory Science, School of Public Health, Babcock University, Ilishan-Remo, Ogun State, Nigeria
3. Department of Veterinary Microbiology and Parasitology, University of Agriculture, Abeokuta, Ogun State, Nigeria.
4. Department of Microbiology and Parasitology, Sacred Heart Hospital,Lantoro Abeokuta, Ogun State, Nigeria.
5. Department of Microbiology, Olabisi Onabanjo University, Ago-Iwoye, Ogun State, Nigeria

ABSTRACT: *Tapinanthus bangwensis* is a parasitic plant with wide distribution and documented antimicrobial efficacies. Inconsistence in its activities has however, been suggestively linked with some factors. Hence, this study was carried out to establish the effect of some extrinsic factors on the antibacterial activities of *T. bangwensis* against some diarrhoeal causing bacteria. Antibacterial activity of *T. bangwensis*, collected from some parts of Nigeria was determined by standard agar-diffusion method. Results from this study showed a significantly higher zone of bacterial inhibition with chloroform extract when compared with ethanol and aqueous extracts ($P<0.05$). Higher antibacterial activities was also observed with extracts obtained from air dried plants than those obtained from sun dried and oven dried plants ($P<0.05$). Steaming method of extraction produced a significantly higher zone of bacterial inhibition than cold and hot methods of extraction ($P<0.05$). Percentage weight yield of active crude compound s of *T. bangwensis* was highest in chloroform (4.63±1.99%) than methanol (2.83±2.06%) and water (2.28±1.90%) ($P<0.05$). A significant positive correlation ($r = +0.91$, $P<0.05$) was observed between percentage weight yield and zone of antibacterial inhibition, exhibited by *T. bangwensis*. Weight yield accounted for 70% of antibacterial activities with a linear relationship of $y = 3x + 5.6$. Antibacterial activities of *T. bangwensis* were however, not affected by its host plants and varying concentrations of its crude extracts ($P>0.05$). Conclusion from this study has shown that solvents and methods of extraction such as mode of plant drying and means of concentrating extracts as important and influential extrinsic factors that determines the antibacterial activities of *T. bangwensis*.

[B.T. Thomas, H. I. Effedua, G.C. Agu, O.S.Musa, P.A. Akinduti, O. Ejilude, A. Oluwadun. **Extrinsic Factors Influencing Antibacterial Activities of *Tapinanthus bangwensis* Against Diarrhoeal Causing Organsims.** Academia Arena, 2012;4(2):1-4] (ISSN 1553-992X). http://www.sciencepub.net. 1

Keywords: Extrinsic Factor; Antibacterial; *Tapinanthus bangwensis;* Diarrhoeal; Organsims

1. Introduction

Tapinanthus bangwensis (order Santalales) belong to the family of Loranthaceae and constitute the largest group of parasitic plants which has about 950 species distributed in 77 genera(Engone and Salle,2006). Loranthaceae; including *Tapinanthus* constitute a great deal of pestilence in the natural forests, plantations, cultivated fruit trees and ornamental plants; causing damages to the host plants(Sonke et al., 2000., Boussim et al., 2004). *Tapinanthus bangwensis* is widely distributed in Nigeria. The plant exists as xerophytes on many host trees. Its leaves and young twigs have in the past been used in folklore treatment of diseases and sterility in cow.Documentations have been made about the antimicrobial efficacy of *T. bangwensis* (Adegbolahun and Olukemi,2010) but its activity tends to vary among investigators. Also, there have been controversies over the hypothesis that the antimicrobial efficacies of *T. bangwensis* is host plant dependent. Hence, we have decided to investigate the impact of host plant factor and other extrinsic factors on the antibacterial activities of *T. bangwensis* against some bacterial pathogens causing diarrhoea.

2. Materials and Methods

2.1. Collection of Plants

Fresh leaves and twigs of *Tapinanthus bangwensis* were collected from Iseyin, Southern part of Oyo State and Chagas village in Abuja, Nigeria.The plants were authenticated by Dr A. E. Ayodele at the department of Botany and Microbiology, University of Ibadan, Nigeria and were designated T1 – T4 on the basis of the host plants from which they were collected. T1 was from Triclisia gilletii (De wild) stainer, T2 from *Parkia biglobosa* (Jacq.) Benth,T3 from *Citrus aurantifolia* (Christm.) swingle and T4 from phyllanthus muellerianus.

2.2.Preparation of Plant Extracts

Fresh Leaves were divided into three groups. Group one were air-dried, Group two were sun-dried and Group three were oven-dried. After drying the leaves were shredded and separately preserved in air-tight cellophane bags.The shredded leaves were milled into powder. Cold extraction of the plant was made by soaking 100g of powdered plant into 400ml each of methanol, chloroform and water respectively in flasks. The flasks were manually agitated at intervals for 5 days. All extracts were then filtered with whatman no 1 filter paper into flask. The filtrates were later concentrated to dryness with the aid of a rotary evaporator. The steam extraction was carried out as described by Adeolu and Oladimeji(Adebolu

and Oladimeji, 2005). The hot extraction involves placing the leaves and twigs of *T. bangwensis* in a pot and boiling for 30 minutes. This was then allowed to cool and the leaves were then squeezed to obtain the extract that was later concentrated by rotary evaporator. The yield of concentrates from the various extracts was then calculated using the following formula:

Percentage weight yield (%) = $W_2 / W_1 \times 100$.
Where
W_1 = Weight of herbal powder before extraction.
W_2 = Weight of concentrate after extraction.

2.3.Statistical analysis

All data were analyzed by SPSS package version 15. Comparison of mean zones of inhibition were determined by ANOVA (Analysis of Variance) while regression analysis was used to determine the linearity between percentage weight yields (%) of plant and their proportional antibacterial activities.

3. Results

The effect of host plants on the antibacterial activities of *T. bangwensis* was determined in table1. Although, the zones of inhibition (mm) varieds with different host plants, but the difference was insignificant (F=1.06, P>0.05). In table 2, when the mean of zones of inhibition of *T. bangwensis* concentrates from different solvents were compared, a significant difference was observed (F=10.13, P<0.05); with highest antibacterial activity being recorded with chloroform. Table 3 displayed various mean of zones of inhibition of *T. bangwensis* extracts processed by different methods of drying. Analyzed data showed that extracts prepared from air-dried plants of *T. bangwensis* hads the highest zone of inhibition of 13.50 ± 3.50mm (F= 6.47, P<0.05). Comparison between antibacterial activities among concentrates of *T. bangwensis* yielded by different extraction techniques was made in table 4. The significantly higher zone of inhibition was observed with steam (13.13±1.59mm) when compared with cold (9.58 ± 0.68) and hot (7.42 ± 0.85) methods of extraction (F=6.66, P<0.05). When means of zone of inhibition of *T. bangwensis* were compared at different concentrations that rangeds from 50–200mg/ml, no significant difference was observed (F=2.23, P>0.05) in table 5. Comparison of percentage weight yields (%) of crude *T. bangwensis* concentrate regarding the type of solvents of extraction demonstrated that the highest yield of 4.63±1.99% was with chloroform (F = 448.17, P<0.05) (Table 6). A significant correlation (r = +0.91, P<0.05) was observed between the percentage weight yields of *T. bangwensis* and its antibacterial activities, with a linear equation: y = 3x + 5.60. Regression determinants showed that percentage weight yield was accountable for 70% of the antibacterial activities (figure 1).

Table 1. Effect of host plant on the antibacterial activity of *Tapinanthus bangwensis*

		Zones of inhibition
Host plants	n	Mean±SEM(mm)
Triclisia gilletii	10	8.43 ± 1.65
Parkia biglobosa	10	6.45 ± 1.94
Citrus aurantifolia	10	8.34 ± 2.63
Phyllanthus muellerianus	10	6.42 ± 2.03

F = 1.06, P > 0.05.

Table 2. Effect of solvent of extraction on the antibacterial activity of *Tapinanthus bangwensis*

		Zones of inhibition
Solvents of extraction	n	Mean±SEM(mm)
Methanol	10	15.64 ± 1.20
Chloroform	10	19.00 ± 1.50
Water	10	11.20 ± 0.85

F = 10.13, P < 0.05.

Table 3. Effect of drying methods on the antibacterial activity of *Tapinanthus bangwensis*

		Zones of inhibition
Drying methods	n	Mean ± SEM (mm)
Air drying	10	13.50 ± 3.50
Sun drying	10	8.88 ± 2.03
Oven drying	10	9.00 ± 1.63

F = 6.47, P < 0.05.

Table 4. Effect of methods of extraction on the antibacterial activity of *Tapinanthus bangwensis*

		Zones of inhibition
Methods of extraction	n	Mean ± SEM(mm)
Steam extraction	10	13.13 ± 1.59
Cold extraction	10	9.58 ± 0.68
Hot extraction	10	7.42 ± 0.85

F = 6.66, P < 0.05.

Table 5. Effect of concentrations on the antibacterial activity of *Tapinanthus bangwensis*

		Zones of inhibition
Concentrations	n	Mean±SEM(mm)
100mg/ml	10	12.05 ± 2.06
150mg/ml	10	14.30 ± 1.99
200mg/ml	10	16.00 ± 1.90
50mg/ml	10	19.50 ± 2.45

F = 2.23, P > 0.05.

Table 6. Effect of Solvents on weight yield of the active ingredients in *Tapinanthus bangwensis*

		Weight yield (%)
Solvents	n	Mean ± SEM (mm)
Methanol	3	2.83 ± 2.06
Chloroform	3	4.63 ± 1.99
Water	3	2.28 ± 1.90

F = 448.17, P< 0.05.

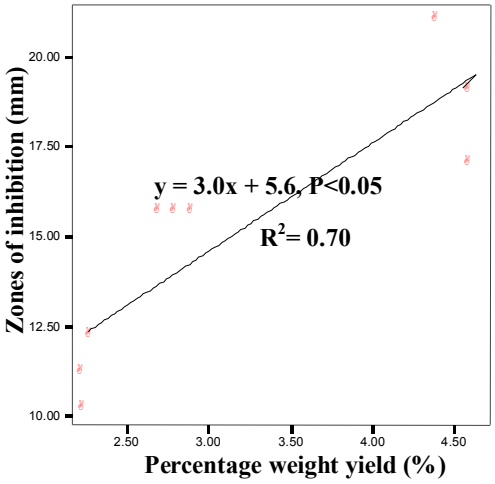

Figure 1. Relationship between inhibitory activities and percentage weight yield of active chloroform extract of *T. bangwensis*.

4. Discussion

Result of this study have shown that the antibacterial activities of *T. bangwensis* were independent of host plant factor. This observation supported the null hypothesis which says that host plant does not influence the antibacterial activities of *T. bangwensis*. The significantly higher percentage yield of crude concentrate of *T. bangwensis* by chloroform in comparison with other solvents demonstrated higher extraction strength with chloroform (P<0.05). Also, significantly the highest antibacterial activity was found in the crude chloroform extract which strongly suggests that the active antibacterial compounds might be organic and less polar in origin.

After processing of *T. bangwensis* leaves by different methods of drying, the highest antibacterial activity was observed in air dried extract while less activity was observed with oven-dried extract and least activity was observed with sun dried extract (P<0.05). Lesser antibacterial activity in sun dried extract may be due to photochemical degradation of the active compounds which in turn may result in structural modification of functional groups required for active antimicrobial activity(Adegbolahun and Olukemi,2010). Also, lesser antibacterial activity in oven-dried extract indicated that the active antibacterial compound of *T. bangwensis* might be heat-labile. This observation was similar to that of Olaniyi et al. (2010), Harnischfeger (2005) and Niggermann and Gruber(2003). Furthermore,the lesser antimicrobial activities in oven-dried extract might also be linked with loss of volatile contents of *T. bangwensis* such as phenols and essentials oils (Rajendran et al., 2007).

Steam method of extraction of *T. bangwensis* has been shown to produce bioactive compound with better antibacterial activities than cold and hot methods of extraction (P<0.05). The weakest antibacterial activity in concentrate of *T. bangwensis* derived from hot method of extraction further re-emphasize the volatile nature of active antibacterial constituents of *T. bangwensis* while lower antibacterial activity in cold method of extraction is a reflection of the decreased solubility of active plant constituent at lower temperature (SOT,2009). Comparison of the antibacterial activity of crude chloroform extract of *T. bangwensis* at concentrations such as 50, 100, 150, and 200mg/ml showed no significant difference (P>0.05). This indicated that *T. bangwensis* exhibited antibacterial activities almost at equal level at concentration range of 50-200mg/ml. Equilibrium of antibacterial activities between the lesser and higher concentrations of *T. bangwensis* clearly shows that the antibacterial quality of the active constituents of the plant is largely dependent on its molecular weight and diffusion rates through agar rather than its concentration. Since higher zones of inhibition in agar diffusion antibiotic susceptibility tests is an attribute of faster rates of drug diffusion and low molecular weight, it can then be inferred that the active antibacterial constituent of *T. bangwensis* might be among compounds with lower molecular weight.

In conclusion, the outcome of this study has demonstrated that antibacterial activities of concentrates from *T. bangwensis* could be best enhanced by methods that include air-drying and chloroform extraction of the plant via steaming.

REFERENCES

1. Engone ONL, and Salle G. Faut il eradiquer phramanthera capitata, parasite des heveas en Afrique? *C.R. Biologies. 2006;* **329:** 185-195.

2. Sonke B, Kenfaek D, and Tindo M. Parasitism de lavocatier (Persea Americana, lauraceae) par les loranthaceae dans la region de Yaounde (Cameroun). *Fruits* 2000;**55:** 325-331.
3. Boussim IJ, Guinko S, Tuquet C and Salle G. Mistletoes of the parklands of Burkina-Faso. *Agro-forest. Syst.2004;***60:** 39-49.
4. Efuntoye M.O, Ayodele AE, Thomas BT and Ajayi TO.Does host plant affect the antibacterial activity of *Tapinanthus bangwensis* (Engl.and k.krause) Danser (Loranthaceae)? *J. Medicinal Plants Res.2010;* **4 (13):** 1281-1284.
5. Adebolu TT, and Oladimeji SA. Antimicrobial activity of leaf extracts of Ocimum gratissimum on selected diarrhea causing bacteria in South Western Nigeria. *Afr. J. Biotech* .2000;**4(7):** 682-684.
6. Adegbolahun OM, and Olukemi OO. Effect of light irradiation on the antimicrobial activity of Zanthoxyloides (lam) methanolic extract. *Afr. J. Pharm. Pharmacol.2000;* **4(4):** 145-150.
7. Olaniyi AA, Ayun JSK, Ogundaini AO, and Olugade TA. Essential inorganic and organic pharmaceutical chemistry. Shaneson C. I. Ltd., Ibadan, 2000:487-512.
8. Harnischfeger G. Development, quality assurance and regulatory aspects of herbal medicinal products. UNIDO-ICS Training course, Panama. 2005.
9. Niggermann B and Gruber C. Side effects complementary and alternative medicine. *Allergy. 2003;***58:** 707-716.
10. Rajendran A, Narayanan V and Gnanavvel I .Photochemical and Electrochemical stabilities of Aloevera sap. *J. App. Sci. Res.* 2007;**3(12);** 1871-1878.
11. SOT.WWW.Solubility of Things.Com.2009.

1/2/2012

Study the Multipath Routing With Self-Healing Technique for Qos in MANET

R. K. Mishra *, Vimal Kumar **

* Dev Bhoomi group of institutions Dehradun
** Research Scholar, Teerthanker Mahaveer University Moradabad.

Abstract: In this paper we describe the multipath routing technique for mobile ad hoc networks. Because we know that Mobile equipments having very powerful and large memory, megabytes of disk space are becoming quite common today. And mobile technology is the best becoming technology for our life and generation. In this Network connectivity options for use with mobile hosts have increased also, including support for growing number of wireless networking product based on radio and infra-red. This type of mobile computing equipments has made the possibilities to share the information between mobile users. Mobile users will meet under circumstances that are not explicitly planned for and in which no connection to a standard network (Internet) is available. The solution to these types of networking problem has come up in the form of mobile ad hoc network. And in this paper we discuss the multipath routing with self healing technique for Qos in mobile ad hoc networks.
[R. K. Mishra, Vimal Kumar. **Study the Multipath Routing With Self-Healing Technique for Qos in MANET.** Academia Arena, 2012;4(2):5-7] (ISSN 1553-992X). http://www.sciencepub.net. 2

Keywords: : multipath routing technique; network;. large memory, mobile

Introduction:

An ad hoc wireless network is a collection of two or more devices equipped with wireless communications and networking capability. Such devices can communicate with another node that is immediately within their radio range or one that is outside their radio range. For the later scenario, and intermediate node is used to rely of forward the packet from the source towards the destination. An ad hoc wireless network is self-organizing and adaptive. This means that a formed network can be de-formed on –the –fly without the need of any system administration. The term "ad hoc" tends to imply "can take different forms" and "can be mobile, standalone or networked". Ad hoc nodes or devices should be able to detect the presence of other such devices and to perform the necessary handshaking to allow the sharing of information and services. [3]

A mobile ad hoc network is self-created and self-organized by a set of mobile nodes called hosts. The nodes are interconnected by single-hop or multiple hop wireless connection, and each node may serve as a packet level router for others nodes in the same mobile ad hoc network. Ad hoc network is the simplest form of wireless LAN which is a network of a few nodes without any bridging or forwarding capability.[1] All nodes are equal and may join or leave at any time, and have equal right to the medium. In fact, it's very much like an Ethernet, where we may add or remove node at discretion. This is the king of radio network deployed in homes of small offices. [2]

Mobile ad hoc networks consist of wireless hosts that communicate with each other in the absence of a fixed infrastructure. Routes between two hosts in MANET may consist of hops through other hosts in the network. The task of finding and maintaining routes in MANET is nontrivial since host mobility causes frequent unpredictable changes. A number of MANET protocols for achieving efficient routing have been recently proposed. They differ in The approach used for searching a new route and / or modifying a known route, when hosts move. It is assumed that each node is aware of the geographic location of all others nodes in MANET of course, for this to work all nodes must be able to see all the other nodes of the network, to be able to establish communication with them. When a node goes out or range, it just looses connection with the rest of the ad hoc network. The vision of mobile ad hoc networking is to support robust and efficient operation mobile wireless networks by incorporating routing functionality into mobile nodes.

Though mobile ad hoc network are attractive, they are more difficult to implement than fixed networks. Fixed networks take advantage of their static nature in two ways. First, they proactively distribute network topology information among the nodes, and each node pre- computes the routes through that topology using relatively inexpensive algorithms. Second, fixed networks embed routing hints in node addresses because the complete topology of a large network is too unwieldy to process of distribute globally. Neither of these techniques works well for networks with mobile nodes because movement invalidates topology information and permanent node addresses cannot include dynamic location information. [3]

Routing of MANETs:

The knowledge of routing protocols of MANETs is important to understand the security problems in MANETs. The routing protocols used in MANETs are different from routing protocols of traditional wired world. Some of the reasons are listed below: [5]

1. Frequent Route updates.
2. Mobility.
3. Limited transmission range.

The performance criteria of nodes in MANETs are different than that of wired networks. Some of the performance Metrics of MANET routing protocols are listed below: [5]

1. Energy consumption.
2. Route Stability despite mobility.

CHARACTERISTICS OF MOBILE AD HOC NETWORK:

MANET has several salient characteristics that have to be taken into account when considering their design and deployment:

1. **Dynamic Topologies:** nodes are free to move arbitrarily; thus the network topology which is typically multi hop, may change randomly and rapidly at unpredictable times, and may consist of both bidirectional and unidirectional links.
2. **Bandwidth:** constrained variable capacity links: wireless links will continue to have significantly lower capacity than their hardwired counterparts. In addition, the realized throughput of wireless communications , after accounting for the effects of multiple access, fading ,noise and interference conditions , etc, is often much less than a radio's maximum transmission rate. As the mobile network is often simply an extensions of the fixed network infrastructure mobile ad hoc users will demand the similar services. These demands will continue to increase as multimedia computing and collaborative network applications rise.
3. **Energy-Constrained Operations:** some or all of the nodes in a MANET may rely on batteries or other exhaustible means of their energy for these nodes, the most important system design criteria for optimization may be energy conservation.
4. **Limited Physical Security:** mobile wireless networks are generally more prone to physical security threats than are fixed-cable nets. The increased possibility of eavesdropping, spoofing, and denial of services attacks should be carefully considered . existing link security techniques are often applied with wireless network to reduce the security threats. As a benefit, the decentralized nature of network control in MANETs provide additional the single points of failure of more centralized approaches.

It is obvious that the routing function is the at most importance for the viability of an ad hoc network. It is also a big challenge since all the characteristics of the mobility and wireless channel previously mentioned, must be , taken into account when designing such protocols.

MULTIPATH ROUTING in MANETs:

To improve the reliability of the mobile ad hoc network for the support of QoS demanding applications, we propose a multipath routing algorithm. [3]

The following assumptions are made for the proper working of our protocol.

- Mobile ad hoc networks considered are of small to medium size networks
- All links are bi-directional.
- Mobile nodes in ad-hoc networks cannot move too fast to render QoS routing impossible and thus the topology of the network will not change significantly while a packet is being transmitted.
- The transmission channel is treated as a pure erasure channel.

Mobile and Wireless Applications are used in these fields:

The following are the application area:

1. Military
2. Radar Technology
3. Aircrafts
4. Internet
5. Banking area
6. Health
7. Transportation
8. Education
9. Entertainment
10. Commercial

Advantages and Disadvantages:

Mobile and wireless networks are increasingly utilized at the edge of the Internet and in localized LANs in place of wired connectivity. These wireless nets, normally built with commercially available wireless routers and network cards based on the Institute of Electrical and Electronics Engineers (IEEE) 802.11 series of standards collectively known as Wi-Fi (wireless fidelity), allow greater flexibility in deploying new nodes or redeploying existing ones without having to acquire or adjust a large wired infrastructure. However, the cost benefits and ease of use associated with wireless networks come at the price of limited bandwidth, limited range and connectivity difficulties due to environmental factors, and security concerns. [4]

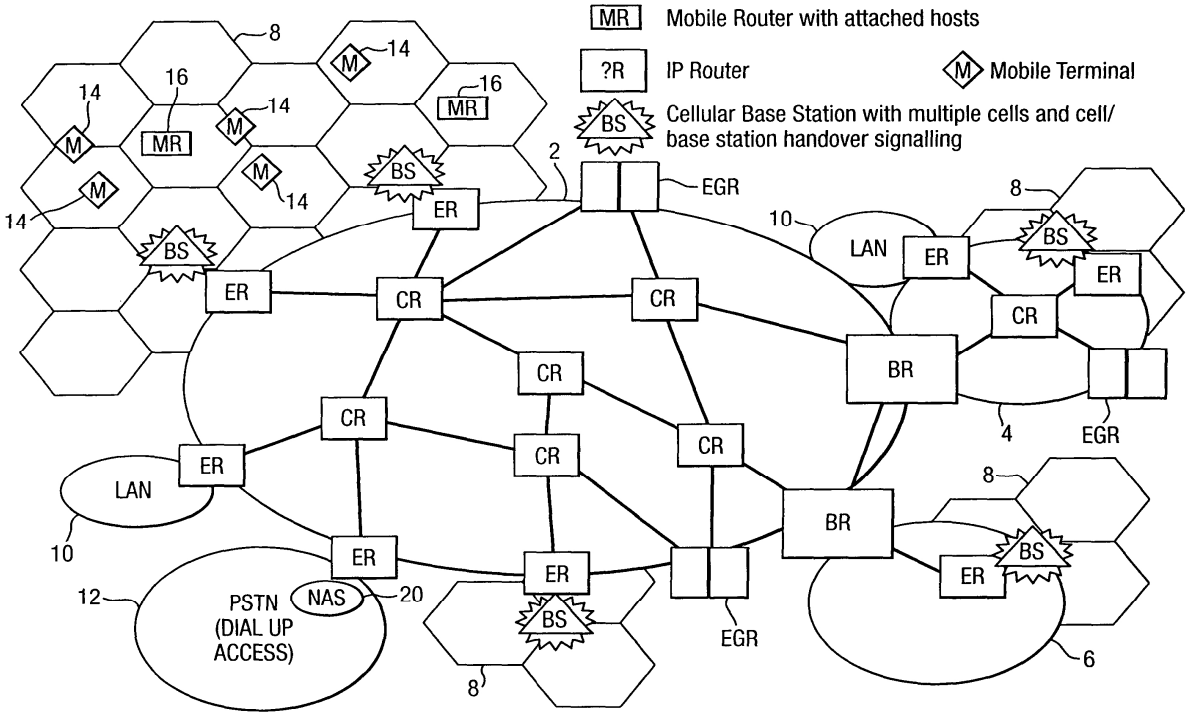

Figure (a)

CONCLUSION

In this paper we present work evaluates the effect of multipath routing in network size and degree for total hop counts, total successful hop counts, delivery rate and MFR routing algorithm in mobile AD Hoc Network. In this we can simulate the routing algorithm result for the success rate greatly depends on network degree. We can change the more than on path and transfer the rate ratio and convert the data ratio density in the present data networks.

References:-

1. Royer EM & Chai-Keong Toh, A review of current routing protocols for Ad-Hoc Networkd, IEEE Personal Commn, Vol 6, no.2, pp 46-55, Apr'1999
2. Shigang Chen & Klara Nahrstedt, Distributed Quality-OfService Routing in Ad-Hoc Networks, IEEE Journal on Selected Areas in Communication, Vol-17, no.8, pp 1488-1504. Aug'1999
3. http://www.bvicam.ac.in/news/INDIACom%202009%20Proceedings/pdfs/papers/252.pdf
4. http://www.au.af.mil/au/awc/awcgate/cst/bh_peacock.pdf
5. http://www.it.iitb.ac.in/~abhiseth/seminar.pdf
6. Figure (a): Google images. www.google.co.in/images/

Investigation of The Laser Nano -Indentation Effects During Irradiation of AISI304 Stainless Steel

Hebatalrahman A[(1)] , Rossetto Gilberto[(2)] and Carta Giovanni[(2)]

Consultant in materials sciences & materials applications, Egypt[(1)]
CNR-Institute of Inorganic chemistry and of Surfaces (ICIS),C.so Stati Uniti,4 35127 Padova Italy [(2)].
Hebatalrahman11@yahoo.com, hebatalrahman@naseej.com

Abstract: In this work, the surface of Austenitic Stainless steel AISI 304 was irradiated by Excimer laser 308nm at constant power 6mJ and repetition rate 200Hz. The selected alloy was irradiated at different number of pulses ranges from 2000 to 50000 Pulses. A significant change in the mechanical properties of AISI 304 is observed based on the microstructure changes. Laser surface irradiation process is a very complicated process and is found to be affected by the microstructure and chemical composition of the alloy. The mechanical properties such as Hardness and reduced modulus of the austenitic stainless steel 304 were improved. Hardness and modulus were decreased with both depth and load. The maximum improvement in nano-hardness and reduced modulus has been investigated in the surface of the sample and rapid decrease in the mechanical properties has been recorded along the depth. Both of quantitative and qualitative techniques were the main tools in results analyses.
[Hebatalrahman A , Rossetto Gilberto and Carta Giovanni. **Investigation of The Laser Nano -Indentation Effects During Irradiation of AISI304 Stainless Steel.** Academia Arena, 2012;4(2):8-15] (ISSN 1553-992X). http://www.sciencepub.net. 3

Keywords: Excimer Lasers, nano-measurements, Quantitative analysis, microstructure

1. Introduction

Stainless steel as alternative to Conventional types of alloys in building applications. In the recent years a need has been developed in several countries for a more comprehensive design specification for cold-formed and hot-rolled stainless steel structural members. Because of the limited life of carbon steel in building and structures that are exposed to moderately to highly aggressive atmospheres, stainless steels, in spite of their higher cost, can be an alternative to carbon steels [(1) ,(3)] . The excellent performance of the austenitic stainless steels in fire conditions and during seismic events is a good reason to introduce stainless steels as structural elements in construction. Attention being paid to crash-worthiness, energy absorption is a key property of the material used for structural parts. Stainless steels and among them austenitic stainless steels have the advantage over aluminum alloys and carbon steels of being highly strain rate sensitive. This means that the faster the loading is applied, the more the material resists deformation [(5),(4)]. This is a particularly good feature for crash worthiness as in all earthquakes the loadings are applied very rapidly. Due to the good energy absorption properties of stainless steel a number of alternative ideas are being continuously developed throughout the building materials [(6),(7)].

2. Experimental Work

The alloys used through this work was supplied by Sandvik Co, France in the form of sheets of stainless steel AISI 304 commercial grade. Table (1) show the chemical composition of the alloy used in the current work. The samples were irradiated by laser table (2) show the laser irradiation conditions of the samples.

Table(1) Chemical composition of Austenitic stainless steel 304

Material	C%	Si%	Mn%	P%	S%	Cr%	Mo%	Ni%
Stainless steel 304 Austenitic	≤0.07	1.0 max	2.0 max	0.045 max	0.03 max	16.5: 18.5	2.5: 3	11.0 14.0

Table (2) Laser Irradiation Conditions

Type	Wavelength nm	No of pulses	Energy per pulse mJ	Repetition rate (Hz)
Excimer	UV 308.6	0,2000,5000,10250, 15000,50000	6	200
duration time=6nano second & total energy =energy per pulse*number of pulses				

Nano- measurements (Indentation data analysis)

Nanoindentation was used to determine film hardness and elastic modulus using a Nanotest 600 instrument from Micro materials Ltd with a Berkovich (three-sided pyramidal) diamond indenter. The peak loads in the rage 1 – 140 mN were used, with loading rate = unloading rate that were varied in proportion to the peak loads starting at a value of 0.05 mN/s for the 1 indentations, while common experimental conditions as initial (contact) load 0.05 mN and holding period at peak load 10 s were used for all the measurements. The indentations were repeated at least five times at each load on different regions of the sample surface apart 100 μm. The hardness and reduced modulus have been determined from these indentation curves using a method originally proposed by Oliver and Pharr, [W. C. Oliver, G. M. Pharr, J. Mater. Res. 7 (1992) p. 1564], which fits a power-law function to the unloading curve. All nano- measurements has been done, the Young's modulus of the samples can be calculated from the reduced modulus via the equation which includes the effects of non-rigid indenters on the load-displacement behavior:

$$1/Er = (1-\nu s^2)/Es + (1-\nu i^2)/Ei \quad (1)$$

where Es and νs are, respectively, the Young's modulus and Poisson's ratio for the specimen, Ei (1141 Gpa) and νi (0.07) the corresponding indenter quantities and Er the reduced modulus, Which has been obtained by the initial slope of the unloading curve[8],[9].

Metallographic Examinations

The specimens were prepared for examination first by grinding on different grades of silicon carbide "SiC" papers coarse grinding followed by fine grinding, finally polishing was conducted with Alumina powder (3μm) size. The details of the microstructure were revealed after etching by standard etching solution of the alloy selected. All specimens had to be etched and polished several times to obtain best results and to produce a uniform level of sample examination[10],[11]. The surfaces of the samples before and after laser irradiation were examined using an Olympus optical microscope Model BHM at selected magnification.

Quantitative Metallography Measurements

A quantitative analysis of the microstructures was produced carried out over 4 fields across the surface to indicate:

1. Average grain size number by linear intercept technique.
2. Average grain diameters D_A using number of modules per unit area
3. Average intercept distance μm
4. Area of average grain section mm^2 x 10^6
5. Average number of grains per mm^3 x10^6
6. Nominal grains per mm^2
7. Nominal grains per mm^2 at 100x

calculations were carried out in several areas in each specimen investigated at 100X projected on a screen measuring 500 mm^2. The measurement is average of over five readings at least for each condition. The scattering value for each specimen was ±1%. All calculations were measured around a circle to consider all directions 360^o

3. Results and discussions

Nano-measurements of stainless steel 304 irradiation by Excimer Laser at 308nm

The nano-indentation measurements were performed on the surface of the stainless steel 304 before laser irradiation in order to determine its hardness and elastic properties. Figures (1) shows the variation of hardness with maximum load for the austenitic stainless steel 304 irradiated by Excimer laser 308nm at 200Hz, 2.2mJ, at different number of pulses. The hardness decreased as the load increased, maximum hardness is at the surface, the higher number of pulses, the higher the hardness at maximum load of 20mN. Figure (2) shows the variation of hardness with Maximum depth for the austenitic stainless steel 304 irradiated by Excimer laser 308nm at 200Hz, 2.2mJ at different number of pulses. The higher number of pulses the higher the hardness at an indentation depth of about 350nm. Figure (3) shows the variation of reduced modulus with load for the austenitic stainless steel 304 irradiated by Excimer laser 308nm, 200Hz, 2.2mJ, at different number of pulses. The change in reduced modulus is less pronounced than variation in hardness at the same range of number of pulses. The gradual decrease in modulus is at maximum load 10mN. Figure (4) shows the variation of reduced modulus with maximum depth for the austenitic stainless steel 304 irradiated at the same conditions. The variation of reduced modulus is significant only at an indentation depth of 400nm. The variation in hardness and reduced modulus with maximum loads and depth respectively, covering the loading range 1 – 200 mN. The sample shows a decrease in the hardness and in the reduced modulus as the indentation load increases; probably the higher hardness near to the surface represents a change in the mechanical properties of the near surface region due to previous spontaneous oxidation of the sample or work hardening due to polishing. Samples with similar preparation conditions have been irradiated by Excimer laser 308nm, 200Hz and 6mJ at 2000, 5000 and 50000 pulses respectively. The hardness value decreased on the surface due to stress relief, which occurs due to laser irradiation. Laser

irradiation effect has been limited to the surface of the sample. This was followed by the value dropped within the range of 0 to 500 nm to the hardness value of the base metal. 2 Gpa. Laser effect was not enough to produce any significant effect on yielding of the material so the reduced modulus almost unchanged with both depth and load.

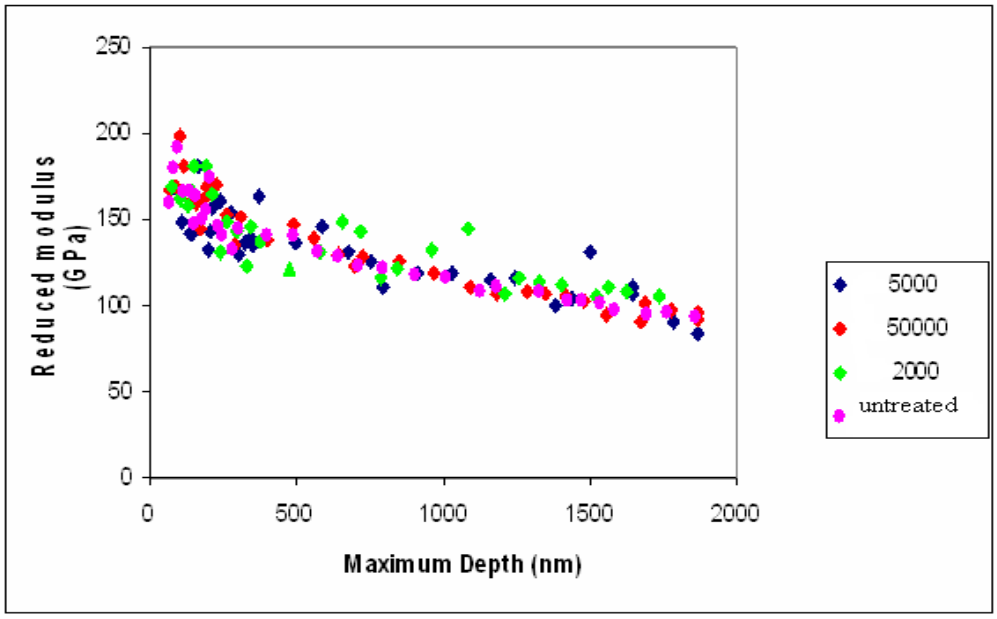

Fig (1) The variation of hardness with maximum load for the austenitic stainless steel 304 irradiated by Excimer laser 308nm, 200Hz, 2.2mJ, at different number of pulses.

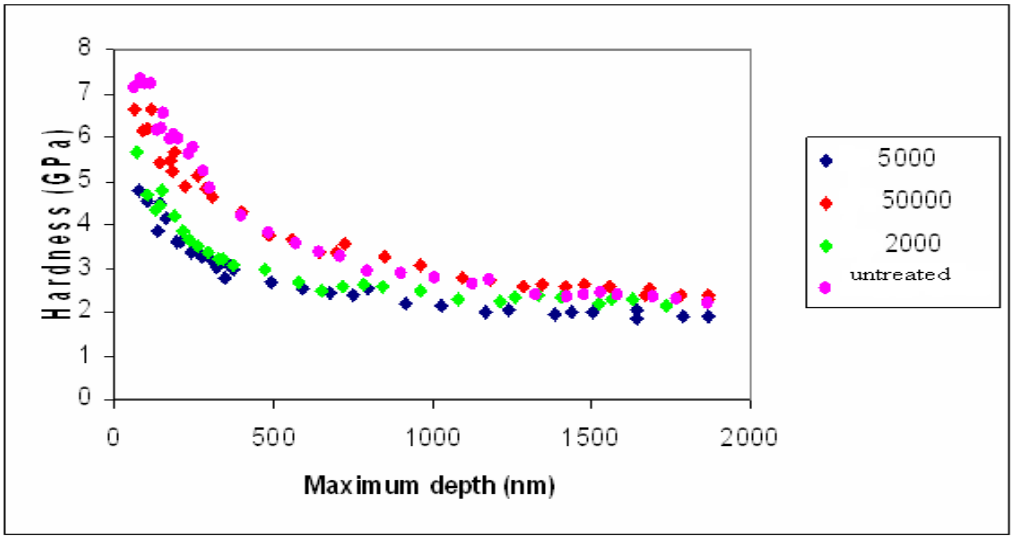

Fig (2) The variation of hardness with Maximum depth for the austenitic stainless steel 304 irradiated by Excimer laser 308nm,200Hz, 2.2mJ, at different number of pulses

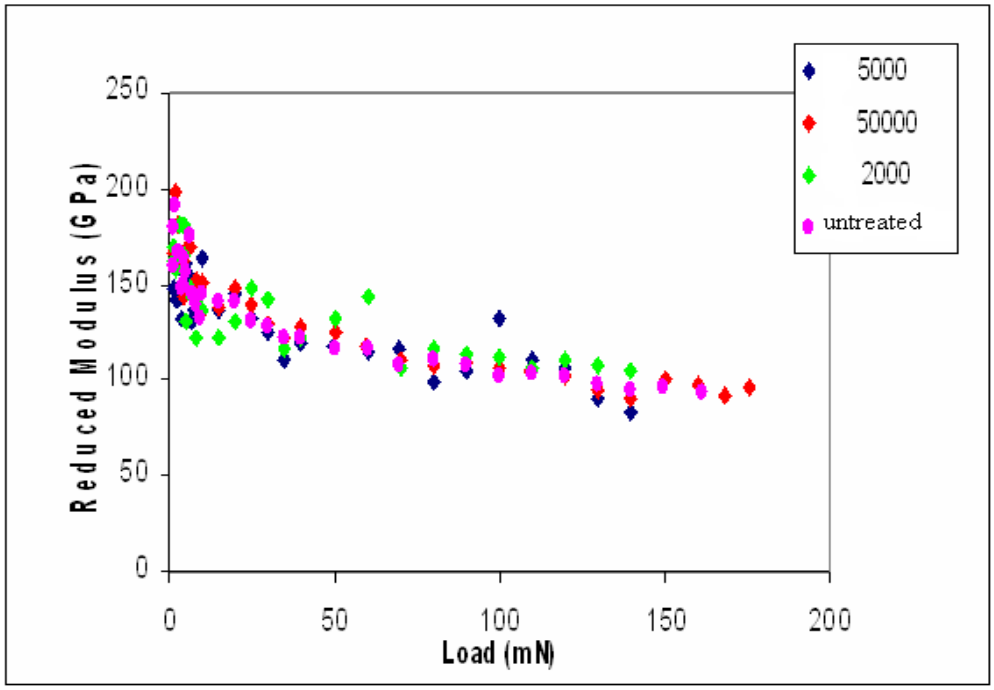

Fig (3) The variation of reduced modulus with load for the austenitic stainless steel304 irradiated by Excimer laser 308nm, 200Hz, 2.2mJ, at different number of pulses.

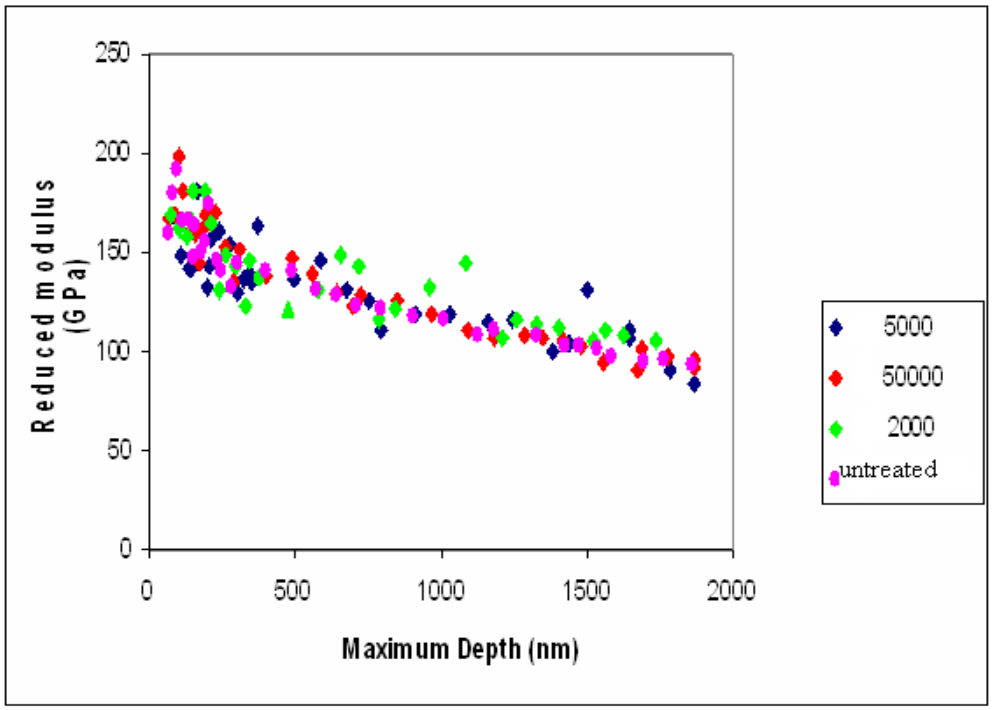

Fig (4) The variation of reduced modulus with maximum depth for the austenitic stainless steel 304 irradiated by Excimer laser 308nm,200Hz, 2.2mJ, at different number of pulses.

Quantitative analysis of stainless steel 304

The variation in mechanical properties such as hardness and modulus was related to the variation in microstructure changes as a function of laser irradiation conditions. Table (4) shows the variation of Grain size, average diameter of the grain, average intercept distance and average number of grains per unit area and unit volume. Quantitative analysis gives us the size, distribution and shape of the microstructure. Fig (5) and Fig (6) show the variation in grain size number and average diameter of the grain with number of pulses respectively. By comparing these figures with hardness-number of pulses curve and Modulus-number of pulses curve the following features appeared:-

* There was good agreement between variations that occurred in the microstructure and the variation in mechanical properties
* Microstructure changed due to laser irradiation.
* All transformations in our study range in solid state

Pulse laser treatment in normal atmosphere is an attractive technique that differs from usual coating methods. A new very thin layer with different microstructure and different mechanical characteristics will be formed on the alloy surface. The laser interaction is the basis for an effective treatment. To induce the chemical-physical reaction with the atmospheric environment high power, short pulse lasers are used.

When comparing these techniques with common surface treatment methods, for instance in the laser nitriding process [(1),(2)], the depth of nitriding is about 400nm for the iron and stainless steel after 256 pulses. Many aspects of Excimer laser nitriding in iron and steels like the influence of laser fluence and gas pressure, the phase formation and thermal stability [(4),(3)] and the mass transport mechanism[(5),(6)] make the nitriding process very complicated and less economic.

Other irradiation techniques have many disadvantages over the Gamma radiation doses extended up to more than I Mrad which the samples started to change its color to the brown-black indicated the carbonization or burning [(11),(8)].

Table (4) Quantitative analysis for stainless steel 304 irradiated by Excimer Laser 308nm, 200Hz, 6n

Micro-grain size measurements	Before irradiation	2000 pulse & 5000	15000pulse & 10250	50000 Pulse
ASTM grain size number	8	9	8.3	8
Average diameter of grain µm	22	16	20	22
Average intercept distance µm	20	14.1	17.7	20
Area of average grain section mm^2 x 10^6	504	225	400	504
Average number of grains per mm^3 x10^6	0.0707	0.2	0.1000	0.0707
Nominal grain per mm^2	1980	4440	2500	1980
Nominal grain per mm^2 at 100x	128	256-287	161.3	128

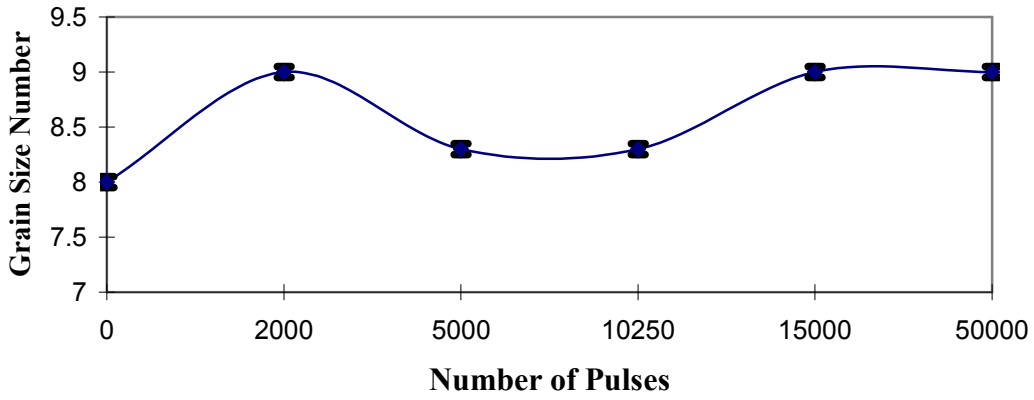

Fig(5)The relation between Number of Pulses and Grain size Number for stainless steel 304 irradiated by 308nm,6mJ,200Hz

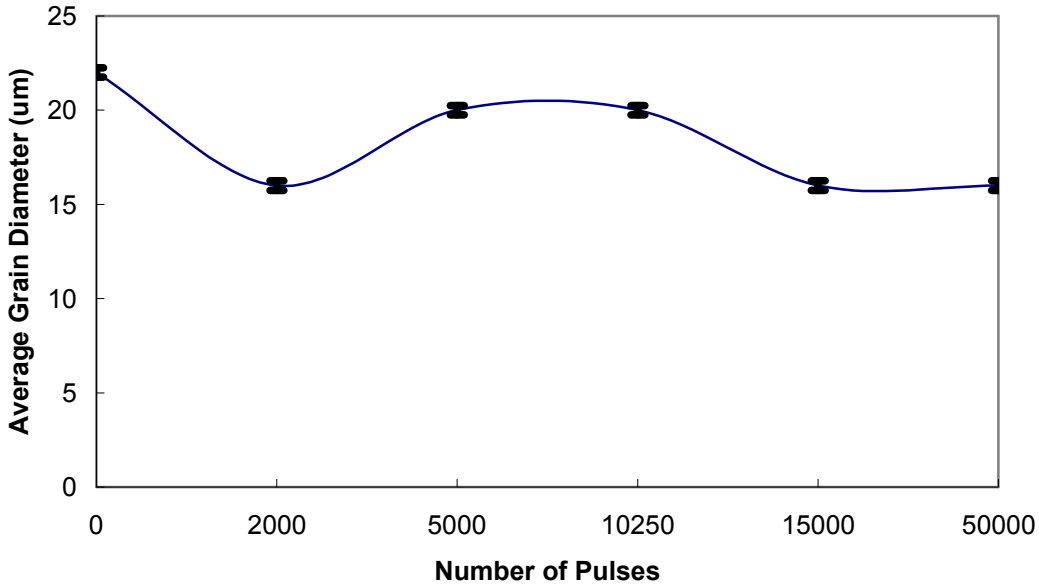

Fig (6)The relation between Number of Pulses and Average Diameter of The Grain(um) for Stainless steel 304 irradiated by 308nm,6mJ,200Hz

The qualitative analysis of stainless steel 304

A wide range of microstructure variations can be obtained as a result of variation in number of laser pulses. Fig (7) shows the variation in microstructure of stainless steel 304 irradiated by Excimer laser 308nm at different number of pulses 2000, 5000, 10250, 15000 and 50000 respectively. The microstructure was compatible with the quantitative analysis mentioned in the above section; laser irradiation leads to change in grain size. At lower number of pulses, grain size number increases and average diameter of the grains decreases (grain refinement). When the number of pulses increased over 10250 pulses, grain growth happened, which is the main reason for the decrease in mechanical properties at higher number of pulses over 10250. Fig (7) shows the variation in microstructure of stainless steel 304 irradiated by Excimer laser 193nm

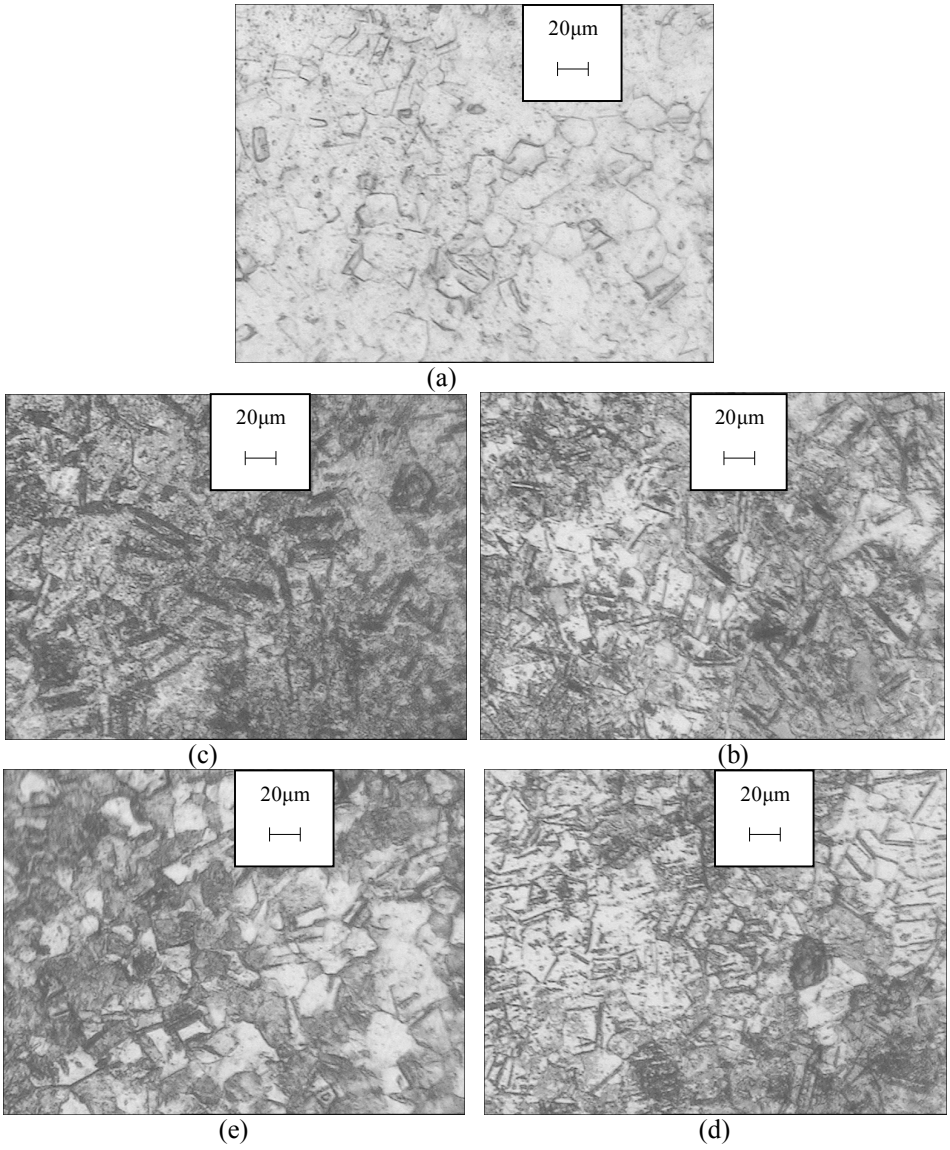

Fig (7) The Effect of Excimer Laser irradiation at 308nm, 6mJ, 200Hz at 300 x Different Number of Pulses on the microstructure of austenitic stainless steel 304. (a) Untreated (b)2000pulses (c)5000pulses (D)15000pulses (e)50000pulses

4. Conclusions

Based on the experimental results observed in this work, the following conclusions may be drawn:

1) The optimized experimental conditions to obtain improvement in the mechanical properties for austenitic stainless steel AISI 304 during laser irradiation in our study range can be summarized as Excimer laser at 308nm, 200Hz, 6mj and 5000pulses.

2) Laser irradiation of austenitic stainless steel is recommended for building elements to improve mechanical properties and enhance surface finish.

3) A significant change in the mechanical properties of the selected alloy is based on the microstructure changes.

4) Laser surface irradiation process is a very complicated process and is found to be affected by the microstructure and chemical composition of the alloys.

5) The mechanical properties such as hardness, modulus of the austenitic stainless steel were improved at the surface of the samples. Hardness and modulus were decreased with both depth and load

References

1. Namba, Y., 1986, ‘‘Laser Forming in Space,’’ *International Conference onLasers*, C. P. Wang et al., eds., STS Press, Las Vegas, NV, pp. 403–407.
2. Scully, K., 1987, ‘‘Laser Line Heating,’’ J. Ship Prod., 3, pp. 237–246.
3. Arnet, H., and Vollertsen, F., 1995, ‘‘Extending Laser Bending for the Generation of Convex Shapes,’’ Proc. Inst. Mech. Eng., 209, pp. 433–442.
4. Vollertsen, F., 1994, ‘‘Mechanisms and Models for Laser Forming,’’ *LaserAssisted Net Shape Engineering, Proc. of the LANE*, M. Geiger et al., eds.,Meisenbach, Bamburg, Germany, 1, pp. 345–360.
5. Geiger, M., and Vollertsen, F., 1993, ‘‘The Mechanisms of Laser Forming,’ ’Annals of the CIRP, 42, pp. 301–304.
6. Chen, G., Xu, X., Poon, C. C., and Tam, A. C., 1998, ‘‘Laser-Assisted Microscale Deformation of Stainless Steels and Ceramics,’’ Opt. Eng., 37, pp. 2837–2842.
7. Chen, G., Xu, X., Poon, C. C., and Tam, A. C., 1999, ‘‘Experimental and Numerical Studies on Microscale Bending of Stainless Steel With Pulsed Laser,’’ASME J. Appl. Mech., 66, pp. 772–779.
8. Zhang, X., and Xu, X., 2001, ‘‘Fundamental and Applications of High Precision Laser Micro-Bending,’’ IMECE, ASME, New York.
9. Feng, Z., Zacharia, T., and David, S. A., 1997, ‘‘Thermal Stress Development in a Nickel Based Superalloy During Weldability Test,’’ Weld. Res. Suppl., Nov., pp. 470–483.
10. Lewis, R. W., and Ravindran, K., 1999, ‘‘Finite Element Simulation of Metal Casting,’’ Int. J. Numer. Methods Eng., 47, pp. 29–59.
11. Taljat, B., Zacharia, T., and Wang, X., etc., 1998, ‘‘Numerical Analysis of Residual Stress Distribution in Tubes With Spiral Weld Cladding,’’Weld. Res. Suppl., Aug., pp. 328–335.
12. Taljat, B., Radhakrishman, B., and Zacharia, T., 1998, ‘‘Numerical Analysis of GTA Welding Process With Emphasis on Post-Solidification Phase Transformation Effects on Residual Stresses,’’ Mater. Sci. Eng., A, 246, pp. 45–54.
13. Maykuth, D. J., 1980, *Structural Alloys Handbook*, Metals and ceramics information center, Battelee Columbus Laboratories, Columbus, OH, 2, pp. 1–61.
14. Takeuti, Y., and Komori, S., 1979, ‘‘Thermal-Stress Problems in Industry 3: Temperature Dependency of Elastic Moduli for Several Metals at Temperatures From 2196 to 1000°C,’’ J. Therm. Stresses, 2, pp. 233–250.

12/12/2011

The Effect of Laser Parameters on The Surface Characteristic of Irradiated Stainless Steel 304

Hebatalrahman, A*

Consultant in materials sciences & materials applications, Egypt
hebatalrahman11@yahoo.com; hebatalrahman@naseej.com

Abstract: In these work, the effect of laser parameters such as wavelengths, number of pulses and energy per pulse were studied. The effect of number of pulses were studied in the range from 0 to 15000 at constant wavelength, the effect of energy per pulse was investigated at 3.5mJ and 6mJ. The commercial grade of polished stainless steel AISI 304 was considered as the base material in current study. Ultra violet excimer lasers at 193nm and 308nm were studied, Infra red lasers 1064nm was also tested. The superficial hardness and modulus were evaluated at different lasers parameters selected in these work to determine the optimum conditions. The total absorbed energy was calculated at all test conditions and compared with measured values. The optimum conditions to improve the mechanical properties at minimum energy were mentioned.
[Hebatalrahman,A**. The Effect of Laser Parameters on The Surface Characteristic of Irradiated Stainless Steel 304.** Academia Arena, 2012;4(2):16-25] (ISSN 1553-992X). http://www.sciencepub.net.4

Keywords: Surface treatment, stainless steel alloys, Laser applications, mechanical properties

1. Introduction

The use of stainless steel in building applications is not a new idea; the use of what we now know as austenitic steel can be traced back to at least the 1930'. Stainless steel is about 70% iron [(1),(2)]. It is special because of the presence of chromium element in the alloy. This element plays a key role in the corrosion resistance of stainless steel, but getting it into the steel is the tricky part [(3),(4)]. This means that the chromium atoms are an integral part of the structure of the steel [(5),(6)]. We describe the structure as a 'substitutional solid solution' - the chromium atoms simply substitute for iron atoms in the crystal structure. (This is opposed to the impurities in stainless steel - carbon and nitrogen - which are in 'interstitial solution' - where they fit in between the iron atoms). How much chromium is the next important Over the years, materials engineers have determined that at least 12% (by weight) of chromium is necessary to make stainless steel. This created some new problems; however, this composition had low ductility (the ability of a metal to be permanently stretched by plastic deformation) and toughness (resistance of the material to growth of a crack). These qualities were the result of the crystal structure of the material. Most iron-chromium alloys, like iron, are body-centered-cubic configuration. This crystal orientation prevented good forming and flexibility [(7),(8)].

The most common stainless steel is "AISI304" austenitic stainless steel. The "18-8" means that it contains 18% by weight chromium and 8% by weight nickel. This composition has the face-centered cubic crystal structure (FCC). It is almost always ductile, readily drawn into wire [(9):(15)].

Stainless steel is increasingly being sought out for structural applications. Engineers and architects are particularly drawn to the competitive life-cycle cost, potentially high strength, high corrosion resistance and aesthetically pleasing finishes of the material. Evidence of growing industry demands are seen daily in applications like plane and three-dimensional trusses, mullions in facade structures, canopies, roof sheeting, silos, portal framed overhead wiring structures (for railway services), and general construction in chemical, marine and other corrosive environments[(16),(17)].

The materials were chosen primarily for the resistance to corrosion that they could provide in what was considered to be a harsh service environment. There are many other examples of the use of stainless steels in the construction industry, on both a small and large scale. However, most of the common examples of the use of stainless steel as a primary structural engineering material have been in buildings or as critical components in structures as opposed to the widespread use as structural engineering materials in their own right [(18)].

Many designers and client bodies are more open to the use of stainless steel. The drivers for this apparent change in attitude do not appear to be clearly defined but include:

• An increased awareness of the future burden of using materials that is not inherently durable in the service environment [(19)].

• An increase in desire to reduce or eliminate the need for maintenance (both planned and unplanned) that can arise with accepted structural materials.

• In some applications it is now perceived as politically undesirable to produce structures that are not inherently durable.

These factors do not necessarily provide an "open door" for the use of stainless steel as a structural material as there will be competition from other materials; however; this change in attitude does provide a climate in which stainless steels may be considered more favorably than in the past[13],[15]. The problem of durability with conventional construction materials in relation to bridges but could be applied equally to other building, architecture and structures and the possible scope for increasing replacement of these materials with various types of stainless steel[20],[21].

2. Experimental work

Laser Surface Irradiation

The irradiation is done on one side of the sample and covers all the surface area of the sample. The main goal of this work is optimize condition for laser irradiation of the samples by Excimer laser at 193nm and 308nm Table (1) shows data for used rare gas halide Excimer laser.

Table (1) Data for Excimer Laser (rare gas halide)

Gas type	λ (nm)	r(A)	ω (Cm^{-1})	σ (Cm^2)	τ (ns)
ArF	193	2.2	-	12	4.2
XeCl	308	2.9	194	50	11

λ = transition wavelength
r(A) = equilibrium inter-nuclear separation
ω = fundamental vibration frequency of the excited state
σ = stimulated emission cross section
τ = radiative life time (pulse duration)

The number of pulses and the effect of energy per pulse on the hardness were recorded to indicate the energy required (fluence) to improve the mechanical properties. Beam in the shape of a rectangle with width (w=4mm) and length (l=10mm) was used in the laser process the power density ranges from (0.75 W/Cm^2 to 0.1 W/Cm^2) without any focusing. The laser irradiation condition is listed in Table (2)

Table (2) Laser Irradiation Conditions

Type	Wavelength nm	No of pulses	Energy per pulse mJ	Repetition rate (Hz)
Excimer	UV 308.6	0,2000,5000,10250, 15000,50000	6	200
Excimer	UV 193	0,2000,5000,10250, 15000,50000	6	200
Nd-YAG	IR 1064	5000	1.9:2.2	10
duration time=6nano second & total energy =energy per pulse*number of pulses				

Superficial Hardness

The hardness of the specimens were measured by using Superficial Rockwell hardness tester with ball diameter 1/16" at load 30Kg. Each hardness value is at least an average of 5 readings and they are good to ± 4%.

Elastic modulus

To obtain the elastic modulus, the unloading portion of the depth-load curve is analyzed according to a relation, which depends on the contact area:

$$C = v^{0.5}/(2E_rA^{0.5}) \quad (1)$$

where C is the contact compliance and E_r is the reduced modulus defined by

$$1/E_r = (1-v_s^2)/E_s + (1-v_i^2)/E_i \quad (2)$$

where v_s the Poisson's ratio for the sample, v_i, the Poisson's ratio for the indenter (0.07), E_s the Young's modulus for the sample and E_i, the Young's modulus for the indenter (1141 GPa).

3. Results and discussions

The effect of both number of pulses and energy have been investigated in order to select the best

irradiation conditions and the alloy potential for producing improvement in mechanical properties

Effect of Number of Pulses

Table (3) shows the effect of the number of pulses on the superficial hardness at constant wavelength of 193nm Excimer laser and constant energy ratings 6mJ/pulse for austenitic stainless steel 304.

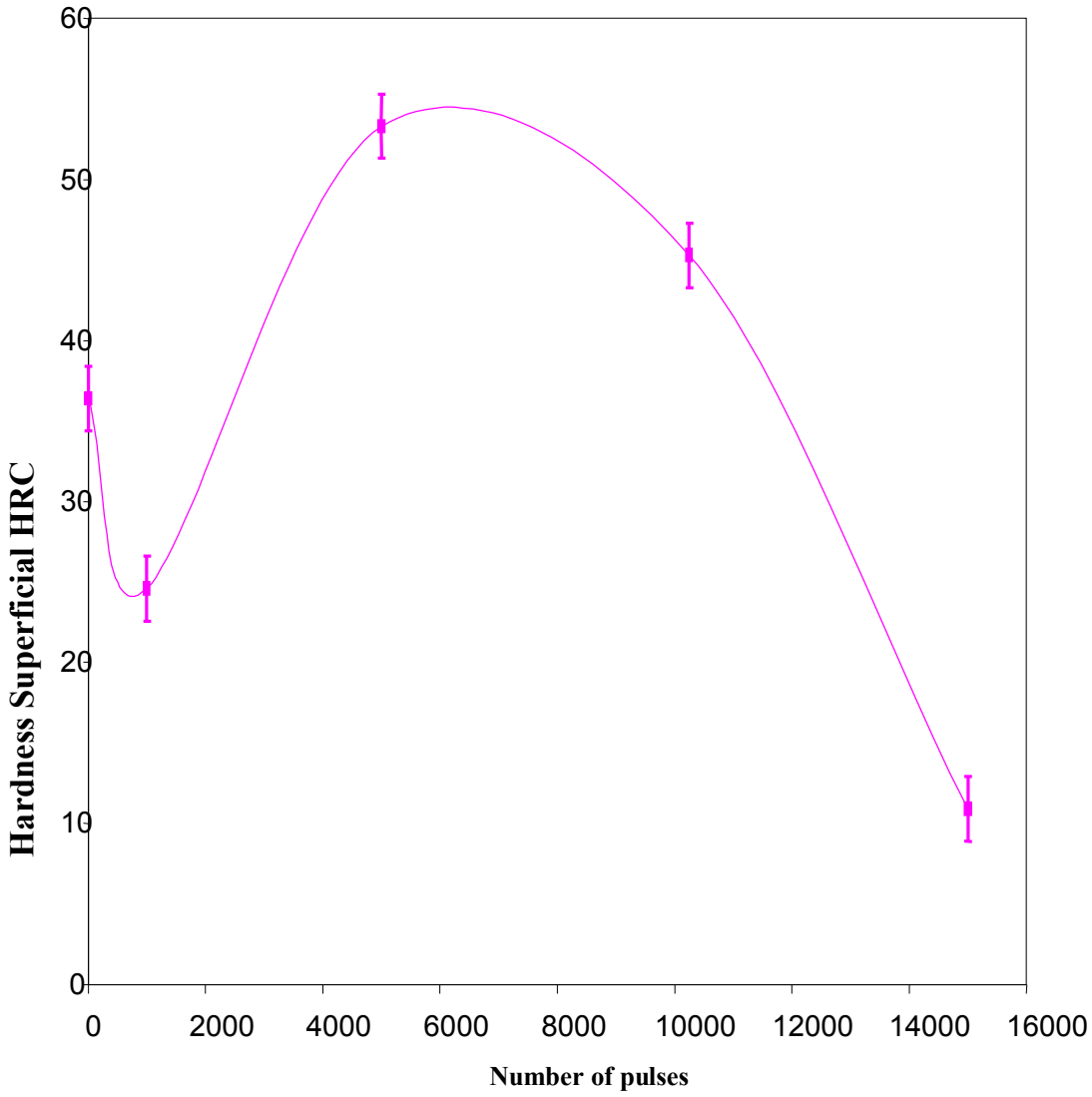

Fig(1) The Variation of Superficial Hardness HRC with Number of Pulses for Stainless Steel 304 Irradiated by Excimer Lasers at,193nm,3.5mJ,200Hz.

Table (3) the superficial hardness as a function of the number of pulses for austenitic stainless steel 304

Number of pulses	0	1000	5000	10250	15000
Hardness	36.4	24.6	53.3	45.3	10.9

As shown in Figure (1) the hardness decreases gradually with the increasing number of laser pulses, after about 1000 pulses the hardness was increased gradually with the increase in number of pulses. Significant improvement in hardness was recorded around 5000 pulses. Rapid decrease in hardness was recorded at 10250 pulses, which continued with increasing in the number of pulses.

Effect of Laser energy

In order to study the effect of laser energy, different energy values were investigated (3.5mJ/pulse & 6mJ/pulse) at constant wavelength of 193nm and constant number of pulses of 5000pulses. Table (4) shows the superficial hardness of the austenitic stainless steel 304 at different power rating.

Figure (2) shows the significant improvement in the hardness at 3.5mJ/pulse. At 6mJ/pulse, the hardness was decreased and became less than that of the base metal before laser irradiation. Accordingly, a power value of 3.5mJ/pulse was selected for the work conducted throughout the research.

Table (4) Effect of Power changes on superficial hardness for stainless steel 304 at constant number of pulses of 5000 and 193nm.

Energy/pulse mJ	0	3.5	6
Hardness	36.4	53.3	13.9

Effect of Laser Wavelength

Nd-YAG is one of the most commonly used laser types in Egypt, stainless steel 304 was irradiated with the fundamental beam 1064nm to show the effect of IR irradiation on the superficial hardness. The number of pulses was 5000 pulse, Table (5) shows the average hardness values of the measured specimens with scattering less than $\pm$ 2%.

Table (5) Effect of laser irradiation by Nd-YAG 1064nm on superficial hardness for stainless steel 304,5000pulse,2mJ/pulse

Conditions	Hardness
Untreated	30
Treated part	45.1

Figure (3) shows superficial hardness of stainless steel 304 before and after laser irradiation with Nd-YAG 1064nm and Excimer laser 193nm & 308nm respectively.

From the above results, Ultraviolet laser irradiation of stainless steel 304 is better. Excimer laser produces improvement in the hardness about 66.5%. The improvement in hardness was higher than the improvement with IR laser (50%) for the same number of pulses 5000 and same energy 6mJ/pulse. The phenomena occur because the energy of the Excimer laser is higher than that of the Nd-YAG laser. Excimer laser has low wavelength and higher frequency while Nd-YAG laser has higher wavelength and lower frequency.

From the pilot study mentioned above, the austenitic stainless steel produces promising improvement in hardness when irradiated by UV lasers. The depth of penetration and reduced modulus should be measured for this type of steels to identify the laser irradiation effect on the mechanical properties.

The effect of laser types on the mechanical properties

The variation of hardness at maximum load with number of pulses at 308nm and 193nm Excimer laser irradiation was shown in Fig (4). The hardness value at 2000 is very close to the non irradiated samples. Improvement in the hardness was significant only at pulses between 5000 and 15000. When the number of pulses increased the hardness value decreased due to sample burning. Fig (5) shows the variation of Modulus at maximum load with number of pulses, the value of modulus increased until 2000 pulses, the modulus value almost remained constant between 2000 and 15000 pulses. The decreasing rate in modulus after 15000 pulses was very slow. The effect of the number of laser pulses on the hardness and modulus when stainless steel 304 was irradiated at 193nm. The maximum improvement in hardness was shifted to about 2000 pulse and another peak appears near 15000 pulses. The beam energy at 193nm pulses is larger than the beam energy at 308nm. According to the energy equations and principles[12],[13]. low wavelengths means higher frequency and higher amount of energy absorbed.

Laser irradiation works as method of hardening and softening at the same time. The initial microstructure of the irradiated alloy (the room temperature microstructure) plays the significant role in that case. The decrease in hardness of stainless steel after laser irradiation is due to the formation of higher energy phases but these phases have lower hardness.

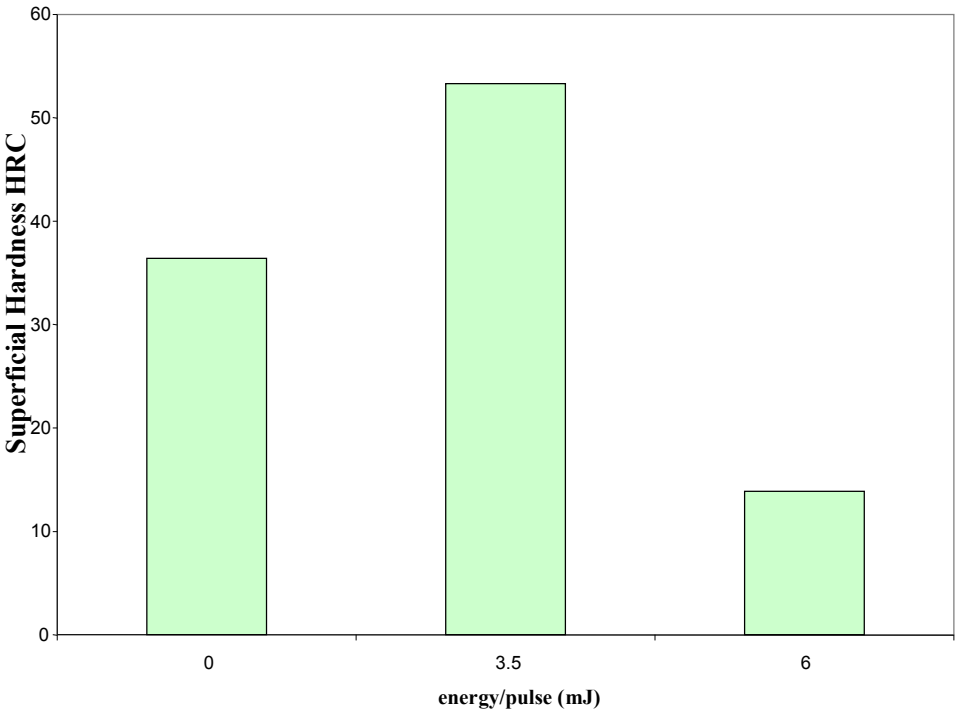

Fig (2) The variation of Superficial Hardness HRC with Power for Austenetic Stainless Steel 304 Alloy Irradiated by Excimer Lasers at , 193nm,5000 Pulses,200Hz

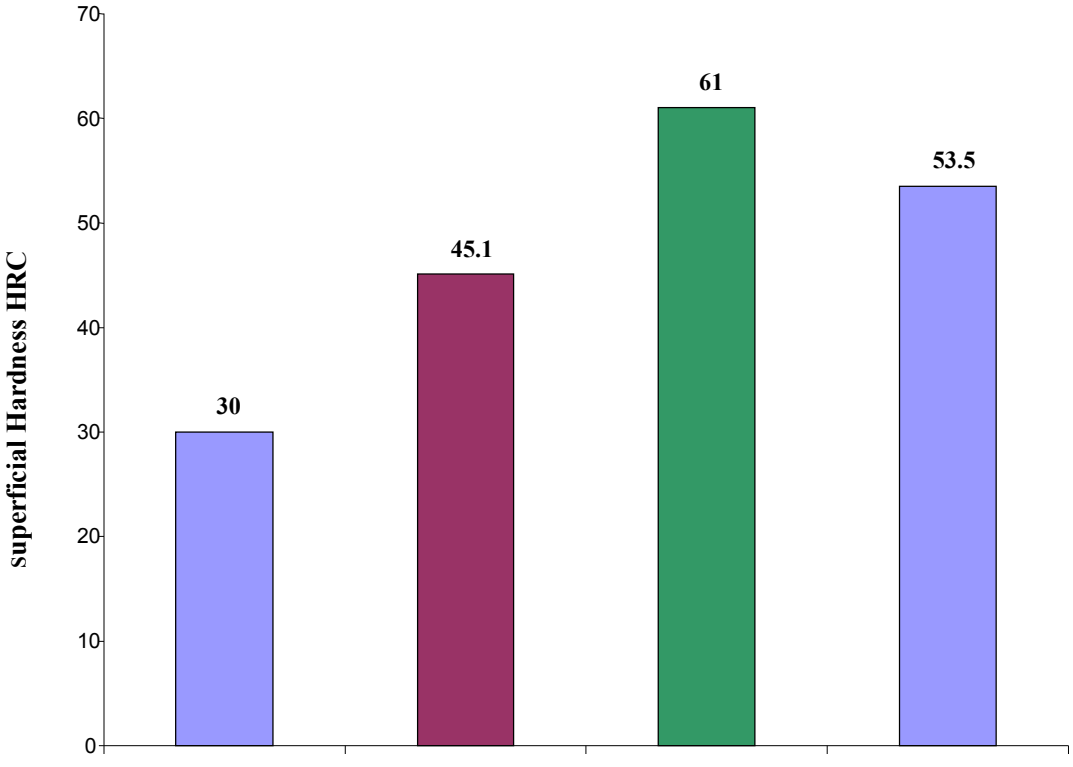

Fig (3)The Effect of Laser Wavelength on The Hardness of Austenetic Stainless Steel 304

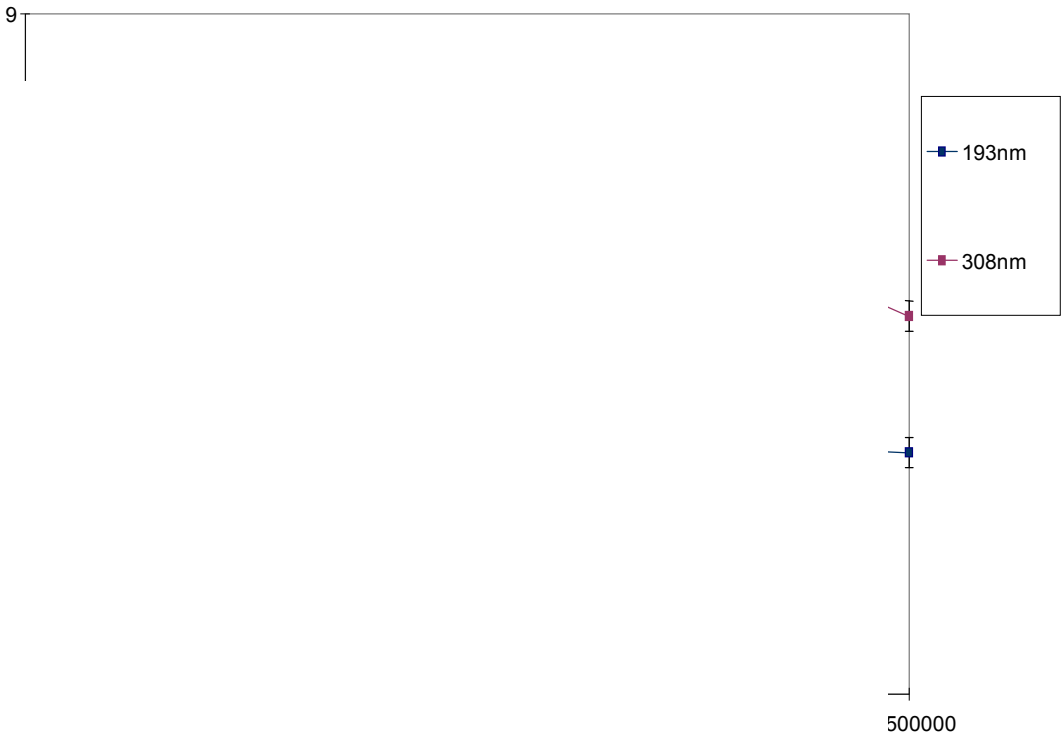

Fig(4)The variation of Hardness at Max Load with Number of Pulses for stainless steel 304 irradiated with Excimer Laser at 200Hz,6mJ

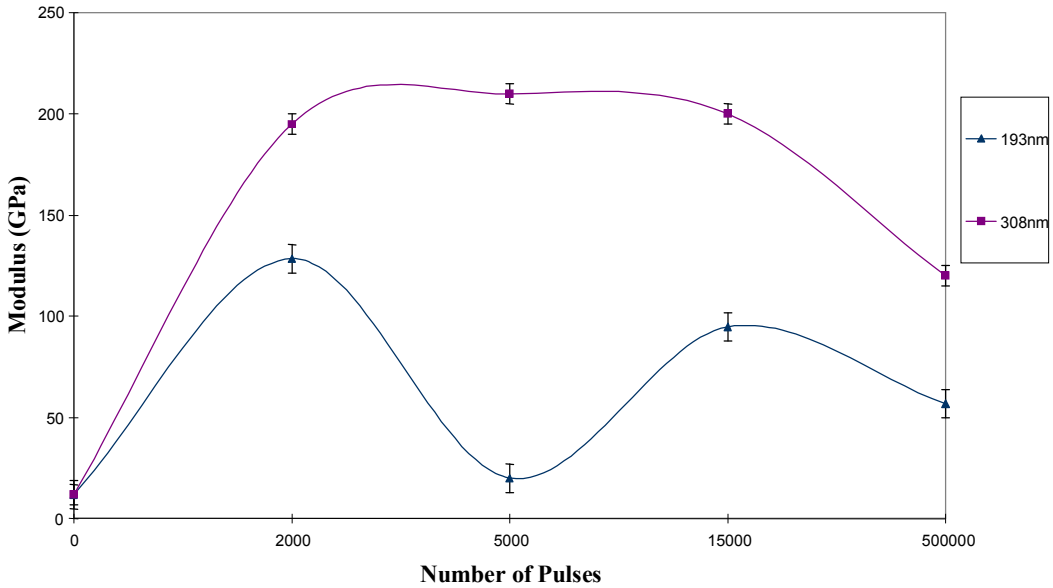

Fig(5) The variation of Modulus at Max Load with Number of Pulses for stainless steel 304 irradiated with Excimer Laser at 200Hz,6mJ

When comparing these figures with the similar graphs at laser wavelength 308nm. The samples show a decrease in the hardness and in the reduced modulus as the indentation load increases; probably the higher hardness near to the surface. The effect of laser irradiation at 193nm was more pronounced than at 308nm. The UV laser has less wavelength and higher frequency so more energy has been resulting from UV light for the same power and number of pulses. High power rating produces higher improvement in the properties at the same laser wavelength and number of pulses.

The effect of laser energy (calculated)

Figure (6) shows the variation of energy absorbed versus the increase in number of pulses at energy per pulse 6mJ and 3.5mJ respectively. When the number of pulses increases, the absorbed energy increases. At 6mJ, the amount of total energy at the same number of pulses was increased. At low value of energy per pulse 3.5mJ, the amount of absorbed energy at the same number of pulses was low. The gap between the two values at 6mJ and 3.5mJ increases linearly with the increase in number of pulses.

* At 5000 pulses total energy at 6mJ equals 2500mJ and total energy at 3.5mJ equals 2000mJ. At 15000 pulses total energy at 6mJ equals 10000mJ and total energy at 3.5mJequals 7000mJ. At 50000 pulses total energy at 6mJ equals 30000mJ and total energy at 3.5mJ equals 15000mJ.

There are many reasons for the disagreement between the current work and some published results [9], [10]. The beam-metal interaction and in the case where the fluence is high enough to rise the surface temperature instantaneous and reflectivity changed. This effect is quite complex, the laser rays dissipated, thus reducing the effective energy really impinging on the target. The thermal effect due to collision between lasers and atoms inside the structure when taken into account in the total energy balance, it tend to reduce the efficiency of heating and melting (i.e. the amount of heat able to form and propagate microstructure changes) ; accordingly, it affects the amount of heat actually absorbed inside the material.

The ultra violet laser is a clean source of high energy density. Surface irradiation processes involve non equilibrium phenomena due to high heating and cooling rates induced by the laser irradiation. The inherent rapid cooling due to high thermal conductivity of steel makes lasers very attractive since the irradiated parts contain various microstructures with metastable and stable phases, fine grain, minimum segregation, and extended solid solutions which improve the mechanical and metallurgical properties of the irradiated parts.

The amount of heat used for irradiation along the depth is considered to be proportional to the input heat flux along the direction of that unit depth. This assumption is based on the fact that in the absence of conduction loss, the amount of irradiated material, that is the amount of heat used for irradiation increases as the input heat flux increases and vice-verse. So the amount of heat used for irradiation can be expressed as a function of temperature and physical parameters such as thermal conductivity, density and specific heat.

The suitability of Laplace transformation analytical model was investigated by comparing simulations to experimental measurements of pulsed laser heating. The data is from laser irradiation of stainless steel 304 designed to evaluate the validity of the classical thermal diffusion model on a microsecond time scale.

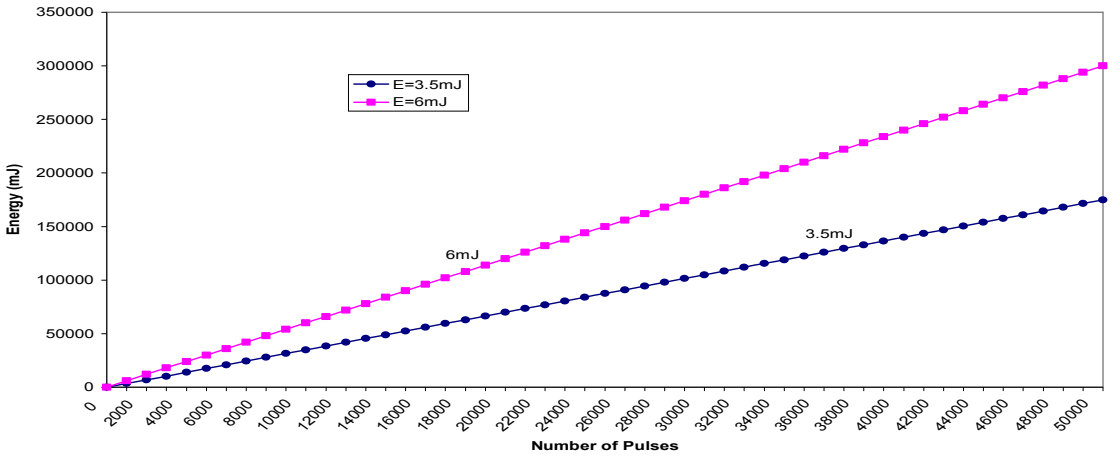

fig(6) The variation of Temperature with Number of Pulses for Steel irradiated by Excimer Laser 308nm, 200Hz at different values of energy per pulse

Conclusions

1. The maximum improvement in superficial hardness were achieved at 5000 pulses.
2. More improvement in mechanical properties were recorded with ultra violet lasers 193nm and 308nm because they are high energy lasers.
3. The increase in the energy per pulse increase the total energy absorbed which have significant influence in the mechanical properties.
4. There are good agreement between the calculated and measured value of the absorbed energy at different number of pulses and different energy per pulse.
5. The total energy calculated is higher than the actual energy used in phase transition due to losses resulting from reflectivity, surface roughness and scattering due to interaction with atoms inside the structure.
6. Higher energy phases were formed when the total energy absorbed increased but sometimes in the case study considered in these work higher energy phases with low hardness values.

References

1. Gang-Chang Ji, Chang-Jiu Li, Yu-Yue Wang and Wen-Ya Li , Microstructural characterization and abrasive wear performance of HVOF sprayed Cr_3C_2–NiCr coating, Surface and Coatings Technology, Volume 200, Issue 24, 1 August 2006, Pages 6749-6757
2. F. Gärtner, T. Stoltenhoff, J. Voyer, H. Kreye, S. Riekehr and M. Koçak, Mechanical properties of cold-sprayed and thermally sprayed copper coatings, Surface and Coatings Technology, Volume 200, Issue 24, 1 August 2006, Pages 6770-6782.
3. C. Batista, A. Portinha, R.M. Ribeiro, V. Teixeira and C.R. Oliveira, Evaluation of laser-glazed plasma-sprayed thermal barrier coatings under high temperature exposure to molten salts, Surface and Coatings Technology, Volume 200, Issue 24, 1 August 2006, Pages 6783-6791
4. Huiling Li, Xiaoyan Zeng and Huifen Li, Study on thick film resistor and electrode fabricated by laser micro-cladding electronic pastes, Surface and Coatings Technology, Volume 200, Issue 24, 1 August 2006, Pages 6832-6839
5. J.L. Endrino, G.S. Fox-Rabinovich and C. Gey , Hard AlTiN, AlCrN PVD coatings for machining of austenitic stainless steel, Surface and Coatings Technology, Volume 200, Issue 24, 1 August 2006, Pages 6840-6845
6. C. Navas, R. Colaço, J. de Damborenea and R. Vilar, Abrasive wear behaviour of laser clad and flame sprayed-melted NiCrBSi coatings, Surface and Coatings Technology, Volume 200, Issue 24, 1 August 2006, Pages 6854-6862
7. Y. Sun, S. Hanaki, M. Yamashita, H. Uchida and H. Tsujii,, Fatigue behavior and fractography of laser-processed hot work tool steel, Vacuum 73 (2004), p. 655.
8. A. Persson, S. Hogmark and J. Bergstrom, Thermal fatigue cracking of surface engineered hot work tool steels, Surf. Coat. Technol. 191 (2005) (2–3), p. 216.
9. G. Hanna, T. Glatzel, S. Sadewasser, N. Ott, H.P. Strunk, U. Rau, J.H. Werner "Texture and electronic activity of grain boundaries in Cu(In, Ga)Se2 thin films"Applied Physics A 82, 1-7, 2006
10. N. Ott, H.P. Strunk, G. Hanna, R. Kniese "Electro-optical properties of the microstructure in chalcopyrite thin films", Springer Series in Materials Science, 179-191, 2006
11. S. Kunsági-Máté, C. Schür, Nikolett Szalay, Tamas Marek, H.P. Strunk Dynamics of As atoms in the reconstruction layer of the As-rich GaAs(001) c(4x4) surface, Lecture Series on Computer and Computational Sciences, 4, 1816-1819, 2005.
12. S. Kunsági-Máté, C. Schür, Eszter Vegh, Tamas Marek, H.P. Strunk A dynamic microscopic model for the formation of excess arsenic in GaAs layers during growth at low temperature, Lecture Series on Computer and Computational Sciences, 4, 1812-1815, 2005
13. T. Marek, C. Schür, S. Kunsági-Máté, Surface orientation as a control parameter for the growth of non-stoichiometric gallium arsenide,Phys. Stat. Sol. (a), 202, 15, 2980-2991, 2005
14. H. Scheel, G. Frank, H.P. Strunk, Electron radiation deamage in Cu(In,Ga)Se2 analysed in-situ by cathodoluminescence in a transmission electron microscope Phys. Stat. Sol. (a), 202, 2336, 2005
15. S. Kunsági-Máté, C. Schür, E. Végh, T. Marek, H.P. Strunk Molecular - dynamics-based model for the formation of arsenic interstitials during low-temperature growth of GaAs, Physical Review B 72, 075315-1 bis 5, 2005
16. L.V. Taveira, G. Frank, H.P. Strunk, L.F.P. Dick, The influence of surface treatments in hot acid solutions on the corrosion resistance and oxide structure of stainless steels Corrosion Science, 47, 757-769, 2005
17. M. Albrecht, L. Lymperakis, J. Neugebauer, J.E. Northrup, L. Kirste, M. Leroux, I. Grzegory, S. Porowski, H.P. Strunk, Chemically ordered AlxGa1-xN alloys: Spontaneous formation of natural quantum wells, Physical Review B 71, 035314-1 bis -5, 2005

18. M. Halbwax, D. Bouchier, V. Yam, D. Déarre, Lam H. Nguyen, Y. Zheng, P. Rosner, M. Benamara, H.P. Strunk, C. Clerc, Kinetics of Ge growth at low temperature on Si(001) by ultrahigh vacuum chemical vapor deposition, Journal of Applied Physics, 97, 064907-1 bis -6,2005
19. G. Alexe, H. Heinke, L. Haase, D. Hommel, J. Schreiber, M. Albrecht, H.P. Strunk Nondestructive evalution of misfit dislocation densities in ZnSe/GaAs heterostructures by x-ray diffuse scattering , Journal of Applied Physics, 97, 103506-1 bis -6, 2005
20. C. Grazzi, A. Castaldini, A. Cavallini, H.P.D. Schenk, P. Gibart, H.P. Strunk GaN epitaxial layers on inhomogeneous buffer layer: electrical and optical properties European physical journal-applied physics, 27, 193-195, 2004
21. L. Lymperakis, J. Neugebauer, M. Albrecht, T. Remmele, H.P. Strunk Strain induced deep electronic states around threading dislocations in GaN Physical Review Letters, 93, 196401, 1-4, 2004
22. N. Ott, M. Nerding, G. Müller, R. Brendel, H.P. Strunk , Evolution of the microstructure during annealing of porous silicon multilayers Journal of Applied Physics, 95, 2, 497-503,2004
23. H. Plagwitz, M. Nerding, N. Ott, H.P. Strunk, R. Brendel, Low-temperature formation of local al contacts to a-Si:H-passivated Si Wafers, Prog. Photovolt: Res. Appl., 12, 47-54, 2004
24. Lam H. Nguyen, V. LeThanh, D. Dèbarre, V. Yam, M. Halbwax, M. El Kurdi, D. Bouchier, P. Rosner, M. Becker, M. Benamara, H.P. Strunk Selective epitaxial growth of Ge quantum dots on patterned SiO_2/Si(001) surface, Applied Surface Science, 224, 134-138, 2004
25. N. Ott, G. Hanna, U. Rau, J.H. Werner, H.P. Strunk Texture of Cu(In, Ga)Se_2 thin films and nanoscale cathodoluminescence, Journal of Physics Condensed Matter, 16, 85-89, 2004
26. T. M. Yue, J. K. Yu and H. C. Man "The effect of excimer laser surface treatment on pitting corrosion resistance of 316LS stainless steel",Surface and Coating Technology, Volume 137, Issue 1, 1 March 2001, Pages 65-71
27. W. A. England, M. J. Bennett, D. A. Greenhalgh, S. N. Jenny, and c. F. KNIGHTS: Corros. Sci., 1986, 26, 537.

12/12/2011

Analytical Solution to Predict Transient Temperature Distributions during Laser Surface Hardening.

Hebatalrahman, A*

Consultant in materials sciences & materials applications, Egypt
hebatalrahman11@yahoo.com; hebatalrahman@naseej.com

Abstract: This paper introduces a new analytical solution to predict transient temperature distributions in a finite thickness plate during laser surface hardening. This analytical solution was obtained by solving a transient one-dimensional heat conduction equation with convection boundary conditions at the surfaces of the work piece. To calculate the temperature field analytically in laser surface hardening processes, laser beam absorptivity was evaluated as one of the most important parameters, the laser and materials parameres were determined. It was extremely difficult to find an accurate value for laser beam absorbtion rate. Therefore, in this paper, absorptivities were determined theoretically under various hardening conditions, including variations in hardened thickness beside variation in surface and subsurface temperature.Owing to the simplicity of the solution method, the analytical model developed may be easily implemented for simulation work for analysis and prediction of laser surface hardening processes under various hardening conditions.
[Hebatalrahman,A. **Analytical Solution to Predict Transient Temperature Distributions during Laser Surface Hardening.** Academia Arena, 2012;4(2):26-36] (ISSN 1553-992X). http://www.sciencepub.net. 5

Keywords: laser hardening, model, temeperature, energy distributiin.

1. Introduction

Heat transfer is energy in transit, which occurs as a result of a temperature gradient or difference. This temperature difference is the driving force that causes heat to flow. Heat transfer occurs by conduction during laser irradiation of metals and alloys. Conduction of heat in solids is thought to be due to motion of free electrons[(1),(2)], lattice waves, magnetic excitations, and electromagnetic radiation. The motion of free electrons occurs only in substances that are considered to be good electrical conductors. The theory is that heat can be transported by electrons, which are free to move through the lattice structure of the conductor, in the same way that electricity is conducted [(3),(4)]. This is usually the case for metals. The molecular energy of vibration in a substance is transmitted between adjacent molecules or atoms from a region of high to low temperature[(5),(6)].

In 2000 the using of UV light in material processing is studies by H.Endert and others, the effect of new ultraviolet lasers upon the material surfaces produce color and properties change which may be explained in terms of microstructure changes[(7),(8)].

The ultra violet laser is a clean source of high energy density [(9)]. Surface irradiation processes involve non equilibrium phenomena due to high heating and cooling rates induced by the laser irradiation. The inherent rapid cooling due to high thermal conductivity of steel makes lasers very attractive since the irradiated parts contain various microstructures with metastable and stable phases, fine grain, minimum segregation, and extended solid solutions which improve the mechanical and metallurgical properties of the irradiated parts[(10);(14)].

The amount of heat used for irradiation along the depth is considered to be proportional to the input heat flux along the direction of that unit depth [(15)]. This assumption is based on the fact that in the absence of conduction loss, the amount of irradiated material, that is the amount of heat used for irradiation increases as the input heat flux increases and vice-verse. Therefore, the amount of heat used for irradiation can be expressed as function of temperature and physical parameters such as thermal conductivity, density and specific heat [(17);(19)].

2. Theoretical Investigation of the problem

Analytical model for the computation of temperature and heat flux distribution in a semi-infinite solid when subjected to spatially decaying, instantaneous laser source is investigated. The appropriate dimensionless parameters are identified. The reduced temperature and heat flux as a function of these parameters are presented in mathematical formula. Temperature and energy are presented as a function of different laser parameters[(20),(21)].

Mathematical model gives us description for the material behavior specifically the values that can not be measured. Stainless steel 304 has been chosen as an example for characterizing laser irradiation of the alloys[(22),(23),(24)]. The reflection was about 85%, and scattering was about 4% [(25)]. The reflectivity of stainless steel is nearly constant in the range from 300K to 1800K [(26), (27)]; which is the case in this investigation. Fig (1) shows Schematic representation of Steps of the analytical solution.

The analytical solution of the heat equation includes phases transition for pure metals in the solid state.

$$K(T)[\frac{\partial^2 T_s}{\partial z^2}]=\rho(T)C_p(T)\frac{dT}{dt}+\rho(\frac{d(z_m-s)}{dt})H \quad (1)$$

The heat equation in one dimension includes phase transition

$$\rho(T)C_p\frac{dT}{dt}=k[\frac{\partial^2 T_s}{\partial z^2}]-\rho(\frac{d\Delta z}{dt})aH \quad (2)$$

$$T(z,0)=T_s=2q_s\frac{(Dt)^{1/2}}{K(\pi)^{1/2}} \quad (3)$$

$$-k(dT/dz)=\frac{Q}{a\eta}=I\eta=(\frac{3P}{\pi r^2})(\eta)(1-\frac{r}{R}) \quad (4)$$

where $z_m-s=\Delta z$

$$\frac{dT(z,t)}{dz}=0 \quad (5)$$

Differentiating equation was solved by laplace transform and inverse laplace transform techniques to give it is interest to Calculate the heat flux at any z

$$-q=-k\frac{\partial T}{\partial x}=\frac{3P\eta}{\pi r^2}(1-\frac{r}{R})e^{[3P\eta(1-r/R)/\pi r2(T-Ts)]}\frac{z}{k}+$$
$$[\frac{3P\eta}{\pi r^2}(1-\frac{r}{R})(T-T_s)]\frac{2Dt}{k^2}\text{erf}[\frac{z}{2\sqrt{Dt}}+[\frac{3P\eta}{\pi r^2}(1-$$
$$\frac{r}{R})(T-T_s)](Dt)^{1/2}-\frac{\mu k}{2}(\frac{d\Delta z}{dt})H\ e^{(-\mu z+D\mu 2t)}\text{erf}[\frac{z}{2\sqrt{Dt}}-\mu(Dt)^{1/2})-$$
$$\frac{\mu k}{2}(\frac{d\Delta z}{dt})H[[\mu+\frac{3P\eta}{\pi r^2}(1-\frac{r}{R})\frac{1}{k}[(T-T_s)]/[\mu-$$
$$\frac{3P\eta}{\pi r^2}(1-\frac{r}{R})(T-T_s)]\ e^{(\mu z+D\mu 2t)}\text{erf}[\frac{z}{2\sqrt{Dt}}+\mu(Dt)^{1/2})]$$
$$+([\frac{3P\eta}{\pi r^2}(1-\frac{r}{R})\frac{1}{k}(T-T_s)]\frac{2Dt}{k^2})\text{erf}[\frac{z}{2\sqrt{Dt}}$$
$$+\frac{3P\eta}{\pi r^2}(1-\frac{r}{R})\frac{1}{k}(T-T_s)\sqrt{Dt}\ ]+\frac{\mu k}{C_p}(\frac{d\Delta z}{dt})H\ e^{(-\mu z+D\mu 2t)}+\frac{k}{2C_p}\frac{d\Delta z}{dt}H\ [2[\frac{3P\eta}{\pi r^2}(1-\frac{r}{R})\frac{1}{k}(T-T_s)]]^2$$
$$[\mu-\frac{3P\eta}{\pi r^2}(1-\frac{r}{R})\frac{1}{k}\ (T-T_s)]e^{[z\frac{3P\eta}{\pi r^2}(1-\frac{r}{R})\frac{1}{k}(T-Ts)}$$
(6)

List of symbols

Symbol	Unit		Definition
Q	joule	J	Energy
I		W/m^2	irradiance
Z	mm		Distance
P	watt	W	Laser power
T	kelvin	K	Temperature
t	Sec	s	Time
ρ	Kg/m3		Density
A			Absorptivity
a	cm^2		Area
ρ	g/m^3		Density
η			Efficiency
C_p	J/kg.K		Heat capacity
D	cm^2/sec		Thermal diffusivity
I_o	J/cm^2		Energy released by laser source
K	W/cm.K		Thermal conductivity
P	watt		Laser power
q	J/cm^3		rate of heat generated per unit volume
r	cm		The beam radius
s			Laplace transform variable
T			Temperature
t	sec		Time
x	cm		Spatial variable
Z	mm		Distance
μ			Absorption coefficient

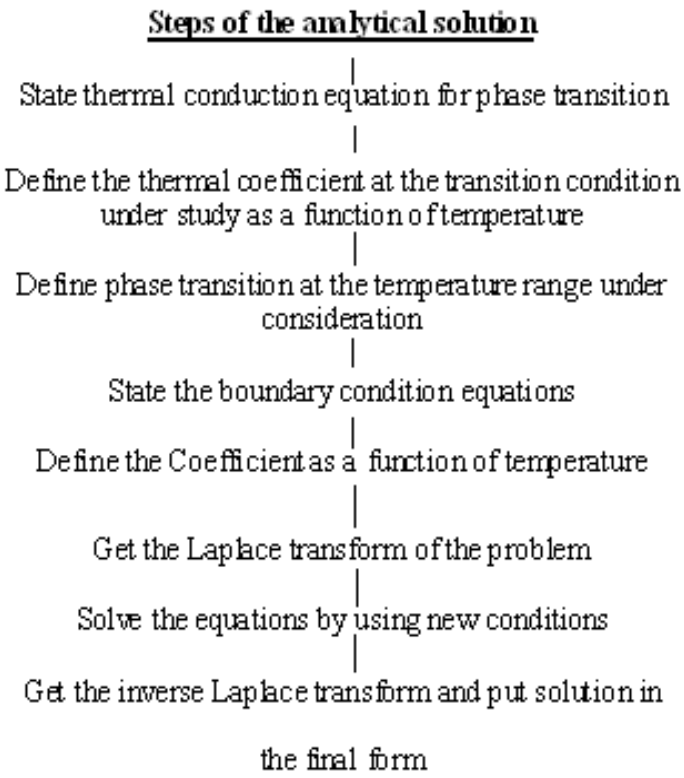

Fig (1) **Schematic representation of Steps of the analytical solution**

3. Results & discussions

Heating & phase transformation stages

The process of heating begins by absorbing the laser energy and converted it into heat. This heat source is considered as laser beam irradiation. The absorbed energy heats up the surface layer and the heat propagates into the metal by conduction. The heating of a semi-infinite insulated rod of Steel sample was done by laser radiation of intensity 150 W/cm^2.Energy per pulse was 6mJ and the total energy was 30J at 5000 pulses and Fluence 0.75J/cm^2. The problem is analyzed in one dimension using the heat transfer differential equation. The boundary conditions include the heat flux at one end and room temperature of 300K at the other end. The initial condition of the sample is the room temperature at 300K. The sample is semi-infinite. There is a sensible temperature variation at the interaction zone.

The problem is solved by the analytical solution method described before by Laplace transformation method. Figure (2) shows the variation of temperature with time at position (50μm) in the metal sample during laser irradiation. The temperature increases with increasing time and the rate of increase depends on the distance from the surface. The steps of temperature rise at different times (5 μs, 10 μs, and 15μs) with laser irradiation are shown in Figure (3). At all times during the laser irradiation process the surface temperature is higher than the substructure temperature and the temperature gradient is continuous until inside of the samples reach room temperature. The curves show the different stages of the heating process. Figure (4) shows the temperature distribution versus depth inside the metal after phase transition. The temperature at the surface reaches the phase transition 1183K (910°C –γ formation) after 20μs. Phase transformation process is a function of temperature, so all corresponding processes such as hardening and softening is a function of temperature. Every phase has formation energy. The energy of formation is a function of temperature. Temperature rises due to laser irradiation. The alloy absorbs photons of light at specified power and number of pulses, then the alloy reaches the energy of phase transition at critical temperature of phase transformation. Theoretical model explains the physical phenomena of phase transition which is considered as the main reason for hardening or softening resulting from laser interaction with the surface of the alloys [19].

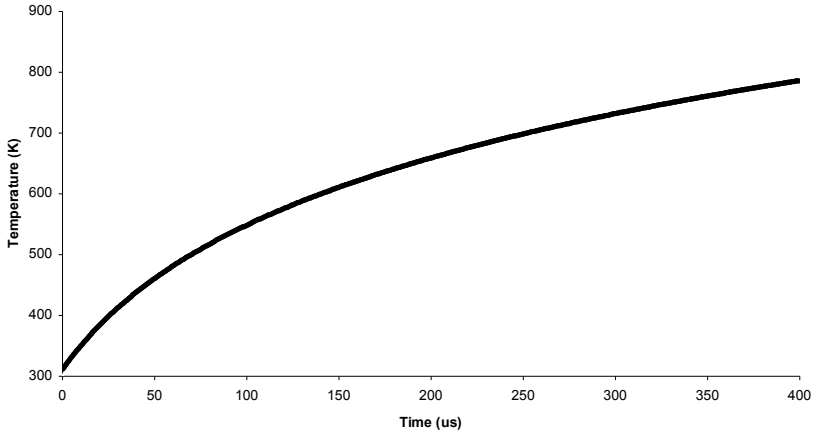

Fig(2)The Variation of Temperature of Steel with time at the surface point z4=50um During The First Pulse

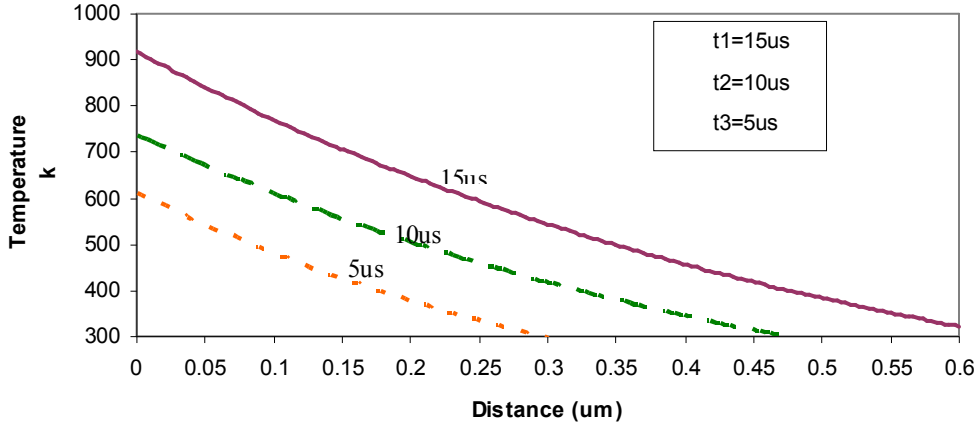

Fig (3) The variation of temperature with distance in analytical solution before phase transition of steel

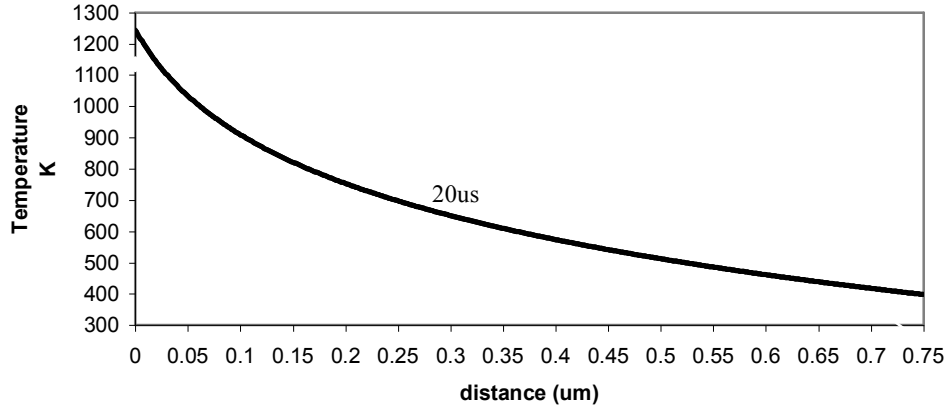

Fig(4) Heating of steel along the distance when irradiated by lasers after phase transition and before melting at 20us

Comparing results with published

When comparing the experimental results with the mathematical model the increase in total laser energy leads to increase in the Gibbs's free energy absorbed and rise in the temperature of the alloys, this may produce suitable conditions for the formation of more energy phases. Figure (5) shows the variation of the irradiated depth with time when the sample irradiated by 308nm excimer laser. Irradiated depth increases exponentially with irradiation time. The increase in irradiation time increases the amount of absorbed energy, the energy absorbed can penetrate extra depth. Some literature [(10), (13)] observed several thermally induced effects when an intense laser radiation is incident upon a surface. A possible explanation for this phenomenon was given that the point of maximum temperature before the phase change occurs at the exposed surface lies inside the body because of the heat loss to the surroundings. The phenomena investigated analytically by calculating the temperature profile in a semi-infinite body with an exponentially decaying source and convective boundary condition. The position of the maximum temperature is a strong function of the physical parameters.

Fig (6) shows the variation of irradiated depth versus number of pulses. The irradiated depth increases linear as the number of pulses increase. At 50000 pulses the irradiated depth expected was 25μm. The irradiated depth at low number of pulses from 2000 to 15000 pulses was limited to less than 10μm. In the experimental results, the irradiated depth was less than the calculated depth. The irradiated depth measured in experimental work was limited to 200nm at all number of pulses. The deviation between experimental results and theoretical results was for the following reasons:

1-Error in experimental measurements

2- The mathematical model neglected the scattering of laser beam between atoms distribution inside the alloy (only consider surface scattering).

3-Degree of surface finish was calculated by theoretical model

4-Experimental method based on certain approximation to calculate irradiated depth.

The deviation between experimental work and the theoretical model was in the acceptable range recommended in the literature.

Fig (7) and Fig (8) show the variation of temperature versus energy in the range from 0 to 50000 pulses at the energy per pulse was 3.5mJ and 6mJ respectively. The amount of total energy at 50000 was 170000mJ when the energy per pulse was 3.5mJ and at 6mJ was 290000mJ. When the energy per pulse increased, the total energy absorbed also increased at the same number of pulses.

The effect of number of pulses

Fig (9) shows the variation of temperature with number of pulses. The temperature rises linear with increase in the number of pulses in the range from 0 to 15000 pulses. At a high number of pulses more than 20000 pulses, the temperature was changed exponentially with an increase in the number of pulses. According to the theoretical results the temperature reach to 1800K (melting point) when the number of pulses more than 50000pulses, which is the critical point in our study range that deal with transformation in solid state only.

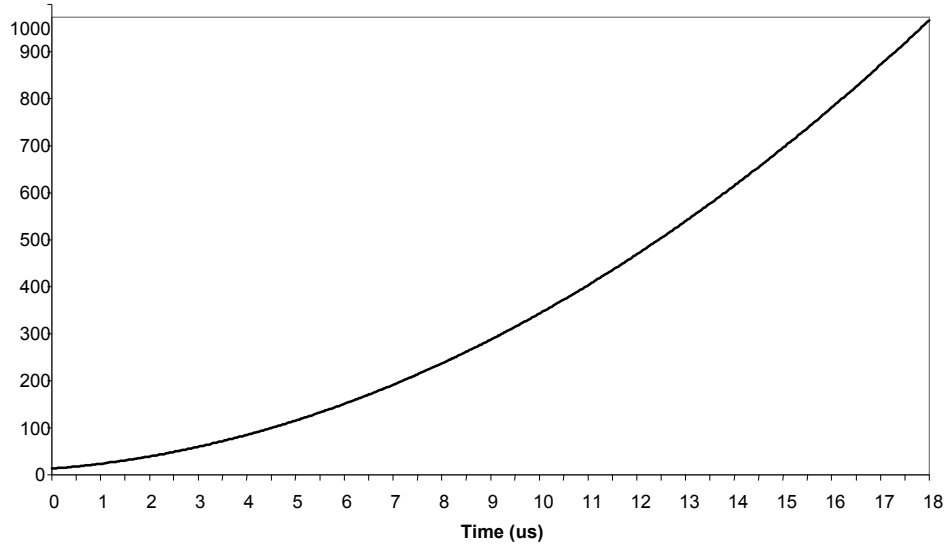

Fig (5) The Variation of The Irradiated Depth with Time for Steel irradiated by Excimer Laser at 308nm,200Hz,6mJ

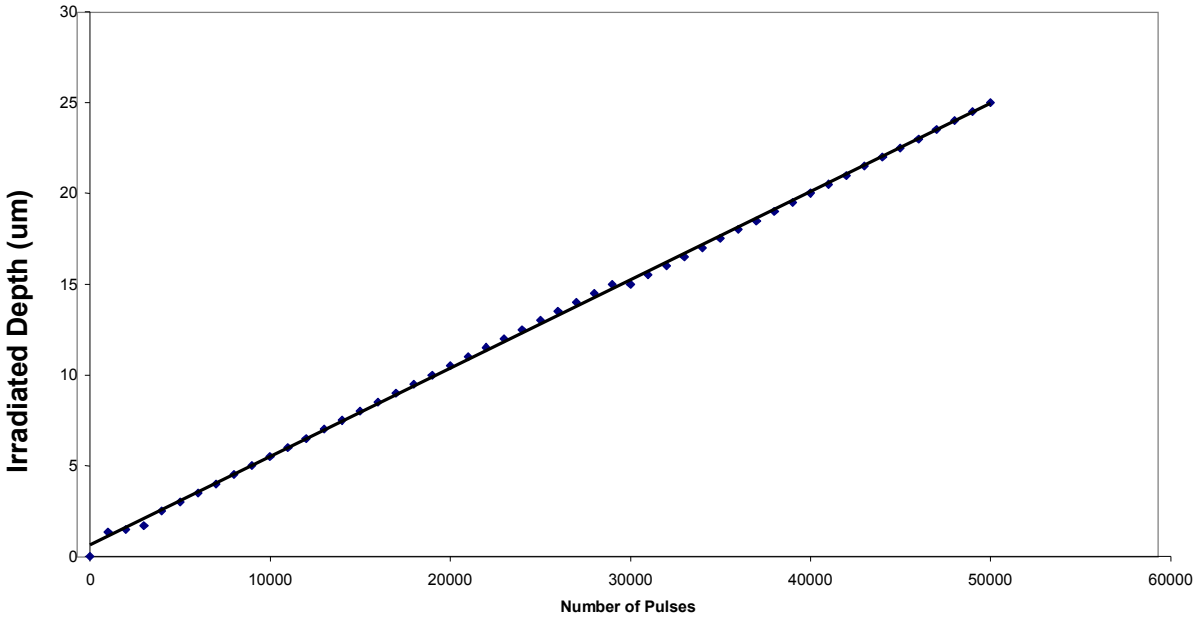

Fig (6) The Variation of irradiated Depth with Number of Laser Pulses For Steel Alloys Irradiated by Excimer Laser 308nm,200Hz,6mJ

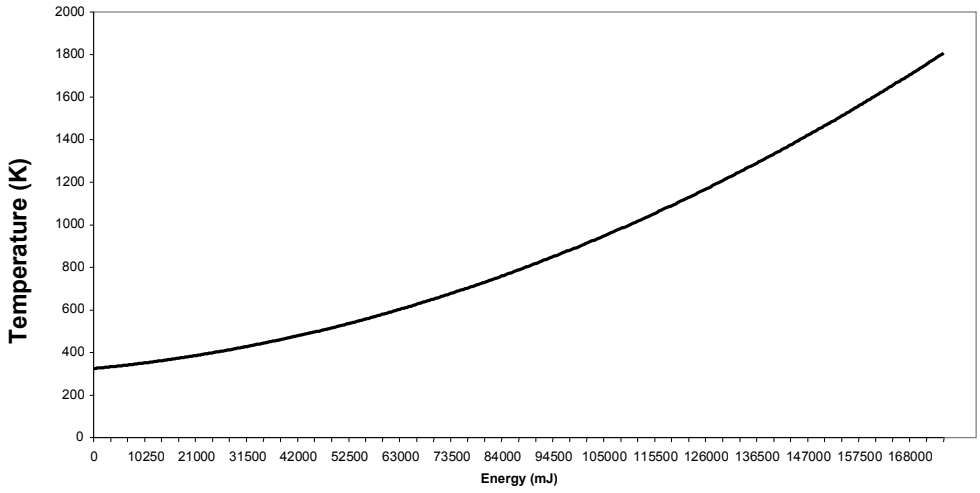

Fig (7) The variation of Temperature with Energy for Steel irradiated by Excimer Laser 200Hz when the energy per pulse 3.5mJ

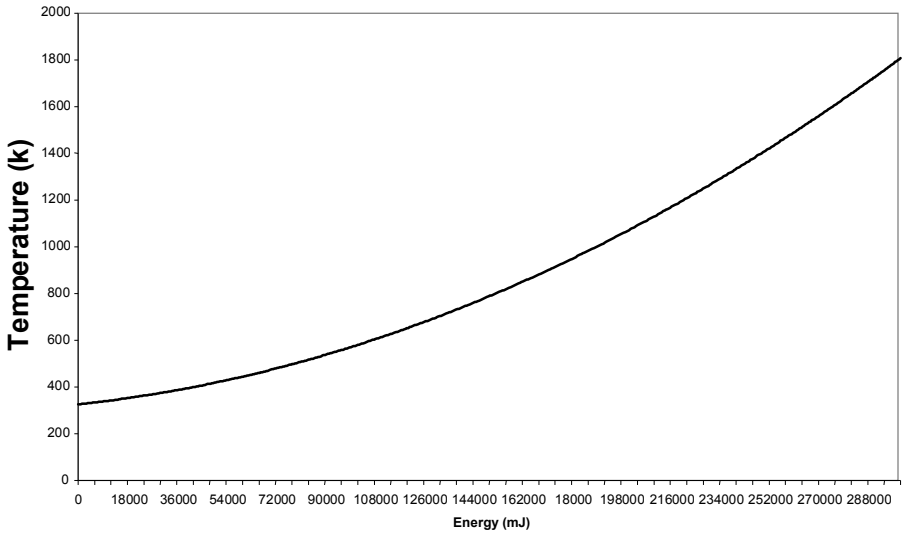

Fig (8) The variation of Temperature with Energy for Steel irradiated by' Excimer Laser 200Hz when the energy per pulse 6mJ

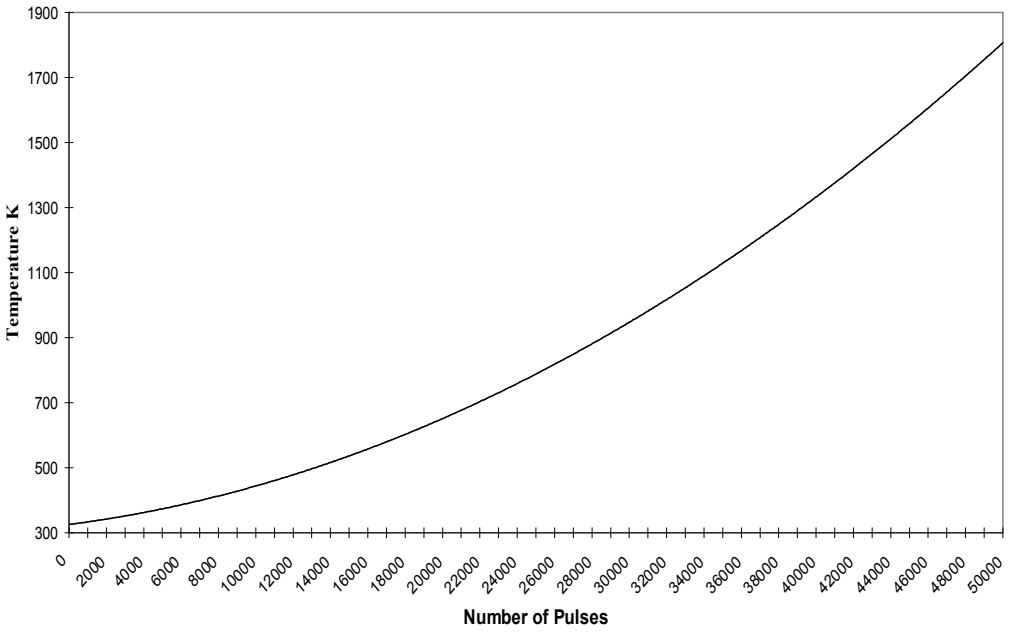

Fig (9 The Variation of Temperature with Number of Laser Pulses For Steel Alloys Irradiated by Excimer Laser 308nm,200Hz,6mJ

Fig (10) shows the variation of temperature versus irradiated depth. The increase in irradiated depth occurred as result of the increase in temperature of the sample surfaces. The increase in the surface temperature means the increase in the total amount of energy absorbed due to increase in number of pulses at constant repetition rate, wavelength and energy per pulse. Fig (11) shows the temperature variation with the rate of laser interaction with the alloy (velocity of interaction) as shown in the figure in solid state before melting point at 1800K. The rate of laser interaction was constant. When the temperature was more than 1800K (liquid state) the rate of interaction was linear and increased gradually with temperature rises.

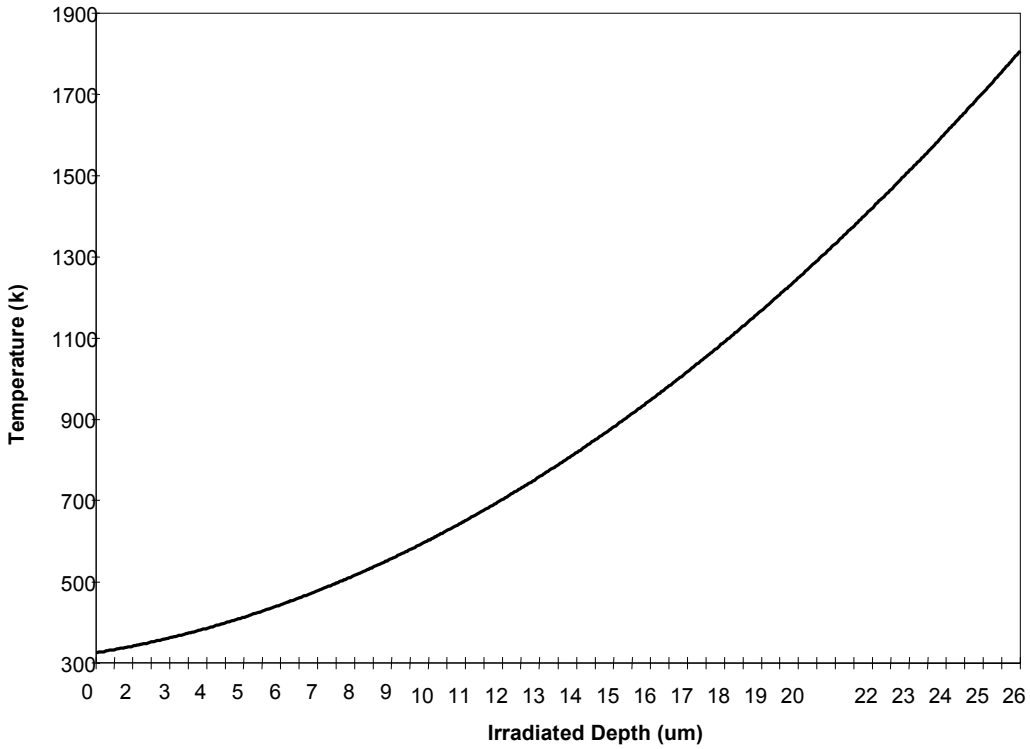

Fig (10) The Variation of Temperature with irradiated Depth for Steel irradiated by 308nm, 6mJ,200Hz

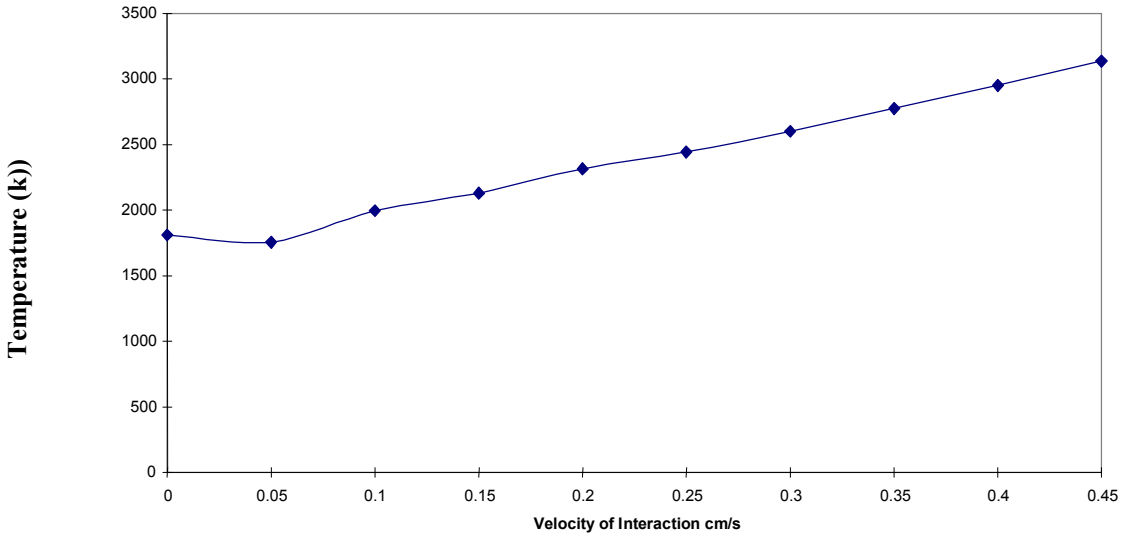

Fig (11) The Variation of Temperature with Interqaction Time for Steels when irradiated by Excimer Laser 308nm,200Hz,6mJ

Comparing theoretical & experimental results

Fig (12) shows the relation between temperature and measured depth for stainless steel 304. Comparing these curves with Figure (10), it shows that both theoretical and experimental results have the same trend.

There are some deviation in values between theoretical study and experimental work due to error in the experimental work and precaution of the model

explained before. The results in literature concur with our results [13], [14]. The experiments in the literature use steel 45 and the relation between temperature and depth have the same trend. The deviation between experimental results and different methods of theoretical investigation was about ± 6% to ±20% [38], [39]. Our results were in the same range of deviation 17% approximately.

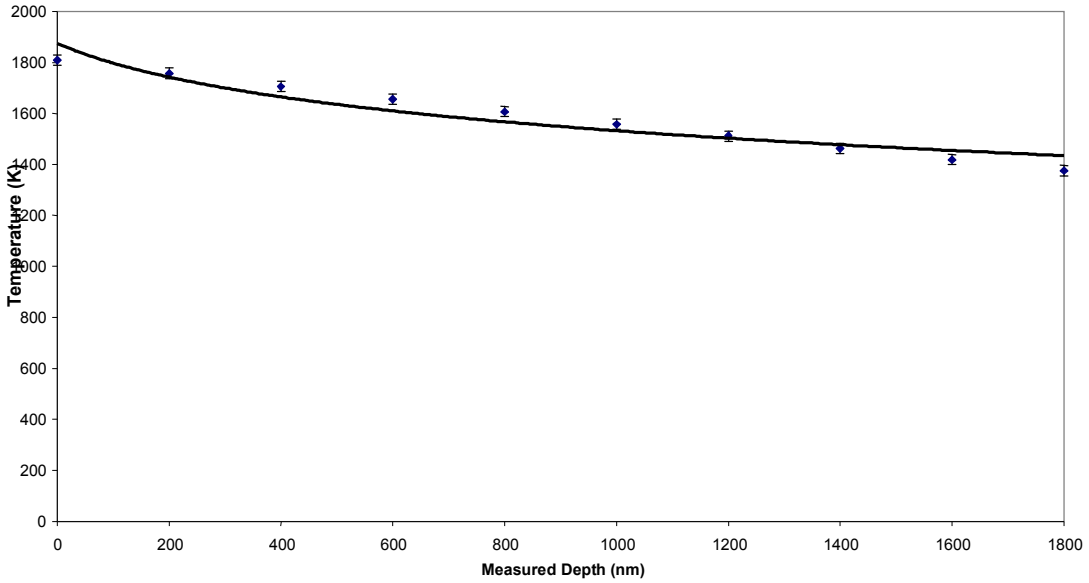

Fig (12) The variation of Temperature with Depth for Stainless Steel 304 irradiated by excimer Laser 308nm,6mJ,200Hz at Different Number of Pulses

The above theoretical results show those at all times during laser irradiation process the surface temperature is higher than the substructure temperature and the temperature gradient is continuous to the room temperature [5]. When comparing the experimental results with the published thermo-mechanical mathematical model, the increase in total laser energy leads to an increase in the Gibbs's free energy absorbed. The absorbed energy causes increasing in the temperature of the alloys; this may produce suitable conditions for the formation of high energy phases [17]. Under the action of external force resulting from the laser photon energy, the external force resulting from laser photons leads to the interaction of dislocations which form dislocation pile up of various degrees of stability and mobility. Frank –read source is also formed [15]:[11]. The light photons of energy go through the surface and absorbed into the metal causing the atoms to move around their position and some atoms may be moved inside the structure[14]. The photon energy is transformed into kinetic energy and causes some change in the arrangement of atoms inside the structure; this disturbance causes the improvement in the properties due to redistribution of atoms and some hard phases may appear. The improvement in mechanical properties as a result of laser irradiation occurred [9],[11].

Pulse laser treatment in normal atmosphere is an attractive technique that differs from usual coating methods, is a new, very thin layer with different microstructure and different mechanical characteristics will be formed on the alloy surface[19],[17]. The laser interaction is the basis for an effective treatment. To induce the chemical-physical reaction with the atmospheric environment high power, short pulse lasers are used [18]. These results agree well with published results [10],[12]. In experiments study the laser processing of grey cast iron the longer the interaction time, the deeper is the melt zone. Current results agree well with published results [10] [12]. They prove that, the depth of the transformed zone increased with increasing interaction time at a laser power of 0.5KW [17].

Literatures recorded systematic discrepancies between the experimental results and the numerical computation [9]. The disagreement increases at high power, in other words, when the amount of absorbed energy increases. The surface absorptive varies with surface temperature thus; with laser beam power (the maximum surface temperature will be greater with a large laser beam power) [15],[18].

4. Conclusions

Phase transformation process is a function of temperature, so all corresponding processes such as hardening and softening is a function of temperature. Every phase has formation energy. The energy of formation is a function of temperature. Temperature rises due to laser irradiation. The alloy absorbs photons of light at specified power and number of pulses, and then the alloy reaches the energy of phase transition at critical temperature of phase transformation.

1. The temperature was changed exponentially with an increase in the number of pulses
2. The deviation between experimental results and different methods of theoretical investigation were about $\pm$ 6% to $\pm$20% [3], [13]. Our results were in the same range of deviation 17% approximately
3. The thermal effect due to collision between lasers and atoms inside the structure; when taken into account in the total energy balance, it tends to reduce the efficiency of heating and phase transitions which mean transformation in solid state (i.e. the amount of heat able to form propagate microstructure changes) ; accordingly, it affect the amount of heat actually absorbed inside the material.
4. Disagreement between the current experimental work and some published theoretical studies [9],[10] have many reasons. The beam-metal interaction, and in the case where the fluence is high enough to rise the surface, temperature instantaneous and reflectivity changed, this effect is quite complex: the laser rays dissipated, thus reducing the effective energy really impinging on the target [6].

References

1. V. Craciun, D. Craciun, N. Chitica, I. N. Mihailescu, L. C. Nistor, Al. Popa, V. S. Teodorescu, I. Ursu, G. Leggieri, A. Luches, M. Martino, A. V. Kuzmichev, V. I. Konov, A. M. Prokhorov: Direct Synthesis Of $TiSi_2$ By A Laser Thermal Self-Aligned Process Journal of Physics D 25 (1992) 1500-1503
2. V. Craciun, I. N. Mihailescu, L. C. Nistor, V. S. Teodorescu, G. Leggieri, A. Luches, M. Martino, A. V. Drigo: Direct Laser Synthesis Of Thin Silicon And Germanium Nitride/Oxynitride Layers,. Nuclear Instruments and Methods In Physical Research B65 (1992) 115-118
3. V. Bohac, E. D'Anna, G. Leggieri, S. Luby, A. Luches, E. Majkova, M. Martino: Tungsten Silicide Formation By Xecl Excimer Laser Irradiation Of W/Si Samples, Applied Physics A56, (1993) 391-396
4. S. Luby, E. Majkova, V. Daniska, A. Luches, M. Martino, A. Perrone: Synthesis Of Tungsten Silicide By Pulsed Laser Irradiation Of Sputtered Alloy Layers, Thin Solid Films, 229 (1993) 24-28
5. S. Luby, E. Majkova, V. Daniska, R. , A. Luches, E. D'Anna, A. Luches, M. Martino: Pulsed Excimer Laser Induced Reactions At The Tungsten-Silicon Interface,. Multicomponent And Multilayered Thin Films For Advanced Microtechnologies O. Auciello And J. Engelmann Eds (1993) 543-549
6. E. D'Anna, S. Luby, E. Majkova, A. Luches, M. Martino: Processing Of W/Si And Si/W Bilayers And Multilayers With Single And Multiple Excimer Laser Pulses, Applied Physics A56 (1993) 429-436.
7. S. Luby, E. Majkova, E. D'Anna, A. Luches, M. Martino, A. Tufano, G. Majni: Tungsten Silicide Formation By Multipulse Excimer Laser Irradiation, Applied Surface Science 69 (1993) 345-349
8. I. N. Mihailescu, N. Chitica, V. S. Teodorescu, M. L. De Giorgi, G. Leggieri, M. Martino, A. Perrone, B. Dubreuil: Excimer Laser Reactive Ablation: An Efficient Approach For The Deposition Of High Quality TiN Films, Journal of Vacuum Science and Technology A 11(5) (1993) 2577-2582
9. E. D'Anna, M. L. De Giorgi, S. Luby, A. Luches, E. Majkova, M. Martino: Excimer (XeCl) Laser Processing Of W/Si Bilayers And Multilayers Up To Si Melting Threshold, Thin Solid Films 228 (1993) 145-148
10. E. D'Anna, G. Leggieri, M. Martino, A. Luches, A. Perrone, G. Majni, P. Mengucci, I. N. Mihailescu: Laser Reactive Ablation Deposition Of Titanium Nitride And Carbide Films, Laser Materials Processing and Machining SPIE 2246 (1994) 96-106
11. A. Luches, G. Leggieri, M. Martino, A. Perrone, G. Majni, P. Mengucci, I. N. Mihailescu: Laser Reactive Ablation Deposition Of Nitride Films Applied Surface Science 79/80 (1994) 244-249.
12. E. D'Anna, G. Leggieri, A. Luches, M. Martino, S. Luby, E. Majkova, G. Majni: Synthesis Of Tungsten Silicide By Multipulse Laser Irradiation Of W/Si Samples In Vacuum, Vuoto XXIII(2) (1994) 79-83
13. I. N. Mihailescu, N. Chitica, A. Lita, V. S. Teodorescu, A. Luches, G. Leggieri, M. Martino, G. Majni, P. Mengucci: Simultaneous

Formation Of Titanium Silicide In One-Step Process In Heterogeneous Phase During Multipulse Laser Treatment Of A Si Wafer With A Thin Ti Coating In Superatmopheric N_2, Thin Solid Films 251 (1994) 23-29

14. E. D'Anna, M. L. De Giorgi, G. Leggieri, M. Martino, A. Luches, G. Majni, P. Mengucci, I. N. Mihailescu: Laser Reactive Ablation Of Thin Nitride Films Journal de Physique IV 4-C4 (1994) C4-51 - C4-54
15. M. L. De Giorgi, G. Leggieri, A. Luches, M. Martino, A. Perrone, I. N. Mihailescu, V. S. Teodorescu, P. Mengucci: Deposition Of TiN Films On Si Wafers By Excimer Laser Ablation Of Titanium In Low Pressure Nitrogen Atmosphere, Vuoto XXIII(3) (1994) 81-84
16. M. L. De Giorgi, G. Leggieri, M. Martino, A. Luches, A. Perrone, G. Majni, P. Mengucci, I. N. Mihailescu, J. Zemek: Laser Reactive Ablation Deposition Of Silicon Nitride Films, Applied Physics A (60) (1995) 275-283
17. E. D'Anna, G. Leggieri, M. Martino, A. Luches, A. Perrone, G. Majni, P. Mengucci, R. Alexandrescu, I. N. Mihailescu, J. Zemek: Excimer Laser Reactive Ablation Deposition Of Silicon Nitride Films, Applied Surface Science 86 (1995) 170-174
18. G. Leggieri, A. Luches, M. Martino, A. Perrone, G. Majni, P. Mengucci, I. N. Mihailescu: Laser Reactive Ablation Deposition Of Titanium Carbide Films, Thin Solid Films 258 (1995) 40-45
19. A. Luches, G. Leggieri M. Martino, G. Majni, P. Mengucci: Titanium Carbide Film Deposition By Reactive Laser Ablation, Surface Modification Technologies VIII T. S. Sudarshan And M. Jeadin Eds. , The Institute Of Materials (1995) 415-419
20. S. Luby, E. Majkova, M. Jergel, E. D'Anna, G. Leggieri, A. Luches, M. Martino, J. Valicek: Intermixing In Immiscible Molybdenum Copper Multilayered Metallization Under Excimer Laser Irradiation, Acta Physics Slovaca 45(4), (1995) 507-518
21. E. D'Anna, A. Luches, M. Martino, M. Jergel S. Luby, E. Majkova, I. Vavra: Influence Of Temperature Time And Depth Profiles On The Pulsed XeCl Laser Crystallization Of Evaporated Silicon Films, Journal Of Non-Crystalline Solids 192&193 (1995) 513-518
22. I. N. Mihailescu, A. Lita, R. Teodorescu, V. S. Teodorescu, A. Luches, M. Martino, A. Barborica: Synthesis And Deposition Of Silicon Nitride Films In Low Pressure Ammonia: A Parametric Study. Journal of Vacuum Science and Technology A 14(4) (1996) 1986-1994
23. M. Dinescu, N. Chitica, V. S. Teodorescu, A. Lita, A. Luches, M. Martino, A. Perrone, M. Gartner: Laser Reactive Ablation: One Step Procedure For The Synthesis And Deposition Of Compound Thin Films. 'Laser Processing: Surface Treatment And Film Deposition J. Mazumder et al. (Eds) Kluwer Academic Publishers (1996) 809-821
24. S. Luby, M. Jergel, E. Majkova, E. D'Anna, A. Luches, M. Martino, M. Brunel, I. Vavra: Pulsed Excimer Laser Crystallization Of Evaporated Amorphous Silicon Films, Physics Status Solidi (a) 154 (1996) 647-656
25. I. N. Mihailescu, E. Gyorgy, M. Popescu, S. Csutak, G. Marin, I. Ursu, A. Luches, M. Martino, A. Perrone, J. Hermann: Laser Ablation In A Reactive Atmosphere: Application To The Synthesis And Deposition Of Performance Titanium Carbide Thin Films, Optical Engineering 35(6) (1996) 1652-1655
26. I. N. Mihailescu, N. Chitica, E. Gyorgy, V. S. Teodorescu, G. Marin, A. Luches, M. Martino, A. Perrone, J. Neamtu: A Parametric Study Of The Deposition Of The TiN Thin Films By Laser Reactive Ablation Of Titanium Targets In Nitrogen: The Role Of The Total Gas Pressure And The Contaminations With Oxides, Journal of Material Science 31 (1996) 2909-2915
27. V. S Teodorescu, I. N. Mihailescu, E. Gyorgy, A. Luches, M. Martino, L. C. Nistor, J. Van Landuyt, J. Hermann: The Study Of Crater Forming On The Surface Of A Ti Target Submitted To Multipulse Excimer Laser Irradiation Under Low Pressure N_2, Journal of Modern Optics 43(9) (1996) 1773-1784

11/21/2011

Unsupervised CBIR by Combining Color, Shape (Features with a Threshold) and Lossless Gray Image Compression

Raj Kumar Mishra, Rajni Singh

DBGI, Dehradun, TMU, Moradabad; er.rajnisingh25@gmail.com

Abstract: Content-based image retrieval (CBIR) uses the visual features of an image such as color, shape and texture to represent and index the image. In a typical content based image retrieval system, a set of images sorted by similarities of their visual features with that of the query image are returned in response to a query. CLUE is a popular CBIR technique that retrieves images by clustering. In this paper, we propose a CBIR system that also retrieves images by clustering just like CLUE. But, the proposed system combines the color and shapes features with a threshold and lossless gray image compression for the purpose. The combination of the colored shape features and compression provides a robust feature set for image retrieval. We evaluated the performance of the proposed system using images from COREL database and compared its performance with that of the other two existing CBIR systems namely UFM and CLUE. Experimentally, we find that the proposed system outperforms the other two existing systems.
[Raj Kumar Mishra. Rajni Singh. Unsupervised CBIR by Combining Color, Shape (Features with a Threshold) and Lossless Gray Image Compression. Academia Arena, 2012;4(2):37-41] (ISSN 1553-992X). http://www.sciencepub.net.

Keywords: Content based image retrieval, image classification, unsupervised learning, spectral graph clustering, lossless gray image compression.

1 INTRODUCTION

The creation of the World Wide Web (in short, WWW) has enabled users to access data in a variant of media formats. This served as a stimulus for organizations having large image collections to convert their collections to digital formats. The number of digital images on the WWW is estimated to be more than hundred of millions. This creates a need for development of novel techniques for efficient storage and retrieval of images.

Content-based image retrieval (CBIR, in short) uses the visual contents of an image such as color, shape and texture to represent and index the image. In a typical content-based image retrieval system (see Figure 1), the visual contents of the images in the database are extracted and described by multi-dimensional feature vectors. The feature vectors of the images in the database form a feature database. To retrieve images, users provide the retrieval system with example images or sketched figures. The similarities/distances between the feature vectors of the query example or sketch and those of the images in the database are then calculated and retrieval is performed with the aid of an indexing scheme. The indexing scheme provides an efficient way to search the image database for images similar to the query images in order to return the relevant images. Generally speaking, content-based image retrieval (CBIR) aims at developing techniques that support effective searching and browsing of large image digital libraries on the basis of automatically derived image features [1].

Unsupervised learning is applied to the class of problems, where one seeks to determine how the data are organized. Here, the system discerns the objects under consideration in different categories on the basis of some similarity measures. The objects that are similar to each other are put in one group (also called a cluster) and the objects that are dissimilar are put into different clusters. CLUE, cluster-based retrieval of images by unsupervised learning, proposed by Chen et al.. [17, 18] is an example of CBIR technique based on unsupervised learning.

In this paper, we propose a CBIR system that is also based on unsupervised learning and combines the color and shape features with a threshold to compute the similarity of the query image with the images in the database.

This paper is organized as follows. In the next section, we discuss the background and related work. In Section 3, we discuss the details of unsupervised content based image retrieval and present the architecture of our proposed CBIR system. In section 4, we present our experimental results. Finally, we conclude in section 5.

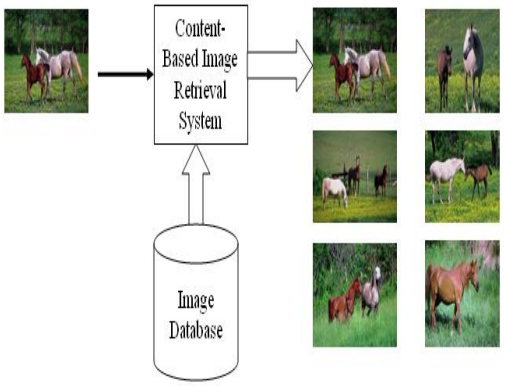

Figure 1. A Content Based Image Retrieval System

2 BACKGROUNDS AND RELATED WORK

In the past fifteen years, many general-purpose image retrieval systems have been developed. Some of these are QBIC System [8], Photobook System [9], Blobworld System [10], Virage System [11], VisualSEEK and WebSEEK Systems [12], the PicHunter System [13], NeTra System [14], MARS System [15], and SIMPLIcity Systems [16].

Existing CBIR systems can be grouped into two major categories: *full-image* retrieval system and *region-based* image retrieval system. Some of the existing CBIR systems may also belong to the both categories. Most of the existing CBIR systems are region-based systems because region-based systems are better than full-image retrieval systems.

In a CBIR system, to search images by their content, two things have to be done [23].

1. The image has to be re-encoded into some mathematical form and stored in a database.
2. There should be a mechanism to compare these mathematical forms.

Re-encoding is needed because an image is a collection of pixels with no meaning by itself. There is a gap between the visual information conveyed by the image and the way it is encoded. The process of re-encoding the image into a mathematical form suitable for comparison purpose is called feature extraction.

Features can also be grouped as low-level and high-level features. Low-level features are features that can be obtained from the pixel itself. Examples are color and texture. High-level features are features obtained from the combination of low-level features. Examples are edge and shape. But, the three of the most widely used features are (i) color (ii) texture and (iii) shape. Details of these features are discussed in [26].

A typical CBIR system views the query image and images in the database (target images) as a collection of features, and ranks the relevance between the query image and any target images in proportion to feature similarities. Images with high feature similarities to the query image may be very different from the query in terms of the interpretation made by a user. This is referred to as the *semantic gap*, which reflects the discrepancy between the relatively limited descriptive power of low level imagery features and the richness of user semantics [17]. Statistical classification methods group images into semantically meaningful categories using low level visual features so that semantically-adaptive searching methods applicable to each category can be applied [19, 20, 16, 21]. The Simplicity system [16] classifies images into graph, textured photograph, or non-textured photograph, and thus narrows down the searching space in a database. There has been work on attaching words to images by associating the regions of an image with object names based on region-term co-occurrence [22]. And semantically precise image segmentation by an algorithm is still an open problem in computer vision [23, 24].

Cluster based retrieval of images by unsupervised learning (CLUE) is an important CBIR technique based on unsupervised learning. CLUE retrieves image clusters by applying a graph–theoretic clustering algorithm to a collection of images in the vicinity of the query. Clustering in CLUE is dynamic.

In this paper, we propose a CBIR system that is also based on unsupervised learning. Color features are computed by color moment and color histogram [2, 3]. Shape features are calculated after images have been segmented into regions or objects [4, 5]. Shape information is captured in terms of edge images computed using Gradient Vector Flow fields [6]. Invariant moments are then used to record the shape features [7]. The proposed system sums up the values of color and shape features, after applying the threshold, for assigning weights to different images. On the

basis of these weights, the relevant images are extracted from the image database.

3. UNSUPERVISED CONTENT BASED IMAGE RETRIEVAL

A CBIR system based on CLUE is shown in Figure 2. In this, the retrieval process starts with feature extraction. The features for target images (images in the database) are usually computed beforehand and stored as feature files. Using these features together with an image similarity measure, the resemblance between the query image and target images are evaluated and sorted. Next, a collection of target images that are "close" to the query image are selected as the neighborhood of the query image. A clustering algorithm is then applied on these target images. Finally, the system displays the image clusters and adjusts the model of similarity measure.

The major difference between CBIR system based on CLUE and the other two CBIR systems lies in the two processing steps, selecting neighboring target images and image clustering, which are the major components of CLUE[18].

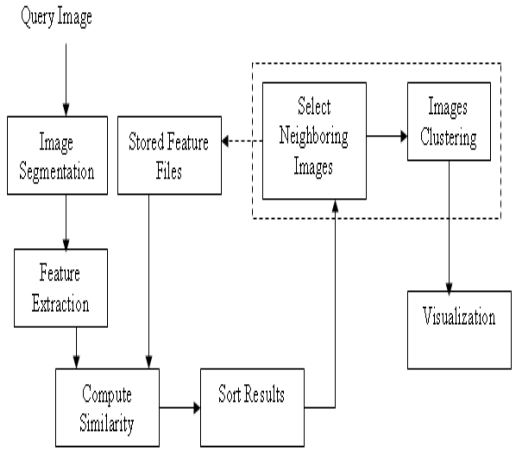

Figure 2. A CBIR system based on CLUE

There are two simple methods to select a collection of neighboring target images for query image [16].

- *Fixed-radius method* (FRM) takes all target images within some fixed radius ε with respect to *i.* For a given query image, the number of neighboring target images is determined by ε.
- *Nearest-neighboring method* (NNM) first chooses k NN of *i* as seeds. The *r* NN for each seed is then found. Finally, the neighboring target images are selected to be all the distinct *target* images among seeds and their *r* NN, i.e., distinct images in *k(r+1)* target images. Thus, the number of neighboring target images is bounded above by *k(r+1)*.

In the field of computer vision, two types of representations are widely used. One is called the *geometric representation,* in which data items are mapped to some real normed color space. The other is referred to the *graph representation* emphasizing the pair wise relationship. Graph representation of neighboring target images is as follows.

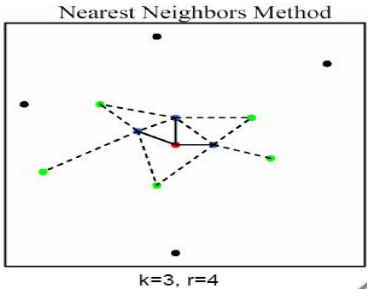

Figure 3 Example of Nearest Neighbor Selection of Images

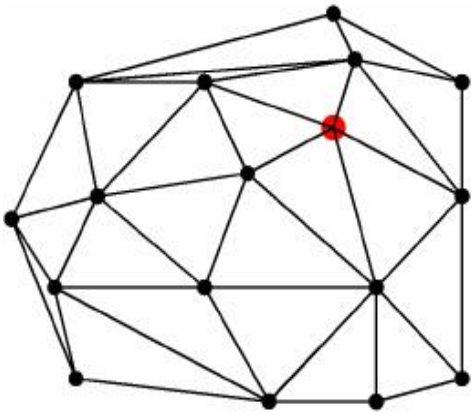

Figure 4 Example of Weighted Graph Representation of Images

A set of *n* images is represented by a weighted undirected graph G = (V, E).The nodes V = {1, 2, …., *n*} represent images, the edge E = {(*i*, *j*) : *i*, *j* ∈ V} are formed between every pair of nodes, and the nonnegative weight w_{ij} of an edge (*i, j*), indicating the similarity between two

nodes, si a function of the distance(or similarity) between nodes(images) *i* and *j*. Given distance d*(i, j)* between images *i* and *j*, the nonnegative weight w_{ij} is given by

$$w_{ij} = e^{\frac{-d(i,j)^2}{s^2}}$$

where, *s* is a scaling parameter that needs to be tuned to get a suitable locality. The choice of exponential decay is based on support from psychological studies. The weight can be organized into a matrix W, named affinity *matrix* with *ijth* entry given by w_{ij}

Under a graph representation, clustering can be naturally formulated as a graph partitioning problem. The CLUE uses spectral graph partitioning methods called the normalized cut (N_{cut}) method for image clustering. A graph partitioning method attempts to organize nodes into groups so that the within-group similarity is high, and/or the between-groups similarity is low.

Given a graph G = (V, E) with affinity matrix W, a simple way to quantify the cost for partitioning nodes into two disjoint sets A and B ($A \cap B = \Phi$ and $A \cup B = V$) is the total weights of the edges that connecting the two sets. In graph theory, this cost is called a *cut*

$$cut(A, B) = \sum_{i \in A, j \in B} w_{ij}$$

which can also be viewed as a measure of the between-groups similarity.

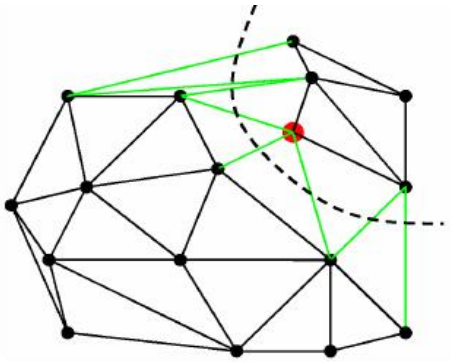

Figure 5 Normalized cut of weighted graph of Images

Finding a bipartition of the graph that minimizes this cut value is known as the *minimum* cut problem. However, the minimum cut criterion favors grouping small sets of isolated nodes in the graph because the cut defined above, does not contain any within-group information. This motivates several modified graph partition criteria including the N_{cut}

$$N_{cut} = \frac{cut(A,B)}{cut(A,V)} + \frac{cut(A,B)}{cut(B,V)}$$

An unbalanced cut would generate a large N_{cut} value.

Finding a bipartition with minimum N_{cut} value is an NP-complete problem. Shi and Malik [27] proposed an approximated solution by solving a generalized eigenvalue problem

$$(D - W)y = \lambda D y$$

Where W is an *n X n* affinity matrix, D = diag[s_1, s_2,…., s_n] is a diagonal matrix with $s_i = \sum_{j=1,\ldots,n} w_{ij}$.

Given a graph representation of images G = (V, E) with affinity matrix W, let the collection of image clusters be {C_1, C_2, …, C_m}, which is also partition of V, i.e.,

$C_i \cap C_j = \Phi$ for $i \neq j$ and $\bigcup_{i=1}^{m} C_i = V$.

Then the representative node (image) of C_i is

$$\arg\max \sum_{j \in C_i, t \in C_i} w_{jt}$$

which can also be viewed as a measure of the between-groups similarity.

Now, we propose the architecture of a CBIR system based on unsupervised learning as shown in Figure 6. The major difference between the proposed CBIR system and the CBIR system based on CLUE lies in the stored features files. In the proposed CBIR system, we store the values of features in the stored features files after combining values of shape and color features of an image with the 80% & 20% (for sketch diagram) threshold. In other words, we take 80% & 20% (for sketch diagram) of the total value of color features and 80 % of the value of shape features for an image and combine the two values and store that combined value into the stored features files as the feature values for the image.

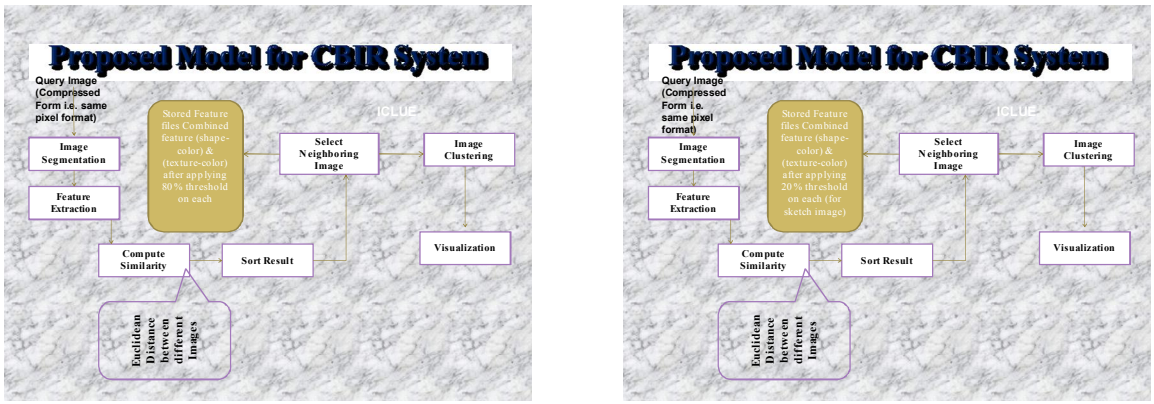

Figure 6 (a) & 6 (b) The Proposed CBIR system

12/12/2011

HYDRATE MANAGEMENT STRATEGIES IN SUBSEA OIL AND GAS FLOWLINES AT SHUT- IN CONDITION

[a] Usman, M.A. [a] Olatunde, A.O, [b] Adeosun T.A and [a] Egwuenu, O.L.

[a] Department of Chemical Engineering, University of Lagos, Nigeria
[b] Department of Mathematics, Yaba College of Technology, Nigeria
abayomi200@yahoo.com, adebaba2001@yahoo.com

ABSTRACT: Flow assurance in deep-water developments has been identified as one of the main technological problems that the oil and gas industry faces today. Extreme conditions such as high pressures and low temperatures promote the formation of gas hydrates that can potentially reduce or completely block the flow path, causing severe financial losses. This work presents an integrated framework of model-based flow assurance management strategy to handling the effect of hydrates. The model-based flow assurance framework determines the operational limits of the production system to avoid the effect of hydrate plugs in the event of unplanned shut-in. P-T curve generated with a PVT sim software using Peng Robinson equation of state predicted the temperature – pressure operating envelop of the system. A Hot Oil return Temperature of 40^0C at the topside of the FPSO was determined with a suitably selected insulation material type and a minimum flow rate of 20,000bpd was determined. The analyses on how long the production system can sustain the available heat in the event of unplanned shut-in before a restart was done and a 10hr flowline cool down was achieved. A maximum of 3.5hrs of blowdown was also determined for the production system, which satisfies the analyses with three different water cuts- 0%, 50% and 70%. The framework is implemented in a state-of-the-art modelling tool (OLGA). The above analyses on these different scenarios are geared towards defining the operating limit of the subsea production facilities to preventing hydrate from forming during unplanned shut-in.

[Usman, M.A. Olatunde, A.O, Adeosun T.A and Egwuenu, O.L. **HYDRATE MANAGEMENT STRATEGIES IN SUBSEA OIL AND GAS FLOWLINES AT SHUT- IN CONDITION.** Academia Arena, 2012;4(2):42-54] (ISSN 1553-992X). http://www.sciencepub.net. 7

Key words: Flow Assurance ,Hydrate, Peng Robinson, Hot Oil Return, Olga, Blowdown

INTRODUCTION

The concept of flow assurance is the ability to produce fluids economically from the reservoir to the production facilities over the life of the field and in all conditions and environments. It governs the success of the fluid movement from reservoir to point of sale. A clear understanding of the concept helps to ensure that any development plan from exploration through production and abandonment of any field is technically viable and designed for optima, operation throughout the field's life. Flow assurance involves: understanding the subsurface, fluid sampling and analysis, well and facilities design, production operations including surveillance, production architecture, interaction among the reservoirs, the wells, the pipelines and the process facilities and the challenges these interaction may present.

The term flow assurance can also be associated to the evaluation of the effects of fluid hydrocarbon solids (i.e asphaltene, wax and hydrate) and their potential to disrupt production due to disposition of inorganic solids arising from aqueous phase (i.e scale) also poses a serious threat to flow assurance. The recent trend to deepwater developments, future oil and gas discoveries increasingly will be produced through multiphase flow lines from remote facilities in deepwater environments. These are multiphase fluids area combination of gas, oil, condensate and water. Together with sand scales, they have the potential to cause many problems including hydrates, wax/asphaltene.

Gas hydrates are solid crystalline compounds formed by the physical combination of water molecules and certain small molecules of hydrocarbon gases (primarily methane, ethane, propane, CO_2 and H_2S), under pressure and temperature considerably above the freezing point of water. Hydrates are formed when the temperature is below a certain degree in the presence of free water. This temperature is called Hydrate formation temperature. Hydrates are like snow in appearance but not as solid as the ice. Water molecules forms the main framework of the hydrate crystal while the gas molecules occupies void spaces -cages in the water crystal lattice They continue to be the most prevalent flow assurance problem in offshore oil and gas operations: an order of magnitude worse than waxes and asphaltenes. The risk of hydrate plugging increases as the oil and gas industry move into deeper water with corresponding higher pressure from the additional liquid head and to longer tie backs in which

the production fluids cool deep into the hydrate stability zone.

The energy industries worldwide incur financial expenses estimated to US$220 million annually (P.K.Notz, Personal communication) for the purchase of methanol for hydrate prevention. Moreover several financial penalties are paid for large methanol storage capacity on offshore platforms and for greater than 50p.p.m methanol contamination in refinery feedstocks. The above analysis of the cost of hydrate prevention shows that about US$600,000 are spent daily worldwide. This is considerably minimal compare to estimated US$6.4 trillion (80million barrels pd of oil production worldwide) generated from oil production on daily basis which could be lost due to total plus off of production system by hydrated if allowed to form.

This work presents an integrated framework of model-based flow assurance management strategy to handling the effect of hydrates. The model-based flow assurance framework determines the operational limits of the production system to avoid the effect of hydrate plugs in the event of unplanned shut-in.

CASE STUDY- A NIGERIAN OIL FIELD STUDY

A typical Nigerian Oil Field Location was studied and used for analyses on how flow assurance challenges as it affects hydrate could be managed in the case of unplanned shut-in in a subsea production flowline Stated below are the relevant information extracted from the field studies;

FIELD LOCATION

The Field development lies offshore Nigeria, located at approximately 120 Kilometres south of Nigerian shoreline adjacent to Bonny Island in water dept ranging between 720 – 860 meters. The field is currently being developed by over 15 production wells producing back to FPSO with about 2,000,000 barrels storage capacity via subsea production manifolds and production flowlines, for processing before production exports to offloading tankers via a buoy. The field is supported by 8 water injection wells and 9 gas injection wells. The field development comprises of 4 umbilicals for distribution of chemicals, hydraulic controls and power supplies through retrievable sub-sea distribution/control units. The field are being developed with 5 drilling centres, DC-01 – DC-05 distributed unequally between two flowline loops. There is one offline subsea production Manifold (SPS) at each drill centres. This provides the facility with the direct tie-in of 4 wells.

The trees in the subsea field lie along two production flow loops, two water injection flow lines and one gas injection flow line. It comprises of three X mass trees:

- Production
- Water Injection
- Gas Injection

All the subsea trees are dual bore type 5” x 2 normal size, rated at API 5,000 psi (accounting for external hydrostatic pressure). All the subsea trees will be installed with tree guide bases and 18 3/4” 10,000 psi wellheads.

The Field Layout

The overall field layout was developed from subsea to topsides to respect the constraints given by the production and injection systems.

In summary the production system consists of

- Spread moored FPSO in 760 m water dept
- 2 X 10” ID production flow loops (PIP flowline or bundle).
- 4 X 10” ID production risers (flexible catenary riser).
- 4X 2.5” ID gas lift injection riser connected to production line riser base.
- 16 oil producers on 2 production loops
- 2 future subsea production wells.
- Umbilicals: 2 per production loop/ water injection line and 1 per gas injection system (methanol lines are incorporated in the umbilicals)

Well Arrangement

Tables 1 and 2 below shows, for each production loop, the distribution of the oil producer wells within each branch of the flow loop.

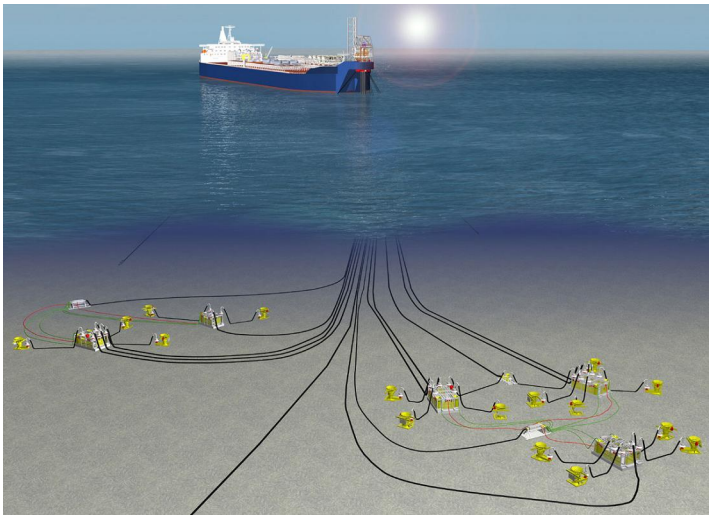

Fig 1: The overall Field Layout

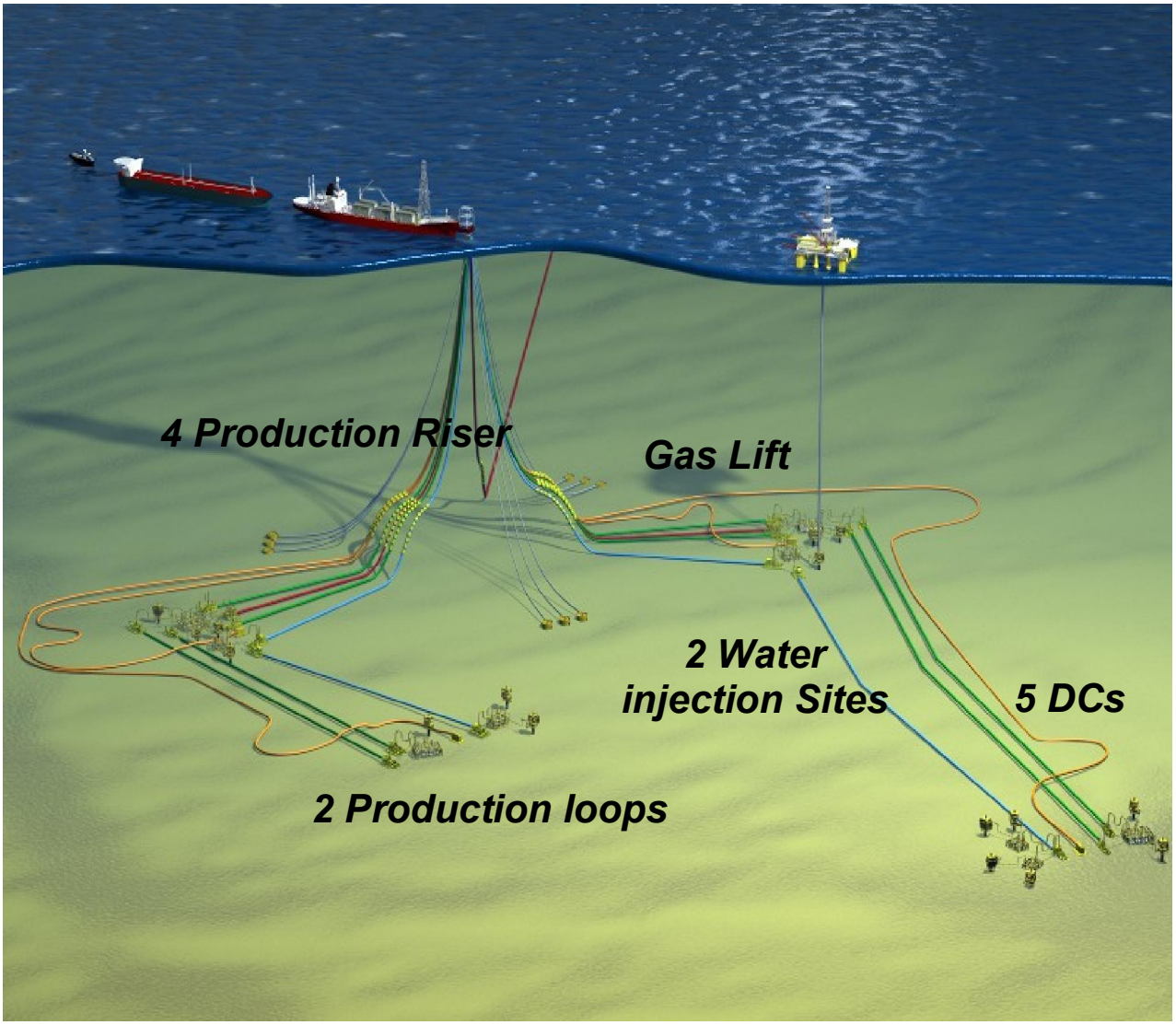

Fig 2: Well Arrangements

Table 1: North Loop Well distribution

Loop	Drilling Centre	Well	TVD (M)	Branch	Reservoir Series	Reservoir pressure (bara)
North	DC01	P630-1	-2807	Right	R-600N	273.8
		P605-2	-2438	Left		
	DC02	P500-4	-2441	Left	R-500 NC	253.5
		P500-5	-2168	Right		
		P630-4	-2668	Left	R-600 N	273.8
	DC03	P500-1	-2344	Right	R-500 NC	253.5
		P500-2	-2461	Left		
		P500-3				
		P500-9				

Table 2: South Loop Well distribution

Loop	Drilling Centre	Well	TVD (M)	Branch	Reservoir Series	Reservoir pressure (bara)
South	DC04		-2306	Right	R-500 NC	
		P605C-1	(HOLD)	N/A	R-500 S^3	
		P500-7	-1746	Right		
		P605-8	(HOLD)	Left		
	DC05	P605-1	-1803	Left	R-605 S	
			-2590	Right	R-605 C	(HOLD)
		P630-9	-2293	Right	R-635 S	
		P670-1	-2126	Left		

PRODUCTION LINES CHARACTERISTICS

Thermal Properties

Table 3: Material Characteristics

Material	K value (W/mK)	Density (kg/m^3)	Specific Heat Capacity (J/kg^{o}C)
Polypropylene (inner layer)	0.240	920	1700
Carbon Steel	45.000	7850	470
Gel	0.170	850	2000
Insulation	0.165	710	1500

Wall definition

Table 4 : The wall material and thickness to be used in all the hydraulic analyses

Pipeline / Section	ID	W.T	Insulation Type	Insulation Thickness (mm)
	Inch (mm)	Inch (mm)		
Flexible production Riser	10 (254.0)			
Production Flowline	10.5 (266.7)	1.25 (31.8)	Insulation	80.0
Production Jumper	7.4 (189.1)	0.59 (15.0)	Insulation	88.9
Manifold	5.2 (131.7)	7.5 (190.5)	Insulation	88.9
Well Jumper	5.2 (131.7)	0.719 (18.26)	Insulation	88.9
Well Spool	(HOLD)	(HOLD)	(HOLD)	(HOLD)
Tree	5.1 (130.3)	7.5 (190.5)	Insulation	88.9
Tubing	5.5 (139.7)	0.36 (9.17)	Gel	39.47

Table 5: Overall Heat Transfer Coefficients

SPS Location	**U VALUE (W/m^{2}K)**
Tubing	5.8
Tree	8.2
Well Jumper	3.4
Manifold	8.2
Production Jumper	2.9
Flowline	3.0
Riser	3.2

Production Flowlines

Table 6: Production Flowline Data

Production Flow Loops Total length	38.8 km
North Flow Loop length	14.3 km
South Flow Loop length	24.5 km
Internal Diameter	10.5 inch (266.7 mm)
Wall Thickness	1.25 inch (31.8 mm)
Pipe Material	Carbon Steel
Insulation Thickness	3.0 Inch (80 mm)
Insulation Material	Insulation (see Table 4-3 for properties)
Internal Roughness	46 μm

Production Riser

Table 7: Production Riser Data

Internal Diameter	10 inch (254 mm)
Wall and Insulation Thickness	97.7 mm
Internal Roughness	1.016 μm

RESERVOIR DATA

Reservoir pressure

The reservoir pressure for the four reference reservoirs used in this paper. These four main reservoirs are considered representative for this field.

Table 8: Reservoir Pressure

Reservoir	Reservoir Pressure (bara)	TVDSS (m/msl)
R-500NC	235.5	2419
R-600N	273.8	2332
R-605S	230.3	1855
R-635S	209.7	2162

Reservoir Temperatures

The reservoir temperatures, at depth, from each of the four reference reservoirs are presented below.

Table 9: Reservoir Temperatures

Well	MD (m)	TVD (m)	Temperature (^{0}C)
P500_1	2638	2275.6	77.2
P500_2	2332	2256.3	76.5
P500_3	2829	1921.0	64.6
P500_4	2496	2122.4	72.0
P500_5	2136	1909.8	64.2

P605C_1	3010	2360.7	80.2
P605C_2	3102	2419.5	82.3
P605_1	1584	1576.3	51.6
P605_2	2175	2167.1	73.4
P605_3	2319	1881.0	60.4
P605_4	2319	1881.0	60.4
P630_1	2609	2609.0	90.7
P630_4	2416	2386.8	82.0
P630_5	2014	1847.7	62.0
P670_1	2205	1955.8	65.8
P670_2	2029	1739.9	58.2

Well Productivity Index

The well productivity index assumed for all simulation is oil PI of 10 bpd/ psi. The table below shows the fluid data for the four reference reservoirs to be used in all hydraulic analyses for the field development.

Table 10: Fluid Characteristics

	Reservoir Characteristics			
	R-500 NC	**R-600 N**	**R-605 S**	**R-635 S**
Bottom Hole Pressure (bara)	253	269	210	230
Bottom Hole Temperature (^{0}C)	81	76	56	67
Saturation Pressure (bara)	245	263	200	225
GOR (Sm^3/Sm^3)	189	186	135	80
Bo Process (Sm^3/Sm^3)	1.54	1.50	1.35	1.20
MW dead Oil (g/mole)	167	172	190	250
Reservoir Viscosity (cP)	0.28	0.34	1.0	2.3
Bottom Hole Density (kg/ m^3)	660	684	741	820

FLUID COMPOSITION

A unified compositional PVT model was built and matched on experimental data from the four main reservoir fluids that made up the field. The well fluid compositions are shown table 11.

Table 11: Reservoir Compositional data

Component	**Reservoir Composition (% mole)**			
	R-500 NC	**R-600 N**	**R-605 S**	**R-635 S**
N_2	0.00	0.10	0.00	0.00
CO_2	0.18	0.58	0.61	0.18
C1	47.63	48.26	41.29	44.19
C2	5.18	7.02	2.98	1.92
C3	5.53	4.11	4.83	1.50
IC4	1.58	1.19	1.56	0.49
NC4	2.87	1.79	3.22	0.83
IC5	1.75	1.43	2.16	0.62
NC5	1.31	1.01	1.31	0.38
C6	3.43	3.06	3.86	1.25
C7	4.23	3.37	4.24	1.71
C8	3.69	3.61	4.16	2.19
C9	2.99	3.19	3.71	2.85
C10	2.49	2.42	3.15	2.50
CN1	10.50	12.20	8.00	22.50
CN2	4.85	3.50	13.80	4.80
CN3	1.80	3.19	0.93	12.09
MW Reservoir Fluid	79	81	98	138

PROJECT DESCRIPTION

No H_2S was detected in the initial reservoir fluid, but the maximum H_2S content to be used for design is currently evacuated at 100 ppmv. This project intended to consider a subsea close loop flowline from the well head up to the riser above the sea water level. The flowline has multiphase fluid from the well head to the process facility. The ambient temperature of the subsea environment is at 4^0C and at a high pressure necessitated by the water head. The Bottom Hole Pressure (BHP) about 260 bara, is assumed to be the highest pressure of the designed subsea system. The diagram below is the actual arrangement of subsea flowline systems from the well head through to the top- side.

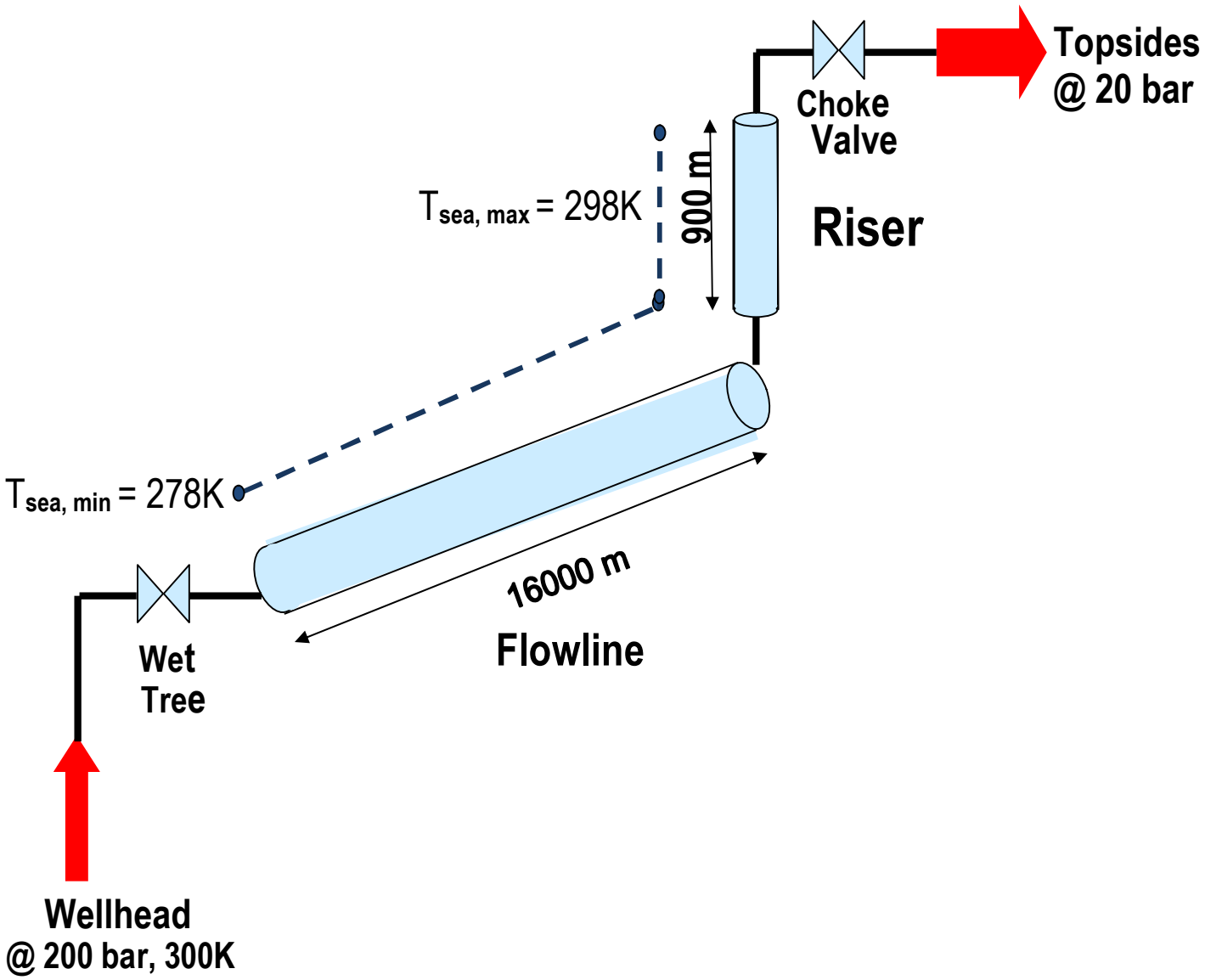

Fig 3: The above is a Schematic representation of the Sub sea flowline – Riser physical arrangement

DESIGN CONDITIONS

Design Assumptions

1) Length of Flowlines
2) Temperature along the pipe length
3) Heat conduction coefficient

Design constraints

1) Multiphase flow liquid
2) Bottom Hole Pressure as the highest pressure (Over 250 bar)
3) Field floor temperature is $4^{o}C$
4) The Hot Oil Return Temperature is at $40^{0}C$
5) Flowline cooling to HDT in 10hrs
6) Riser base is the weakest point
7) U value is = 3.0 W/m^2K

Conditions that necessitates Hydrate Formation

1) High pressure
2) Low Temperature
3) Presence of free water and gas molecules
4) Natural gas at or below its water dew point
5) High velocity or Agitation
6) Presence of more soluble acid gasses such as H_2S and $C0_2$

DISCUSSION OF RESULTS

Pressure temperature gas hydrates curve is generated at in-situ conditions using fluid characterisation software- PVTsim. The unified PVTsim model matched the combined fluid from the reservoirs. Peng Robinson Equation of State (EQS = PR 78 Peneloux) was used to generate the model fluid characteristics. PVTsim gives conservative hydrate formation check curve.

4.5
4.6
4.7
4.8

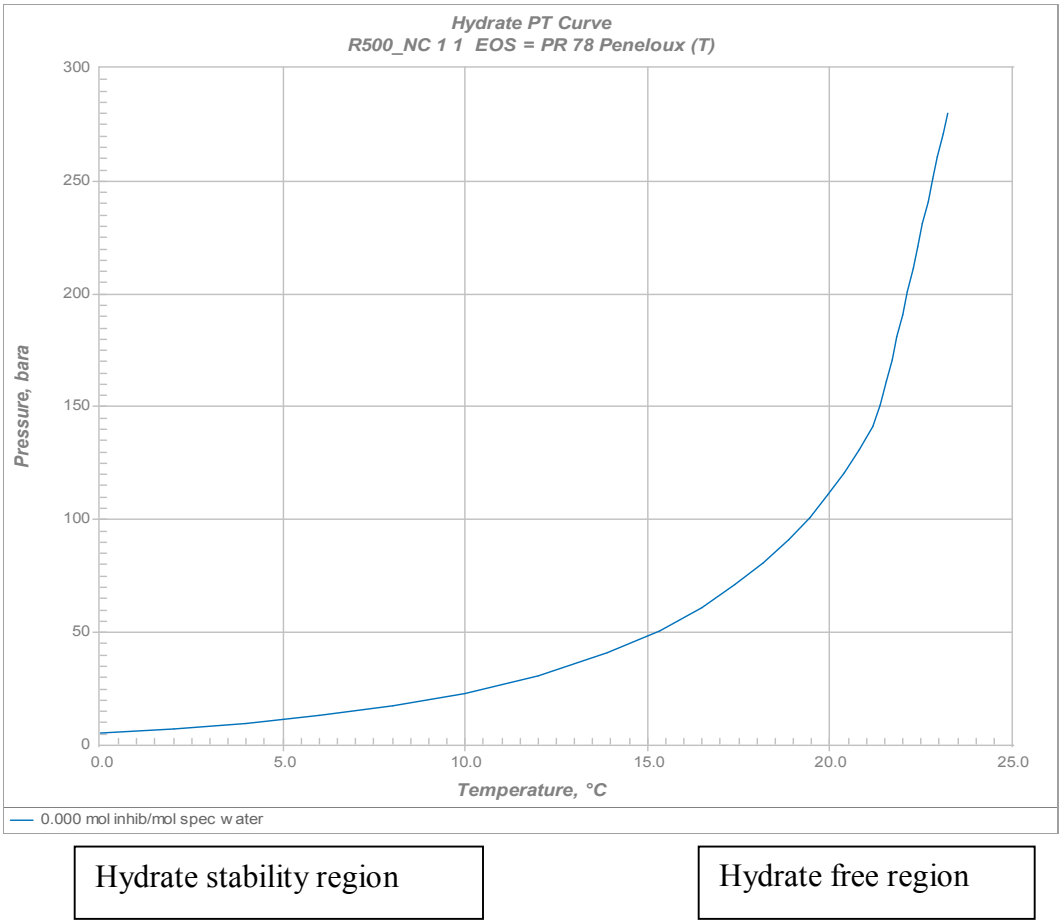

Fig. 4: Pressure- Temperature curve

The pressure – temperature curve is generated considering the reservoir pressure –about 260 bar as the highest pressure and taking the corresponding temperature which forms the HDT. It defines the temperature – pressure envelope at which the system must operate in a steady state and transient conditions in order to avoid the possibilities of hydrate formation. The region to the left of the graph is the hydrate stability region. The stability of hydrates increases with increase in pressure and decrease in temperature. While to the right of the graph is referred to as hydrate free region, at which the system shall operate to avoid hydrate formation. The project flowline was analysed for hydrate formation during steady state normal operations.The flowline temperature profile and hydrate subcooling temperature profile is shown in the graph below.

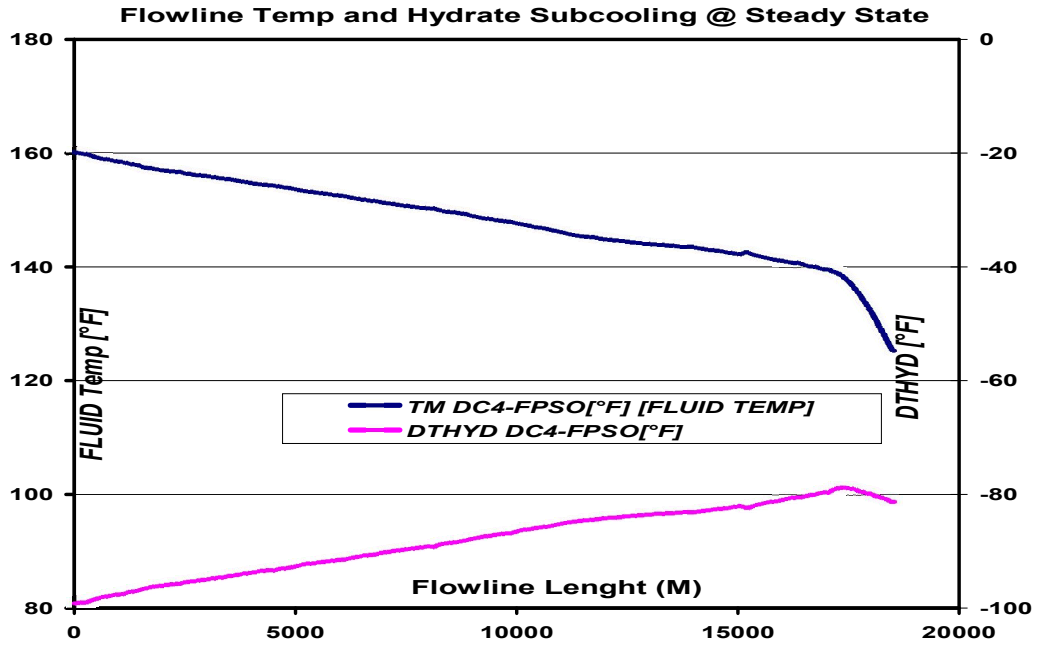

Figure 5- Flowline Temperature Profile in Normal Operations

At steady state normal operations the minimum flowline temperature anticipated is at the top of the riser is 120°F. The OLGA variable DTHYD is the hydrate subcooling temperature, which is the difference of the hydrate formation temperature and the insitu fluid temperature. A negative DTHYD indicates that hydrate formation would not be an issue of concern at steady state normal operations. This also implies that the selected insulation type is adequate at steady state normal operations. The project flowline is analysed based on unplanned shut-in transient condition for hydrate formation during operations

PROCEDURES

- Configure flowline with three different insulation type as shown below

Table 12: Insulation Type Material for Flexibility at FPSO Arrival

INSULATION COMPARISON		
MATERIALS	**THICKNESS (inch)**	**OHTC (U_{id}) [Btu/ft2-h-F]**
TYPE A	3.00	0.49
TYPE B	4.00	0.41
TYPE C	5.00	0.36
WT of steel pipe 1.25 inch		

- Produce a single well at minimum flow rate at 20,000 bpd
- Monitor oil return temperature at the top Side of FPSO @ 40^0C

A sensitivity study was done to get the type of insulation which would give the required hot oil temperature at the FPSO. The required hot oil temperature is 40 °C. A different insulation type of the flexible material at a supply flowrate of 20,000 bbl/d was studied.

The result of the simulation analysis shows that from the three insulation type looked at, it takes approximately 20 hours to heat up the flow line to achieve the required return temperature at FPSO topside. The difference in time required for the three insulation types to attain the return temperature is negligible. But, type A insulation material is selected since it has lower U-value and lower cost.

Hot oiling is a process of pre-heating the process facility (oil flowlines) with hot oil before actual production processes commenced to avoid hydrate formation. In the process heat is transferred from the hot oil to the flowline thereby keeping the flowline at a certain temperature before the actual production process begins. Otherwise there will be temperature drop which will lead to hydrate formation in the production flowline.

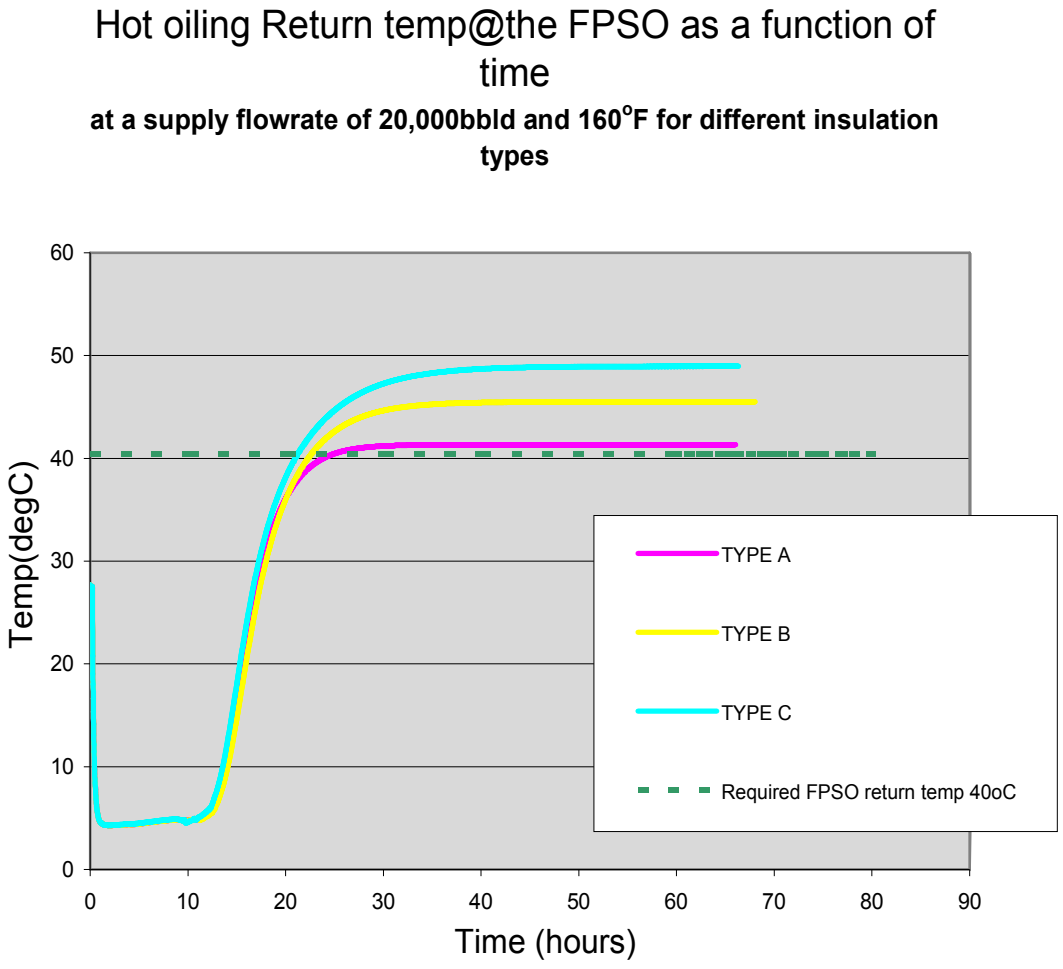

Fig .6: Hot Oil Return Temperature for Different Insulation Type Material.

The three insulation type materials satisfy the FPSO required return temperature at 40°C. Type C material gives the highest return temperature.

Flowline Cool Down Profile

- Achieve steady state production process

- Unplanned shut-in well and flowline
- Monitor the flowline temperature profile over time

The flowline was analysed for hydrate formation during shut down cool down at long intervals of time. As highlighted a flowline cool down to 10 hrs is required to be satisfied in the flow design. This condition is achieved with the insulation material selected which has a U-value of 3.0W/m^{2}k. The flowline, production system should be able to retain and sustain heat up to 10 hours. The graphs below show flowline profile temperatures at different cool down times.

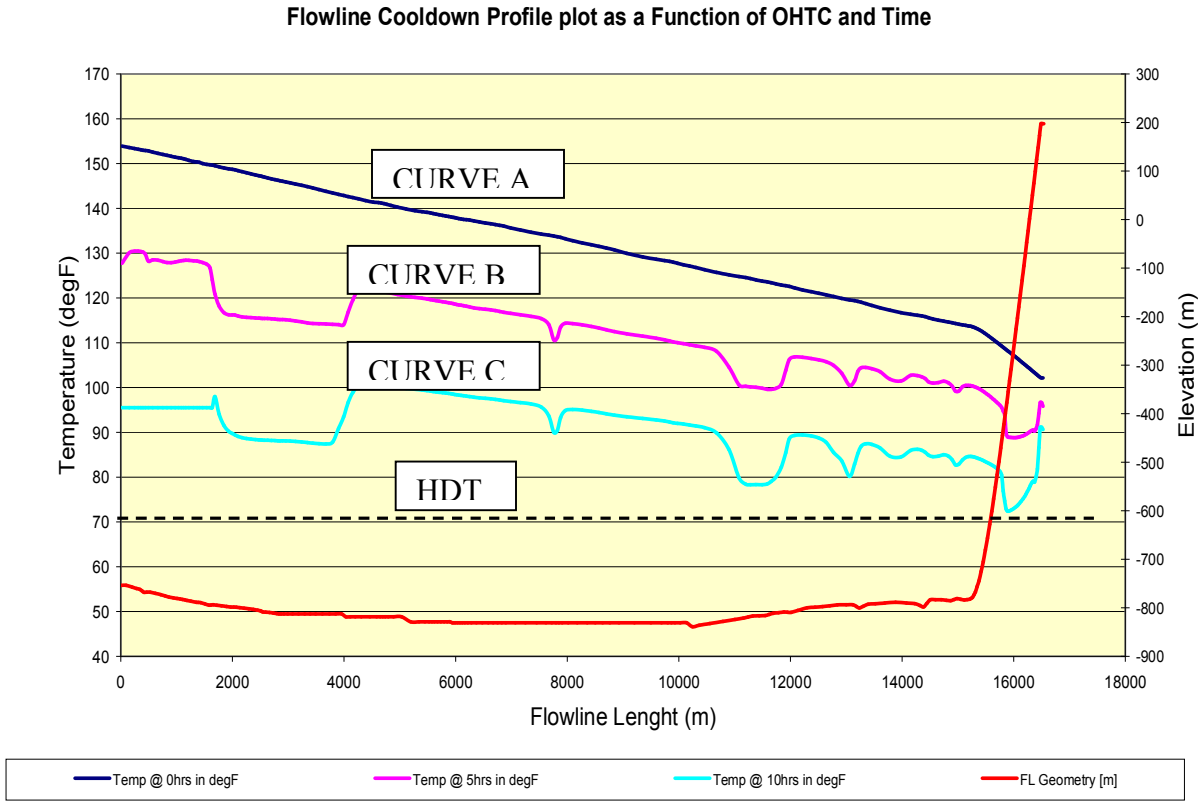

Fig 7: Flowline Cooldown profile

At cool down time 0hr corresponding to flowline shut-in, the temperature ranges profile ranges from 150^{0}F to 110^{0}F as shown in curve A in the graph above.

Also, at cool down time 5hrs corresponding to flowline shut-in, the temperature ranges profile ranges from 130^{0}F to 90^{0}F as shown in curve B in the graph above.

Furthermore, at cool down time 10hrs corresponding to flowline shut-in, the temperature ranges profile ranges from 95^{0}F to 75^{0}F as shown in curve C in the graph above.

The pockets along the slope of the graphs signify more Gas accumulation within those areas compare to other parts along the production flowlines. Gas expands more rapidly than liquids.

From the graphs, it is established that the system gives 10hrs for cooldown without the system temperature falling below HDT. This also infers that the system offers a maximum of 10hr within which to manage the risk of hydrate formation in the event of unplanned production system shut-in.

Flowline Blow Down Operation

- Production at steady state is achieved
- Unplanned shut-in due to sudden disturbance in the production system

- Simulate production shut-in condition
- Allow No Touch- Time of 3 – 4 hrs. This is a suitable time necessary to understand the nature of the shut- in condition
- If production system cannot be restarted after No Touch- Time, blow down flow line to HDP

The system simulation shows that it will take approximately 3.5hrs to blowdown the system to a safe pressure well above Hydrate formation pressure (HDP) in the event of unplanned shut-in.. This simulation is carried out from different water cuts of 0%, 50% and 70% as shown in the graph below.

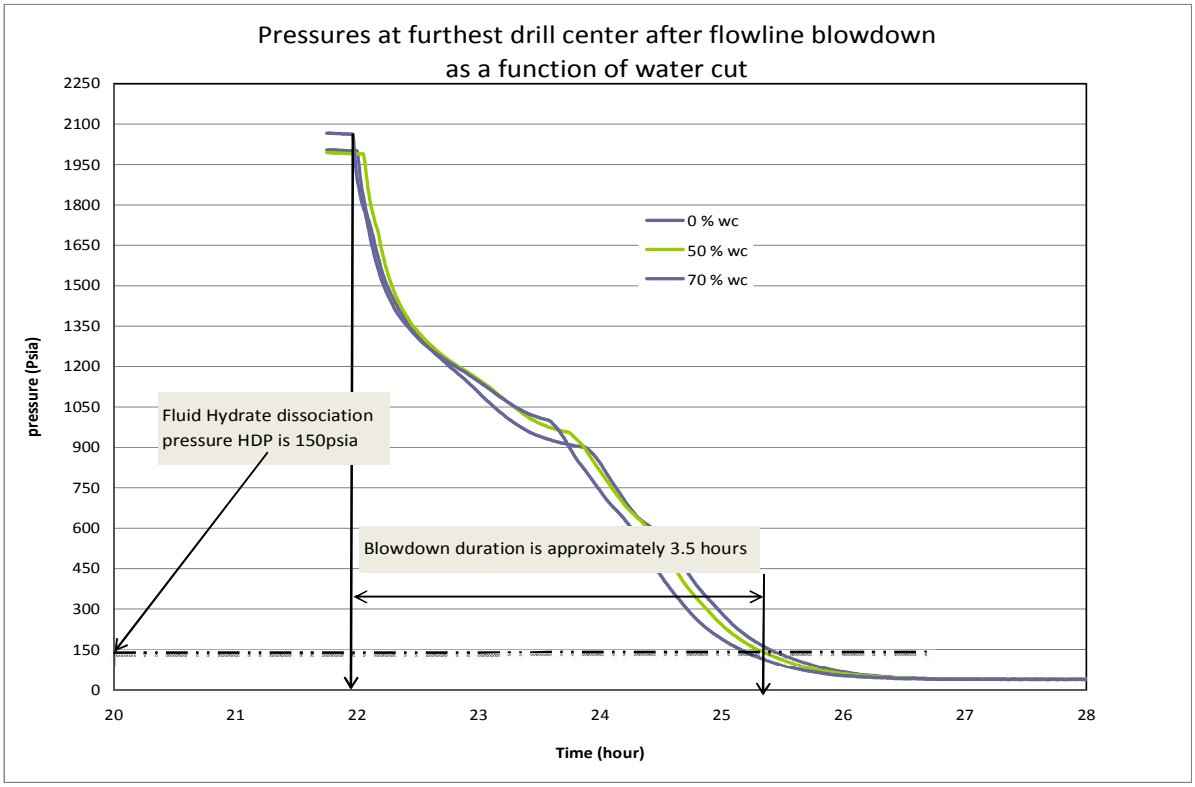

Fig 8: The blowdown pressure against time

A hydrate dissociation pressure of 150 psia (10.4 bara) is anticipated. From the PT- hydrate curve this would have to correspond to a temperature of less than 5°C to form hydrates, (<5°C, 150 psia) Analysis from the P-T curve inferred that the operating temperature of the flowline at any given time must not fall below the HDT- 74^{0}F. This is with only an exception of the use of hydrate inhibitors such as MeOH.

Type A insulation is recommended since it satisfies all flow assurance requirement of Oil Return Temperature of 40^{0}C with minimal cost in the production system.

The system can sustain life fluid for a period of 10hrs on an event of unplanned shut-in. On the other hand, the life fluid should not be allowed to remain in the flowline for more than 10 hrs uninhibited otherwise hydrate will form. A blowdown of 3.5hrs is required on this project to keep the production system free from hydrate plug. But, if blowdown is not feasible may be due to water hold up or steep flowline situations, then dead oiling is recommended.

CONCLUSION

The flow assurance challenges in this projects production system in terms of hydrates are well addressed and taken care of if these findings are adequately and strictly adhered to:

- Operating temperature of the production system must always be above 74^{0}F- HDT
- Operating pressure of the production system must always be above 150 bara- HDP
- FPSO Hot Oil Return Temperature at 40^{0}C at the top side
- The life fluid should not be allowed to remain more than 10hrs uninhibited in the flowline in the case of unplanned shut-in
- A blowdown time of 3.5hr maximum in the case of sudden shut-in

GLOSSARY

The following terms are referred to in this Technical work:

CHC = Cameron Horizontal Connector
Cv = Valve Characteristics
DC = Drilling Centre
FPSO = Floating Production Storage and Offloading Unit
ILT = In line Tee
FWHP = Flowing Well Head Pressure
FWHT = Flowing Well Head Temperature
GOR = Gas to Oil Ratio
MD = Measured Depth
MSL = Mean Sea Level
PI = Productivity Index
PIP = Pipe in Pipe
ROV = Remotely Operated Vehicle
SPS = Subsea Production System
SRB = Sulphate Reducing Bacteria
TOP = Touch Down Point
SOU = Subsea Distribution Unit
SPS = Subsea Production System
SUT = Subsea Umbilical Termination
TVD = True Vertical Depth
WTHP = Well Tubing Head Pressure
WTHT = Well Tubing Head Temperature
XMT = Christmas tree
BIT = Bundle Insulation Test
b/d = Barrels per day
FPSO = Floating Production Storage and Offloading
FSM = Field Signature Method
GOR = Gas-Oil-Ratio (Sm3/m3)
MDT = Modular Dynamic Tester
mScm/d = Million standard cubic meter a day
OCWR = Overall Control of Wells and Risers
OHTC = Overall Heat Transfer Coefficient
OPEX = Operation Expenditures
ppm = Parts per Million
QC = Quality Control
QRA = Quantitative Risk Analysis
RAM = Reliability, Availability and Maintenance
SPS = Subsea Production System
TIT = Tower Insulation Test
UFL = Umbilical and Flowlines
CDT = Cool Down Time
HDT = Hydrate Dissociation Temperature
HDP = Hydrate Dissociation Pressure
HFT = Hydrate Formation Temperature
LDHI = Low Dosage Hydrate Inhibitors
MEOH = Methanol
SCSSV = Surface Controlled Subsea Safety Valve
SSAT = Steady State Arrival Temperature

8/11/2011

UFR = Umbilical Flowline Riser
VIT = Vacuum Insulation Tubing

DEFINITION OF TERMS

Hydrate Dissociation Pressure (HDP) is the minimum pressure at which the system will operate without hydrate plug formation in the production system

Hydrate dissociation Temperature (HDT) is the minimum temperature at which the system will operate without hydrate plug formation in the production system

Flowline cooling to HDT in 10hrs - This in effect means that my production system should be able to retain and sustain heat between 10- hours to keep the system out of hydrate formation

U value (W/m^2K) - This is selected putting design intension, cost etc into consideration . The lower the U-value the better the insulation and the higher is terms of cost

REFERENCES

1. Bai, Y. Bai, Q. (2005), "Subsea Pipelines and Riser", 1st Edition. Elsevier The Boulevard, Langford Lane Kidlington, Oxford, OX5 1GB, UK
2. Cochran, S. and Gudimetla, R. (2004) " Hydrate Management: Its importance to deepwater Gas Development success", Word Oil, Vol. 225, PP.55-61.
3. Davies, S. R. Boxal, J. A. Koh, C. A. Sloan, D. E. (copyright 2008) "Predicting Hydrate Plug Formation in Subsea Tieback", SPE 115763
4. Guo, B. Duan, S. Ghalambor, A (2006) "A Simple Model for Predicting Heat Loss and Temperature Profile in Insulated Pipeline", SPE Production and Operation.
5. Hagesaether, L. Lunde, K. Nygard, F. (2007) "Reality check and aspects of transient operations of gas/ condensate pipelines", SPE projects, Facilities and Construction.
6. Hammerschmidt, E. G. (1939), "Gas Hydrate Formation in Natural Gas Pipelines", Oil and Gas J. , Vol, 37, No.50, 66
7. Hansen, A. B. Rydin, C. (2002) "Development and Qualification of Novel Thermal Insulation System for Deepwater Flowlines and Risers based on Polypropylene"
8. Janoff, D. Davalath, J. (2002) "Application of Insulation Materials for Deepwater Subsea Completion and production Equipment", OTC 14119
9. Luna-Ortiz, E. Lawrence, P. (2008) "An Integrated framework for model-based flow assurance in deep-water oil and gas production", ESCAPE 18
10. Saint-Pierre, T. Constant, A Khoi Vu, A (2002) "The Management of Flow Assurance Constraints", OTC 14169
11. Sloan, E.D. (2000), "Hydrate Engineering", Edited by Bloys, J.B., SPE
12. Zakarian, E. Larrey, D. (2009), "Systematic Investigation of Girassol Deepwater", SPE Production and Operation.

评吴耀琪先生的核育论

郑道

Recommended by Zhang Dongsheng

【摘要】21 世纪科学的“中国弦”或“核弦”，才真正具有生命传承共性的内蕴；“核弦”从种子到繁育，表达了一种自然传承规律。

[郑道．评吴耀琪先生的核育论． Academia Arena, 2012;4(2):55-61] (ISSN 1553-992X). http://www.sciencepub.net. 8

【关键词】核育论 中国弦 生存权 科学权

一、吴耀琪的“核育”原旨与发展

在西南交通大学经管学院教授高隆昌先生的推荐下，我们联系上吴耀琪先生。吴先生邀请我们关注他提出的“核育论”， 希望在哲学层面达成共识。第一是对科学的理解，第二是对科学知识来源的理解，第三是对科学表达工具的理解。于是我们之间进行了一些讨论和交流，现与大家共享。吴先生的自我简历介绍是：“中央党校超越之路研究员，西南交大兼职教授，核育论原创人，太阳热能‘黑箱’专利所有人，生物液态氢燃料模式发起人”。

1、吴耀琪教授对“科学”的理解是分：

1）公开标准；2）公共工具；3）可在实践中验证有作用。

2、吴耀琪教授又进一步综合为：科学的传统与创新。

1）其中他具体对“科学的传统” 的理解是分：a）数量标准，物体标准，单量纲；b）数学工具；c）物理实践，物质实践。

2）他具体对“科学创新” 的理解是分：a）性质标准，用关系显示，双主体。运动标准，多量纲；b）象形工具；c）社会实践。

3、吴耀琪教授提出的“核育论”，具体极大的社会意义和现实意义。因为一般说来，吴耀琪教授以上的理解没错。但吴耀琪教授是在 21 世纪这个特定的时代来谈“核育论”的，这已经不同于 20 世纪时谈的“核育论”。这是一个要求发达国家和发展中国家都要“改革开放”的转型时代，要求发达国家和发展中国家都要“共同富裕” 的文化强国时代。

21 世纪的社会和现实情况是，如果“核育论”是指一般的：1）公开标准；2）公共工具；3）可在实践中验证有作用。那么这一般也只是等价于普通教育或国民教育。即使这具体到对“科学的传统与创新”的理解，一般也只是等价于类似我国 20 世纪时的大众科普教育或大中专学校的科技教育。这种核育论实践，确实是取得了很大的成绩，符合吴耀琪教授的“可在实践中验证有作用”的标准；这正如李国杰先生所说：“青年科技人员更应该对老一辈科学家表示的敬重”。

所以我们不是说 60 年来的这种核育论有错，而是很有建设成就。例如屠呦呦在 2011 年下半年获得的拉斯克临床医学奖，屠呦呦和青蒿素不是一时间也还成为社会的热点吗？但青蒿素是我国 30 年前，得益于中医药古方的启示，而取得的被今天国际上誉为 20 世纪后半叶“最伟大的医学创举”的。因为新中国成立初期，就开始重视科学、重视人才，让从海外回来的科学家和国内自己培养起来的新秀合作，在非常恶劣的环境下，创造的令世界震惊的辉煌成果。老一辈科学家艰苦创业的精神值得继承，今天应有更加积极更有远见的人才引进和国内人才培养计划。

4、但也应该看到在国外，发展中国家在 20 世纪一般的普通教育或国民教育，是类似学校教育；而据说在阿富汗、巴基斯坦的伊斯兰语中，“学校”称为“塔利班”，如果这也是一般的如 20 世纪“核育论”的理解作的标准，那么“塔利班”即学校教育培养出的精英，领导的一些地区群众的活动，也许在联合国内仍是有争议的。

20 世纪的“核育论”，如果实践只有实用标准，这虽是我们中国人两千多年来的成功作法，但没有前瞻性的现代科学原理标准，是有欠缺的。有一则史料是：1864 年，普鲁士和德意志帝国的政治家、外交家、普鲁士王国首相俾斯麦预言：三十年后中国必败，日本必兴。俾斯麦的预言不幸而言中：1894 年，中日甲午战争，清朝政府的海军被日本打败。有人问俾斯麦，你当时何有如此准确的预言？俾斯麦的回答是：当时中国留学生一到欧洲，打听的是哪样东西便宜？哪样的枪炮厉害？好多买点回国，认为就能成为强人强国。这是一种败象。而日本的留学生一到欧洲，问的是欧洲有哪些先进的科学原理、学说？学成回国后，也大肆在国内宣传普及，这是一种兴象。两百多年来，先进的中国人已经注意到要把实用与前瞻性的科学原理结合，但在我国

国内的上下层人中，仍然是有争议和各行其是的。

例如湖南人在我国近代史上一直是开新风的省份，21 世纪湖南省的科技出版社出版的一套丛书，如《黑洞战争》、《存在之轻》、《伟大的超越》、《物理学的困惑》、《看不见的世界》、《量子夸克》等，又开新风。因为如果把这 6 本书综合归纳整理成一本大书，也可以称为“核弦”。我们关注到，我国对此有 90%的成人，包括大学生、教授、院士，看不懂这类前沿科学。甚至我国就是专业从事“核弦”的人，私下也对自己的研究没有信心。原因是，他们自己因为不是中国“核弦”的创始人，老是跟着老外的屁股走，又对中国自己很早以来独立创见的“核弦”或“中国弦”视而不见或看不起，所以有的才私下里对自己的研究说没信心。

那么是谁在强迫他们研究核弦呢？是国际大环境。例如据美籍华人学者、美国杜邦中央研究院退休院士、物理学家、现任《前沿科学》编委的沈致远教授，发表在 2008 年 6 月 1 日《科学时报》上的文章说，全世界有几千物理学家和数学家从事弦论研究，阿根廷、荷兰、瑞士、西班牙、加拿大等都有人在最前沿作出一流贡献。我国从事这方面研究的有几人？有人说真正在做弦论者不超过 10 人，这或许低估了点，但人数之少肯定与大国地位不相称，甚至还比不上某些小国。研究万物之理对物理和数学要求极高，甚至要发展出新数学方法，基础薄弱者不得其门而入。

据另我国不少媒体，宣传美国著名科学家斯莫林的《物理学的困境》一书中也说：“在美国，追求弦理论以外的基础物理学方法的理论家，几乎没有出路。最近 15 年，美国的研究型大学为做量子引力而非弦理论的年轻人一共给了三个助理教授的职位，而且给了同一个研究小组”。“因为弦理论的兴起，从事基础物理学研究的人们分裂为两个阵容。许多科学家继续做弦论，每年大约有 50 个新博士从这个领域走出来”。“在崇高的普林斯顿高等研究院享受有永久职位的每个粒子物理学家几乎都是弦理论家，唯一的例外是几十年前来这儿的一位。在卡维里理论研究所也是如此。自 1981 年麦克阿瑟学者计划开始以来，9 个学者有 8 个成了弦理论家。在顶尖的大学物理系（伯克利、加州理工、哈佛、麻省理工、普林斯顿和斯坦福），1981 年后获博士学位的 22 个粒子物理学终身教授中，有 20 个享有弦理论或相关方法的声誉。弦理论如今在学术机构里独领风骚，年轻的理论物理学家如果不走进这个领域，几乎就等于自断前程。”

如果仅仅是吴耀琪教授对核育“科学”原旨的标准理解也罢，但有的群众也想效仿“塔利班”那种战斗模式。例如有“否定相对论”网友 2012 年 2 月 6 日发表意见说：“当我看到支持相对论时，下面就不用看了。据我观察，人一旦相信了相对论就像相信了法轮功，这个人就算完了。法轮功分子没有一个能够改造过来的，相对论者也没有一个能够改造过来”。

“核弦”来自相对论等 20 世纪前沿科学的发展，而“否定相对论”者希望把 20 世纪以来国际前仆后继的前沿科学当作专政打击的对象，这是一种败象。即使这已不会成为国策，但如果说希望打击专政前沿科学的人是少数，那么国内讨厌类似看不懂的前沿科学的人，也许是多数。即使在号称中国科技城的绵阳，对中国人很早独立创见研究的“核弦”，也有类似“V5V5”的网友 2012 年 2 月 5 日发表意见说：“这种民科脑子真是坏掉了，发这种东西就像在三医院门口唱大戏”。曲高和寡，60 多年来的 20 世纪核育国民教育的实施，彻底改变了人们的生活。

那么我国真的不需要类似“核弦”等 21 世纪前沿科学的发展了吗？造成这种局面，难道和类似吴耀琪教授核育论的“科学”原旨标准理解的 60 多年的国民教育实施实践，没有一点关系吗？这虽不是“橘生淮南则为橘，生于淮北则为枳”，但 20 世纪后期国际的“核弦”核育的大环境，已经使得我国改革开放后国内出国留学西方的人，也不是如新中国成立初期从海外回来的科学家，当时他们在西方的学习，那么得心应手了。

1）据从美国回来的张操教授的博客报导，弦论的迅速发展，量子中国与量子美国的差距，中国人即使曾经在美国获得终生教授的物理学家，也只能“骂娘”。例如张操教授说，王令雋教授就是值得国内人更多关注中的一个。张操说，王令雋教授是他在美国留学时的同学加室友，现在是美国田纳西大学物理系的终生教授。在 2012 年春节的年初三，王令雋教授在回复他的信中，以指责伪科学家欺世盗名，把物理学界搞得污烟脏气为托辞，点名霍金和彭罗斯，把因果律都颠倒了，即他们主张时间是二维的，既有实时间，也有虚时间，而且虚时间比实时间更真实。王令雋最后愤愤地说：“对科学逻辑和事实的违背，莫此爲甚”。

2）张操说，在近日与美国王令雋教授的交流中，王令雋对现代宇宙学作了明确的批判。他张操和王令雋为什么虽然几十年不见，但经过各自独立的探索和思辨，居然是所见略同的朋友？为什么他们非常难得，相互支持，也不那么孤独？张操说，因为真理只有一个。

这说得好。正如张操教授所说，物理学的使命就是认识客观世界，解释客观世界。如果大家都秉着实事求是的科学精神去研究物理学的客观规律，不同的人应该能够得出同样的结论。也就是说，真理应该是收敛的理论。

3）但张操教授真懂量子中国吗？真懂量子美国吗？请听他的分析，张操说：“如果从一大堆假定或原理出发，建立一些方程，然后要求大自然服从这些方程式，并吹口仙气，赋予数学变量以物理意义，物理理论不需要经过科学事实和科学逻辑的检验，学术上就没有是非可言了。像时间倒转，虚时间，高维空间，暗物质，黑洞白洞，时空隧道，真空扰动，宇宙婴儿等等等等，都是一些完全违反科学逻辑和事实的伪科学。既然整个宇宙学界都在玩数学，那谁不可以玩？于是各种五花八门的荒唐理论纷纷出台。这样的理论当然不可能有一致的结论。所以，伪科学的理论是发散的，不收敛的。他们今天说宇宙是封闭的，最终会导致大湮灭；明天又可以说宇宙是开放的，大湮灭不会发生。宇宙的最终命运，湮灭还是不湮灭？只取决于质量密度的 10 的 120 次方分之一的差别。一个理论不稳定到这步田地，不正是这理论荒唐的一个证据吗？所以，只要我们以伽利略的殉道精神坚持真理，一定能够把物理学从这种伪科学中解救出来。不要怕孤独。不要怕路远。做学问要耐得住寂寞，经得起压力。亦予心之所善兮，虽九死其犹未悔”。

4）研究以上张操和王令雋教授的言论，不知张操和王令雋等同仁在美国学到些什么？既然霍金和彭罗斯类似的现代前沿科学都是伪科学，他们何必要到美国去？甚至还呆着不归？他们去美国目的是什么？他们学懂了现代前沿科学了吗？

二、“核弦”等 21 世纪前沿科学错了吗？

格拉肖 1979 年与温伯格、萨拉姆共同获得诺贝尔物理学奖，是世界著名的理论物理学家、美国科学院院士。他 1932 年生于纽约，1954 年毕业于康奈尔大学，1958 年在哈佛大学获得博士学位，1958-1960 年在哥本哈根工作。1966 年到哈佛大学任教，1967 年起任教授。主要研究领域是基本粒子和量子场论。1976 年还获奥本海默奖，1991 年获 Erice 科学和平奖。格拉肖多次来过中国，他的儿子曾在南京大学留学。据何祚庥院士讲，和他一起获诺贝尔奖的温伯格就赞扬过层子模型。据《伟大的超越》一书介绍，格拉肖也曾发誓要让哈佛远离弦理论，但他却无法阻止阿卡尼哈默得和兰德尔等他的学生和班底，成为被公认的当今全球最一流的超弦理论学家。

1、如今要去格拉肖办公室，人们必须穿过一个入口，而入口两边正是阿卡尼哈默得和兰德尔的办公室。阿卡尼哈默得，又翻译为尼玛·阿卡尼-哈米德，是哈佛大学理论物理学家。他的父母是两个伊朗物理学家，他们辞去原来的大学职位来到美国休斯敦，1972 年阿卡尼哈默得在这里出生。不久，他家搬回了伊朗。伊朗 1979 年爆发革命，因为他的父母极高的科学地位以及与西方的联系等政治问题，被迫流亡多伦多。阿卡尼哈默得着迷父母的专业，进大学选择了数学物理专业，拿到了理论物理博士学位，1997 年进入斯坦福线性加速器中心。

莉萨·兰德尔（Lisa Randall）1962 年生于纽约，读高中时就是享有盛誉的“西屋奖学金”的获得者。兰德尔多年来潜心研究引力、时空的额外维度和弦理论。她的代表著作《弯曲的旅行：揭开隐藏着的宇宙维度之谜》一书，由于深入浅出地谈论了宇宙的故事，一举入选《纽约时报》2005 年“100 本最佳畅销书”之列。2007 年，她又被美国《时代》杂志评选为全球“100 名最有影响力人物”之一。她和约翰霍普金斯大学的物理学家拉曼·桑卓姆，提出的兰德尔-桑卓姆（RS）理论，为一种不同于广义相对论的、关于引力如何塑造宇宙的过程，提供了一种数学描述膜世界模型，

1）从阿卡尼哈默得，使我们想到伊朗 1979 年伊斯兰革命后的科学，之所以有很大的发展，也许伊朗国内注意到类似阿卡尼哈默得这样的伊朗人，在西方学习前沿科学的进展方向，而暗中不动声色地在进行追赶。1978 年伊朗前国王巴列维与来访的华国锋举行会谈，1979 年华国锋同志邀请伊朗国王巴列维来我国访问，伊朗国内因动乱，巴列维回国途中，被推翻。当前，世界已进入了高科技时代，实现发展权就是要让人民平等地参与量子世界科学权的发展，全面享有量子世界科学发展的成果。因为减轻和最终消除贫穷，也是量子世界科学权发展的优先选择。

2）阿卡尼哈默得和兰德尔虽是在各自研究，但其成果都能相互配合。阿卡尼哈默得 2006 年 34 岁时就被美国著名的《大众科学》杂志，评为世界上前十位的“科学才子”。他是 30 岁时从哈佛结束全部学业，成为一名物理学教授，选择研究第五维的。目前阿卡尼哈默得是隐藏的额外维度、暗物质、弦/膜理论等研究，在欧洲大型强子对撞机(LHC)上实验检验的推手之一。因为 LHC 将粒子撞碎而释放出的能量，或许就足以使粒子脱离三维空间的束缚，让我们一窥神奇的高维世界。而在现代物理学理论中，两个质子在 LHC 中对撞产生出电子和其他粒子，它们的能量既有可能是 1TeV，也有可能是 1TeV 的整数倍，例如 2TeV 或 3TeV。如果观察到了这种能量倍增现象，这就说明撞击导致了粒子在额外维度中发生振荡。除此之外，不论是常规的粒子过程，还是暗物质粒子之类的奇异过程，都无法作出解释。阿卡尼哈默得说：理论家清楚知道做实验的人在找什么，这次理论家说的是“也许这会发生，也许那会发生。”

而他早在 2004 年就开始担心，许多理论家可能没做好准备，面对欧洲粒子物理实验中心即将得到的大量数据。他对最初大型强子对撞器实验奥林匹

克的构想是，实验者会根据超越“标准模型”的未知物理学，创造出仿真数据组，来当做真实资料分析，接着再将他们的规画公诸在理论学家面前。早在 1998 年，阿卡尼哈默得（Nima Arkani-Hamed）在哈佛大学就和纽约大学的德瓦利（Georgi Dvali）及史丹佛大学的迪摩波罗（Savas Dimopoulos，以上三人简称为 ADD），提出了著名的 ADD 理论，假设了一张三维膜，存在于有两个超大额外维度的空间中。像 RS、ADD 或其他较新的模型，都将被大型强子对撞机检验。

3）从以上可见，从事额外维度、暗物质、弦/膜理论等研究，是为着人类未来寻找更先进的能源、材料和环境而来。吴耀琪教授的“核育论”，虽然不是指“原子核”之类的教育，但人类进行了两千多年的物质结构探索，从原子、原子核的球面图像扩容到孤子链、里奇流的弦链图像，也可称为“核弦”，我们称为“中国弦”。这里“中国弦”和“西方弦”的区别，中国球面图像是扩容的，不像西方弦球面图像和弦链图像是分开的。吴先生的“核育”是指生命传承的共性，核指种子，育指繁育；核育论是一种表达生命传承规律，从哲学到实践层面纵向创新的系统理论。包括行动世界观，包容方法论，象形思维工具。重要功能是为人本世界“怎样做”提供基础理论。

2、其实 21 世纪科学的“中国弦”或“核弦”，才真正具有生命传承共性的内蕴；“核弦”从种子到繁育，表达了一种自然传承规律。到 2012 年“中国弦”用里奇张量、泰勒弦和庞加莱猜想外定理等方法，解决 21 世纪两朵乌云暗物质、暗能量，以及超伴子、EPR 超光速隐形传输、希格斯大质量等难题。李政道先生说：物理学不是数学；数学比较容易，物理更难。所以很少有人读懂物理。例如彭罗斯的《皇帝新脑》一书对爱因斯坦的广义相对论方程包括的韦尔张量和里奇张量，虽说得直观明白：韦尔张量囊括类似平移运动的相对加速度，对球面客体单向的拉长或压扁作用；这与牛顿力学的性质对应；而里奇张量囊括当球面客体有绕着的物体圆周运动时，被绕着的物体的整体都有一个纯粹向内的加速，产生有类似向心力的扩张或收缩的缩约、缩并作用。但几乎没有多少人弄懂。也许是看成类似科里奥利加速度矢量，但科氏力仅是一般的推算分析。

1）里奇张量奇妙的是，似乎已经包含了韦尔张量，即类似牛顿引力在地球的潮汐效应。

能说明射影里奇张量整体效应的，是麦克斯韦的电磁场方程：变化的电场产生变化的磁场；变化的磁场产生变化的电场。所以彭罗斯的解释是：“黎曼=韦尔+里奇”。韦尔张量，韦尔是测量类似自由下落的球面的潮汐畸变，即形状的初始变形，而非尺度的变化。里奇张量，里奇是测量类似球面的初始体积改变。这与牛顿引力理论要求下落球面所围绕的质量，和这初始体积的减少成正比相合。即物体的质量密度，或等效地能量密度（$E=mc^2$），应该和里奇张量相等。

简单地说，黎曼曲率描述的是引力场，黎曼张量只是反映时空几何，描述引力场的是度规里奇张量，是黎曼张量的缩并、缩约。对这种“缩并力”，彭罗斯再解释说，爱因斯坦方程存在一个称作能量----动量的张量，它将有关的物质和电磁场的能量、压力和动量都组织在一起。他把这一张量叫做能量，爱因斯坦方程则粗略是：里奇=能量。正是在能量张量中“压力”的出现以及为使整个方程协调的条件要求，使得压力对体积缩小效应有所贡献。那么不涉及韦尔张量吗？不是的。韦尔张量引起空虚的空间里感受到潮汐效应，爱因斯坦方程意味着存在将韦尔张量和能量相联系的微分方程的结合结构域。彭罗斯对这种韦尔张量重要性的推证，实际上是反过来又把部分里奇张量效应包含在韦尔张量中。但彭罗斯正如牛顿没有解决好韦尔张量超距的引力潮汐畸变一样，也没有解决好里奇张量的超距作用。因为物体在圆周运动的对称点，里奇张量也有类似对称超距的引力。这种作用传输是隐形的，可以是光速，也可以是超光速。

但彭罗斯继续阐述了里奇张量和韦尔张量这种结合结构域的产生原理。他说要理解该结合结构域，还可以射影麦克斯韦的电磁场方程电场 E 和磁场 B 的结合结构域。因为韦尔张量韦尔实际是引力场的测定；韦尔的“源”是能量张量，这与麦克斯韦的电磁场的电场 E 和磁场 B 的源，是麦克斯韦电磁场理论的电荷和电流的结合结构域的情形相似。这种观点实际是将“麦学”引向“里奇张量”和“里奇流”统一的结合结构域；这里“电荷”对应里奇张量圆周运动的“源”效应，是类似彭罗斯的“扭量球”图像。“电流” 类似“里奇流”，对应韦尔张量平移运动的“流”效应，可联系类似傅里叶级数、泰勒级数展开式变换的“孤子链”，以及隐形传输与宇宙弦。

2）以上也包括了我们所说的“中国弦”或“核弦”研究。“中国弦”在 20 世纪 80 年代就开始的这种从“扭量球” 联系类似傅里叶级数、泰勒级数展开式变换的“孤子链”的解读，可对比 2003 年 10 月，彭罗斯到普林斯顿高等研究院与弦论学家威藤讨论后，威藤才把彭罗斯的扭量理论和他的弦论結合在一起，发表的一篇 97 頁的重量級论文。从哈佛大学刚转任到普林斯顿高等研究院的阿卡尼哈默得，正是在这时一头栽进这门新领域的。阿卡尼哈默得说：“我这辈子从未对物理感到如此兴奋。这个领域在全球約 15 人日以继夜地努力下，正迅速发

展”。所谓的“扭量球”，就如看起來像是围绕着一个旋转粒子的面旋、线旋、体旋等三旋动画视频。

3）如此抽象，不知张操和王令雋教授学懂了里奇张量没有？如果没有学懂，又骂是伪科学，他们要去殉道，我们说不必要。如果他们死活要去殉道，百个、千个也难阻挡“量子中国科学百年战略”。但中国科学家中，也有懂得知己知彼的人，如有一个故事是说，中科院今天最著名的数学家之一的王元院士，看不懂他教的研究生张寿武研究的抽象数学。张寿武只是一个 1962 年才出生在安徽和县西埠镇五星大范村的放鸭娃；这类事也出现在中山大学。

当时张寿武还是一个大学生，可以给中山大学的数学教授们讲课。张寿武后来在法国和美国深造后，今天已是公认的世界一流数学家。这说明我国人权的生存权、发展权的基础科学权，从以前的科普教育已到“量子中国”转化的时候。道理是我国 90%的成人，包括大学生、教授、院士看不懂前沿科学类似超弦理论的研究，而现代高科技又源源不绝从这些基础研究中创新出来，如互联网的出现就是著名的一例。这使得我国不得不向西方发达国家用高价购买，而且还买不到。

4）以“量子中国”类似超弦理论的前沿科学领域为例，目前我国数学和物理等技术和相关人才在国际上处于第二方阵前沿，即发展中国家前沿，尚未进入第一方阵。在“量子中国”领域，我国除科学殿堂外，主流长期以来是在做跟踪模仿研究，真正做与国际水平接近的科研工作还不到十年，数学和物理等技术积累远不如国外。至今为止，类似超弦理论的前沿科学领域有较大影响的新学科方向几乎没有一个是国内学者开辟的。为什么大量的人才依然在海外？那里没有世界前沿科学基础研究公认的成果和产品，能有这种现象吗？目前中国有 20 多万留学人员就职于国际知名企业、高水平大学和研究机构，取得副教授或相当职务以上的高层次人才约有 1.5 万人。他们大多在 35-50 岁之间，正处于创新创业黄金时期。所以我们说吴耀琪先生的“核育”概念是个好概念，是说 21 世纪的“核育”主要是指“量子中国”的科学普及教育。

三、中国的生存权、发展权万岁

这是 21 世纪的一场“文化战”----如果把前沿科学当作专政打击的对象的话。

但也可像青蒿素一样把“战争”变成一种“科学转化”。这具体地说，类似青蒿素把中医药变成了一种“转化医学”。然而类似这种转化医学研究，有要解决的两大问题一样：一是中医药语言现代化的转化问题；二是中医临床及中药创新药物研究的现代化问题。语言现代化可以通过规范来解决，而中医药研究现代化却不那么容易。转化医学热潮已经到来，但有一点可以肯定，绝对不是原来的中药开发研究。建立在“量子中国”理念上的转化医学，是中西医的共同点。中医、西医学界应消除隔阂，携起手来，共同服务于人类健康。“量子中国”也一样。

1、但国内类似“否定相对论”者的“文化战”，和青蒿素的“科学转化”类似，解决起来仍然是艰巨的。有两位网友“蒙童”先生与“土生金” 先生的谈话，说明我国又一次正处在“量子中国科学百年战略”的十字路口。蒙童说：“土兄啊，我也是个非专业人士，但关注基础科学的新进展---因为对我的研究课题有着新的启迪.....”。这从蒙童身上，看得出希望有“量子中国科学百年战略”的实施。但“土生金”更强调，原来的科普路线和听令的科学家的作为。

土生金是这样说的：“基础理论研究与应用技术研究有区别，科学发展一日千里，科学技术日新月异。可是，科学知识更要广泛普及；不能通俗易通，为社会公众所理解和接受，再先进的东西，也发挥不出效力，还是没用，等于没有啊。”从土生金身上，看得出含有“赶不上，不如不赶”的意思。土生金的理由还有：“美国养十几只航母，年军费千亿，不打仗，只赔钱，事实上是不良资产。土生金洞察古今，明中华千秋万载之大道：经书用金子写就，不如废铁多多啊。得人心者得天下，科学知识也是一样，即使是真理，不能普及于大众让人接受和认可，智慧之光除了枯萎，最多只是骷髅。学以致用，昨日中国最好的数学家华罗庚，把理论数学推广到应用，为数学力学等方面，做出了极大地贡献。我们建设好人间，让它比天堂更好，必然近在眼前。”

1）我们真诚地希望吴耀琪先生的“核育”不受已有的成就的影响，放眼世界跟上时代。中华民族是世界上最有智慧的民族之一，运用在量子中国与量子日本相互追逐近 60 年上，真是人类科学史上罕见的传奇。大国和平崛起的竞赛，中国传统有两类智慧：第一类战略是说对方错了，另立方法竞争；第二类战略是“田忌与齐王赛马”，相同方法竞争。在与西方的科学竞赛中，由于我国的国情与制度的不同，这决定了我国只能公开选择第一类战略占大多数。但自然科学不同于社会科学，自然规律更多是统一。战略与智慧就成了悖论，但量子中国却“化腐朽为神奇”。

2）这就是众所周知的，量子中国起步较晚；而“里奇张量”也在社会科学领域起作用----但也正是在新中国建立后，才能把这变成创举：毛泽东同志为翻开新中国科学千里之行始于量子足下的第一步，采取了用第一类战略的大多数掩护第二类战略的极少数。坚持第一类战略既能维护我国的原则，也能用 20 世纪前类似促进工业革命的成熟科学原

理，全面推进国家的建设。虽然这使第二类战略的极少数很难生长，但也是对其一种磨炼和自然选择。所以第二类战略必然在第一类战略类似“钱学森之问”的效果的释放中，自然会跟随百年生聚，百年打拼而造福世界造福人类。这难道不是“化腐朽为神奇”吗？因此，有人称它为“量子中国科学百年战略”。

3）吴耀琪教授说他的“核育”，是从哲学到实践层面纵向创新的系统理论。这包括行动世界观，包容方法论，象形思维工具。重要功能是为人本世界“怎样做”提供基础理论；当前的使命主要有传承中华文脉，超越以物为本的科学，建立以人为本的“容学”。

这里可见吴先生的核心是批判，“容学”不容。他说：现在许多人把自己当成了物，违背了人性，就会生病。美国的精神病发病率最高，中国精神病（抑郁症）的增长率最快。而许多人对幸福，可以讲出许多概念与大道理，但是，不知怎样做。其次目前中国的政府或者国有企业的领导，面对巨大物质利益的诱惑，一些人成为“贪官”而毁灭了前程。

2、吴耀琪先生说：“中华文化负责形而上，西方文化负责形而下。我们知道物质向下看，存在分子、原子、量子等运动规律，这是西方文化的贡献。可是，从物质向上看，存在哪些规律呢？这是东方文化的责任”。现代科技的发展，使东、西方文化在系统层次互相促进发展。世界正转向东、西方文化整合的时代。《核育论》应用先进的科技成果研究中华文化系统化的路径，使用象形工具表达研究成果，这样，就让我们在日常生活、工作中使用工具传承中华文脉，并解决面临的难题。但吴先生没有提到量子模具类似孤子链的象形工具，而只留在类似化学量子能的阶段。

1）提供行动种子。提供得时得机的项目。例如，太阳热能“黑箱”项目，生物氢能项目。让资产由百万级变成百亿级。

2）建设人本世界。从世界观，方法论到实践工具，虚、实结合建设人本世界。东、西文化整合，哺育人类共有的文化。

3）吴先生说，理解《核育论》，需要在实践中感受。例如：A）怎样做人；B）幸福怎样做；C）团队怎样做；D）智慧怎样做。社会调查表明：现代人面临难题的根源，主要是人性的迷失。《核育论》以此为机缘，为现代人遇到的难题提供“解脱”的操作方法与工具，通过感受人间的正道，使人心向善，人生圆满。《核育论》将为我们提供关于人的先进定义，科学内涵，以及怎样做人的简便方法与工具，提供“能人”实践模式，让团队释放巨大的聚合能；为领导的精彩人生，提供系统指导方案。

2、我们知道，“核育”概念和提倡“核育”，是一个很好的创见；也需要大家的共同努力，才能完善。《国际歌》中说：“从来就没有什么救世主，也不靠神仙皇帝”。要创造人类的幸福，全靠我们自己！那么我们自己又靠什么呢？我们中国认为，生存权和发展权是首要人权，没有生存权、发展权，其他一切人权均无从谈起。那么生存权、发展权的基础又是什么呢？是科学权！

1）例如说，中国人民有过长期遭受外来侵略和殖民统治的遭遇，国家主权沦丧，社会动荡不宁，人民生灵涂炭，饥寒交迫，毫无尊严可言。这是中国没有黄金和白银吗？这是中国经济不发达，不是世界强国吗？不是。据《白银帝国》一书研究，在西方侵略之前，我国是世界第一经济大国、白银大国。但因我国自古以来就深受儒家文化的影响，中华文明五千年的灿烂，正是有了以儒家文化为代表的中国文化，中国才始终强调是以华夏/汉族为本去同化四方民族。可以说，近代中国人流落在国外，大多数是帮工，而不是传授先进的科学原理。这是因历史上、传统上，士大夫们深受儒家以“夏善变夷蛮”文化的影响，这虽不是主要强调类似西方和反西方民族鼓吹的恐怖和侵略，但客观上也加剧不让中国人有科学权。所以这才是没有在中国发展出强大的近代和现代科学，这也是造成国家不独立、人民的生命安全没有保障的根本。

3、即人权没有生存权、发展权的基础科学权，其他一切人权都无从谈起。

1）中国人民为此进行了 100 多年的斗争，在大陆建立了新中国。我国政府经过 60 多年的努力，其中包括对西方成熟的经典的近代和现代自然科学技术的普及，基本上解决了人民的温饱问题，实现了人民的生存权，这是一项了不起的成就。但中国的总体经济发展水平和人民生活水平与西方发达国家相比还有很大差距，人口的压力和人均资源的相对贫乏还制约着中国社会经济的发展和人民生活的改善。在世界 192 个国家和地区的财富排名表中，中国仍然居倒数第三十一位。

2）由于近代和现代自然科学是不断发展的，特别 20 世纪相对论、量子论、基因学说的出现，1949 年新中国一建立就逼迫我国向量子中国转型。但我国经济基础还比较薄弱，一遇天灾人祸，人民的生存权还会受到威胁。我国现在还有 5000 万贫困人口，约占人口的 5%；已脱贫的人口，还存在防止返贫的任务；我国每年仍净增一千多万人口，人口的压力不断带来生存、就业、住房等一系列问题；在经济体制转型中，如何解决大批城镇职工的下岗问题，使他们实现再就业、享有生活保障和摆脱贫困，也是摆在政府面前的一项严峻任务。我国还有 1.5 亿文盲，每年有许多儿童因贫困而辍学。实践说明，向量子中国转型，必须且必然需要“量子中国科学

百年战略”。

3）但对西方成熟的经典的近代和现代自然科学技术的普及教育实施证明，它们虽然是中国政府和人民维护和促进人民的生存权和发展权仍然的首要任务；这也不是说，成熟的经典的近代和现代科学技术的普及教育不行，恰恰是因为它很成功，所以才有人说：“过去 30 多年，低成本劳动力为经济快速增长做出了巨大贡献，但这不仅在经济上难以持续，也将带来道义上的后果。过去中国人均 GDP 七八百美元，现在已是几千美元了，还照一二十年前的作法是不行的，于情于理也说不通。企业长期依赖廉价劳力搞加工贸易，也缺乏自主创新的动力。伴随着国内外经济的进步，这种落后的发展方式已经越来越行不通，走不动了。”

参考文献

[1][美]伦纳德·萨斯坎德，黑洞战争，湖南科学技术出版社，李新洲等译，2010 年 11 月；
[2]王德奎，三旋理论初探，四川科学技术出版社，2002 年 5 月；
[3]孔少峰、王德奎，求衡论---庞加莱猜想应用，四川科学技术出版社，2007 年 9 月；
[4]王德奎，解读《时间简史》，天津古籍出版社，2003 年 9 月；
[5][美]弗兰克·维尔切克，存在之轻，湖南科学技术出版社，王文浩译，2010 年 4 月；
[6][美]保罗·哈尔彭，伟大的超越，湖南科技出版社，刘政译，2008 年 4 月；
[7][美]L·斯莫林，物理学的困惑，湖南科技出版社，李泳译，2008 年 4 月：
[8][美]斯蒂芬·韦伯，看不见的世界，湖南科学技术出版社，胡俊伟译，2007 年 12 月：
[9][英]安德鲁·华生，量子夸克，湖南科技出版社，刘健等译，2008 年 4 月；
[10]叶眺新，中国气功思维学，延边大学出版社，1990 年 5 月；
[11]刘月生、王德奎等，“信息范型与观控相对界”研究专集，河池学院学报 2008 年增刊第一期，2008 年 5 月。

2/11/2012

一个备用的教案

谭天荣

青岛大学 物理系 青岛 266071
ttr359@126.com

Abstract: 按照我的意见，《自然辩证法》是一本没有定稿的书，其中的某些论点，对于一个没有自己重踏恩格斯的思路的读者是不可能理解的。这里我举一个例子，在该书的开头，恩格斯写道："力学，出发点的惯性，而惯性只是运动不灭的反面表现。""惯性"这一用语在这本书中只在这里惊鸿一瞥，以前不曾出现，以后也不再出现。这句话是什么意思，众说纷纭，迄今没有一个哪怕是字面上说得通的看法。爱因斯坦是诚然一个卓越的物理学家，但他肯定不知道恩格斯这里说的是什么意思。

[谭天荣．一个备用的教案． Academia Arena, 2012;4(2):62-63] (ISSN 1553-992X). http://www.sciencepub.net.9

Keywords: 力学; 惯性; 物理学; 数学; 《自然辩证法》

我是一个物理教师，也教过几年高等数学。有一次当我讲完关于"导数"的定义时，一个学生问我一个课外的问题：为什么"负一"乘"负一"等于"正一"。当时已经下课了，我在自己家里为他给出如下回答：

我们开始学算术时，总是把一个算术式与某一"日常生活中的实例"联系起来，例如，把"一加一等于二"这个算术式与"一个桃子加上一个桃子得到两个桃子"这一实例联系起来。一个算术式有了这样的实例，我们就理解了，一旦没有这样的实例，这个算术式就成了"无法理解"的。

像这样，我们把分数"三分之二"理解为三个人分两个桃子时，每个人分得的份额；把"负数"理解为家庭收支中的"债务"，等等。但我们的日常生活领域太狭窄，远不能为所有的算术式提供实例，我们不理解为什么"'负一'乘'负一'等于'正一'"，正是因为我们一时找不到对应于这一算术式的实例。或许，有人生活经验极为丰富，能为这个算术式乃至其他更复杂的算术式找到实例，但只要他局限于"寻找对应的实例"这样的理解方式，他就早晚会遇到一个界限，在这个界限之外的算术式，就成了他所不理解的。

然而，如果放弃这种理解方式，就有可能越过这一界限，例如，"负一乘负一等于正一"这个算术式可以按照如下方式来理解：

第一，三加负一等于二，二加负一等于一；

第二，二乘一等于二；

第三，从第一步与第二步我们得到："三加负一"乘"二加负一"等于二；

第四，展开"三加负一"乘"二加负一"，得到四项之和，其中有三项不涉及负数与负数之积，从而是我们已经接受的算术式；而第四项则正是"负一"乘"负一"。借助于已知的运算规律，可将前面三项合并，得到"一"。于是我们得到："三加负一"乘"二加负一"等于"一"加上"负一乘负一"。

第五，从第三步与第四步我们得到："'一'加上'负一乘负一'等于二。"

第六，将"一"移项，从第五步得到"'负一乘负一'等于'正一'"。

在这六步中，我们一方面应用了已经接受的算术式，另一方面又应用了算术中的交换律、结合律、分配律以及移项等已知规律，这就表明，按照这些已知规律，我们可以从已经接受的算术式"推导出""负一乘负一等于正一"这一算术式。这样，我们就按照算术自身的规律理解了这一算术式。

一般地说，我们学习算术可以分成为三个阶段：第一阶段，从与日常生活的实例对比中来理解某些个别的算术式，同时从这些个别的算术式总结出一般的运算规律；第二阶段，按照第一阶段总结出运算规律，从一些较简单的算术式导出较复杂的算术式，不再要求这些较复杂的算术式与日常生活的实例相互对应。第三阶段，从最简单的算术式和最简单的运算规律开始，导出全部算术式，从头到尾摆脱与日常生活的实例相互对应这一环节。这个第三阶段所用的方法就是所谓"公理化"的方法，这种方法对于我们学习算术乃至学习数学的其他分支都是极为重要的。

上面就是我的回答。不久，这位学生又问我关

于复数的问题，他的提问和我的回答至今我记忆犹新。我原准备就这一问题给学生们上一节课，还为此准备了一个教案，下面是这个教案的要点：

关于复数的故事，可以从“数学怪人”卡丹的一道题说起，“如何把 10 分成两部分，使得其乘积为 40？”这道看来平淡无奇的算术题的求解把我们带进了怪异的复数王国。对于这一意外的结果，卡丹这样说：“算术是如此微妙地发展着，而它的尽头，却……是既精致而又无用的。”

在以后的发展中，复数运算不仅越来越精致，而且也越来越有用，但数学家们却继续拒绝承认复数是“数”。直到“数学王子”高斯和与他同时代的其他人把复数表成平面上的一点，并给出复数加法与乘法的几何意义，复数才最终登上了数学的大雅之堂。

对于我来说，接受复数是在接受了“域”的概念之后。“域”虽然是一个“高等代数”的概念，但只要学过“分数”，我们就可以这样理解它：“域”是一个“数的集合”，在这个集合中，可以定义加减乘除四则运算，而且其中的加法和乘法运算，满足交换律、结合律、交换律等运算规律。有了“域”的概念，“复数”就可（借助于实数）定义如下：

第一，每一个实数都是一个复数；

第二，“负一的平方根”是一个复数；

第三，全体复数构成一个“域”。

由此可见，掌握“域”的概念之后，对“复数”这一概念的引进可大大简化。

有了“域”的概念，我同样容易地接受了“非标准分析”中的“超实数”，因为“超实数”可（借助于实数）定义如下：

第一，每一个实数都是一个超实数；

第二，某一无穷小量（其绝对值大于零而小于一切正实数的量）是一个超实数；

第三，全体超实数构成一个“域”。

关于有理数、实数、复数和超实数的理论，统称为“数系”的理论。对于这一理论，“域”是一个关键的概念。

马克思在他的《数学手稿》中曾对“导数”有过一些议论，作为一个外行人在工作之余想一想数学问题，无论对错都是无可非议的。不幸的是，当“马克思主义”蜕变为一种宗教以后，他的数学手稿也被提升为数学的“最高成果”，这就引起了完全多余的麻烦。对于数学我所知甚微，不可能在这里评论马克思的《数学手稿》的学术价值的问题。但对于马克思在手稿中提出的一个论点我不妨说两句，马克思谴责数学家们忌讳把“零”作为一个分数的分母，说这是一种“形而上学的恐惧”，这一点我不敢苟同。如果允许零作为分母，除法就不再是一个“代数运算”，而“分数”就不再是一个“域”。这样，整个算术的大厦就成了一片废墟。

恩格斯曾说马克思是一个精湛的数学家，在我看来，这表明恩格斯对于数学也只是一个“半通”（这是他对自己的评价）。

在《自然辩证法》一书中，恩格斯一方面对数学提出许多深刻而又中肯的意见；另一方面也提出了某些错误的看法而不自知。但是，其中有一论点恩格斯自己也知道错了，那就是他说：“虚数的荒谬的，但有时候应用虚数也能得出正确的结论。”错在何处，恩格斯没有说。其实，恩格斯对虚数的这种看法，和 17、18 世纪大多数数学家对虚数的看法差不多，问题仅在于到了恩格斯所处的时代，数学家们已经认识到复数并不是荒谬的，而作为一个哲学家，恩格斯本应走在数学家们前面的……。

恩格斯对虚数的看法是一种落后于时代的看法，这一看法说明恩格斯也是一个人，而不是无所不知的神。至于马克思关于“零可以作为分数的分母”的意见，就不是落后不落后的问题，它是一个错误，而且是一个致命的错误。

不过话又说回来，对于数学，马克思充其量是一个业余爱好者，不论他有怎样的错误，都可以一笑置之，这件小事丝毫无损于这位伟大的思想家的声誉。至于“最高成果”之说，那就不能由马克思负责任了。

一个相关的问题是爱因斯坦对恩格斯的《自然辩证法》一书的评价，这个问题一向很敏感，而且不完全是一个学术问题。按照我的意见，《自然辩证法》是一本没有定稿的书，其中的某些论点，对于一个没有自己重踏恩格斯的思路的读者是不可能理解的。这里我举一个例子，在该书的开头，恩格斯写道：“力学，出发点的惯性，而惯性只是运动不灭的反面表现。”“惯性”这一用语在这本书中只在这里惊鸿一瞥，以前不曾出现，以后也不再出现。这句话是什么意思，众说纷纭，迄今没有一个哪怕是字面上说得通的看法。爱因斯坦是诚然一个卓越的物理学家，但他肯定不知道恩格斯这里说的是什么意思。如果一个人连恩格斯说的是什么都不知道，他能对《自然辩证法》提出中肯的意见吗？

这个教案还有一些细节，就不在这里叙述了。由于这个教案不在教学计划之内，我一直没有用。时至今日，看来我是再也用不上了。

2/22/2012

Academia Arena

(*Academ Arena*)
ISSN 1553-992X

学术争鸣

Call for Papers

Academia Arena is published bi-linguistically with English and Chinese for the scientists and Engineers by Marsland Press in USA. The journal founded in January 1, 2009 aims to present an arena of science and engineering. The Editor-in-Chief, Associate Editors-in-Chief and Editors have backgrounds in Philosophy, Science, Technology, Cosmology, Mathematics, Physics, Chemistry, Biology, Medicine, Civil, Electrical, Mechanical Engineering, etc. Papers submitted could be reviews, objective descriptions, research reports, opinions/debates, news, letters, and other types of writings. All manuscripts submitted will be peer-reviewed and the valuable manuscripts will be considered for the publication after the peer-review.

学术争鸣于2009年元月1日在美国纽约马斯兰德出版社发刊，主要目标为提供科学家与工程师及社会工作者学术辩论的发表园地，专业领域包含哲学、科学、技术、宇宙学、数学、物理、化学、生物学、医学、土木、电机、化工、机械工程，等，编辑群将以最专业客观的立场为所有投稿作者服务。

Here is a new avenue to publish your outstanding reports and ideas.

Papers in all fields are welcome, including articles in natural science and social science.

Please send your manuscript to: aarenaj@gmail.com

For more information, please visit: http://www.sciencepub.net/academia

Marsland Press
PO Box 180432
Richmond Hill, New York 11418, USA
Telephone: (347) 321-7172
E-mail: sciencepub@gmail.com;
editor@sciencepub.net
Emails: editor@sciencepub.net; aarenaj@gmail.com
Website: http://www.sciencepub.net/academia

Volume 4, Number 2 (Cumulative No.32) February 25, 2012 ISSN:1553-992X

Academia Arena

Marsland Press
PO Box 180432
Richmond Hill, New York 11418, USA

Websites:
http://www.sciencepub.net/academia
http://www.sciencepub.net

Emails:
aarena@gmail.com
editor@sciencepub.net

Phone: (347) 321-7172

Cover design: MA,Hongbao
Photograph: YOUNG, Mary